Study on Development of Cobalt Phosphide Nanoparticle Catalysts for Environmentally-benign Hydrogenation Reactions

MIN SHENG

September 2022

Study on Development of Cobalt Phosphide Nanoparticle Catalysts for Environmentally-benign Hydrogenation Reactions

A dissertation submitted to

THE GRADUATE SCHOOL OF ENGINEERING SCIENCE

OSAKA UNIVERSITY

in partial fulfillment of the requirements for the degree of

DOCTOR OF PHILOSOPHY IN ENGINEERING

BY

MIN SHENG

September 2022

Abstract

This thesis deals with the studies on the development of cobalt phosphide nanoparticle catalysts for environmentally-benign hydrogenation reactions. The present thesis consists of five chapters.

In Chapter I, the author surveys the fundamental background of metal phosphides and focus on the exploration of cobalt phosphide as a potential catalyst for organic synthesis. The characteristics and preparation methods of cobalt phosphides were systematically summarized. Finally, recent reports on the catalysis of cobalt phosphides were specifically reviewed.

In Chapter II, the author describes a well-defined cobalt phosphide nanoparticle (nano-Co_2P) catalyst for selective hydrogenation of nitriles to the corresponding primary amines. nano-Co_2P was successfully prepared via a phosphorus-alloying strategy and showed significantly high activity in nitrile hydrogenation even under 1 bar H_2 pressure, which is the first example of a non-precious metal catalyst for promoting this transformation under ambient H_2 pressure. In addition, nano-Co_2P catalyst was applicable to the gram-scale reaction, giving the desired primary amine in high yields.

The author demonstrates in Chapter III that an Al_2O_3-supported nano-Co_2P (nano-Co_2P/Al_2O_3) can serve as a highly efficient catalyst for the selective hydrogenation of furfural derivatives. In contrast to conventional non-precious metal catalysts, nano-Co_2P exhibited unique air-stable metallic nature, which enables easy and safe handling. Furthermore, the spent nano-Co_2P catalyst was reusable without significant loss of its activity and selectivity.

The next chapter represents unique catalysis of a newly synthesized single-crystal cobalt phosphide nanorods (Co_2P NRs) for reductive amination of carbonyl compounds to primary amines using aqueous ammonia or ammonium acetate as green amination reagent. The Co_2P NR is the first cobalt catalyst to achieve reductive amination under just 1 bar of H_2 and a wide range of carbonyl

compounds including aldehydes and ketones could be selectively transformed into the corresponding primary amines in high yields.

Finally, the author mentions the hydrogenation of nitriles catalyzed by a hydrotalcite (HT, $Mg_6Al_2(OH)_{16}CO_3 \cdot 4H_2O$)-supported cobalt phosphide nanorod catalyst (Co_2P NR/HT) in Chapter V. Co_2P NR/HT exhibited a broad substrate generality including aromatic, heteroaromatic, aliphatic nitriles, dinitriles as well as sulfur-containing nitriles under mild conditions. Moreover, Co_2P NR/HT is the first example of hydrogenation of nitriles to primary amines under ammonia-free conditions using non-precious metal catalyst.

Preface

This dissertation is a collection of the author's studies which were carried out from 2017 to 2022 under the supervision of Professor Tomoo Mizugaki and Professor Koichiro Jitsukawa at the Division of Chemical Engineering Department of Materials Engineering Science, Graduate School of Engineering Science, Osaka University.

Taking the advantages of sustainability and economy, heterogenous catalysts based on earth-abundant non-precious metals have attracted enormous interest in both academia and industry. Up to date, nickel and cobalt sponge metal catalysts (Raney catalysts), sufferring from low activity and safety problems caused by the air-sensitivity (pyrophoricity), are still widely employed in industrial hydrogenation reactions with low efficiency and potential dangers. Thus, the development of non-precious metal-based heterogenous catalysts with high activity and air-stability plays a pivotal role toward environmentally-benign chemical processes and is highly demanded.

In this thesis, the author demonstrates that the "phosphorus-alloying strategy" is a promising nanotechnology to develop a new class of air-stable and highly active non-noble-metal catalysts. The developed cobalt phosphide nanoparticle catalysts exhibit excellent catalytic performances in various liquid-phase hydrogenation reactions with easy and safe handling, which can be leading candidates to substitute the conventional sponge metal catalysts.

The author strongly believes that this study will be a milestone attempt for developing air-stable and highly efficient non-precious metal catalysts via "phosphorus-alloying strategy" for organic synthesis and provide the worthwhile background for future researchers to realize efficient, sustainable, and environmentally-benign reaction processes for valuable chemical productions.

Contents

Chapter I.

General Introduction

1. Preliminary

Catalysis is firstly introduced in 1836 by Berzelius [1], which is one of the most important domains of chemistry. About 90% of commercial chemicals involve catalysis at some stage in the production process, including fine chemicals, food manufacturing, and energy processing [2]. Since the beginning of the 20th century, catalysis has started to draw a tremendous interest and enable many "dream reactions" come true in the chemical industry. For instance, Haber–Bosch process, the production of ammonia from dinitrogen and hydrogen catalyzed by an iron catalyst regarded as an industrial landmark innovation, is achieved in 1913, which makes the manufacture of ammonia economically feasible and significantly alleviates the worldwide food supply problems by the increase of nitrogen fertilizers [3-5]. Up to now, the Haber Bosch process is undoubtedly considered as one of the most important inventions of the 20th century. Over the past decades, various challenges in climate change, pollution, and sustainable energy also have found their solutions in a catalysis way [6]. As a result, catalysis has made significant contributions not only improving the quality of human living standards but also notably increasing our life expectancy.

Since the large amounts of waste generated every day by chemical processes, there is a growing demand for more environmentally acceptable processes that shift traditional focus of process efficiency and chemical yield to eliminate unwilling wastes and avoid the use of toxic and/or hazardous reagents. This trend has become known as 'Green Chemistry', advising nowadays chemists to solve energy and resource consumption problems. In this context, catalysis has been listed as one of the 12 principles of Green Chemistry in 1998. Spontaneously, catalyst is regarded as a necessary and critical tool towards Green Chemistry [7-8]. For example, the reduction of ketone to the corresponding secondary alcohol can be achieved by using sodium borohydride with an atom economy about 80%. While the reaction using molecular hydrogen ends up everything in the product and shows a 100% atom economy, in other words, there is no waste. However, this reaction does not occur to any

2

extent under normal conditions, unless the copresence with a catalyst such as palladium-on-charcoal (Pt/C). For this reason, chemical procedures using stoichiometric reagents that create unwanted byproducts like inorganic salts are gradually replaced by catalytic alternatives, which are atom-efficient and environment-friendly.

Catalysts are generally divided into two types, homogeneous and heterogeneous catalyst, depending on whether they occupy the same phase as the reaction mixture. Although homogeneous catalysts show high catalytic performance because of the high-degree interaction between catalyst and reactant molecule, they are hard to be separated from reaction mixture and generally unrecyclable. On the contrary, heterogeneous catalysts can be separated easily in a straightforward manner, such as filtration, and effectively recovered. Thus, most chemical industries tend to use heterogeneous catalyst in accordance with the need of sustainable development. In the meantime, heterogeneous catalysts based on non-precious metals (e.g. Fe, Ni, Co), which are earth abundant, low cost, and relatively low toxicity, have received great interest in recent times and are regarded as a better option than their noble-metal based competitors [9]. However, conventional non-precious metal heterogeneous catalysts typically exhibit low activity and/or poor durability, which hinders their further applications [10].

In terms of the critical role of non-precious metal heterogeneous catalysts in sustainable chemical processes, the study on development of non-precious metal-based heterogeneous catalyst with high performances through the sophisticated design and synthesis, such as alloying with other metals or non-metal elements, is of considerable interest.

2. Background

"Metal phosphide" is a kind of compounds that contain phosphorus and metals. The first successful synthesis of metal phosphide is recorded in the 18th century [11]. However, no notable use of metal phosphides is found for nearly 200 years until the early reports about the applications for metallurgy and pesticides [12]. Importantly, nickel phosphide ($NiP_{0.584}$) was found to be active for a gas-phase hydrogenation reaction in 1958, revealing the catalytic potential of metal phosphides for the first time [13]. However, the following investigations indicated that metal phosphides genarally exhibit poorer catalytic activity than the in-situ generated metal (0) nanoparticles [14-15] or their metallic counterparts [16-19] and thus gradually slipped out of the popular consciousness. Since the pioneer works by Robinson *et al.* and Oyama *et al.* in 1990s [20-21], metal phosphides captured attentions again by their high performance in hydrotreating reactions. Notably, a density functional theory (DFT) study in 2005 predicted that the (001) plane of Ni_2P is a potential material as hydrogen evolution reaction (HER) catalyst [22], which has been later experimentally proven by Schaak and coworkers in 2013 [23], unveiling the upsurge of metal phosphides in electrocatalysis and photocatalysis fields [24-25].

Cobalt (Co) belongs to the group VIII-B of the periodic table and is one of the most promising materials as non-precious metal heterogeneous catalysts. Among them, cobalt phosphides have attracted enormous concentrations during the past decades owing to their unique catalysis. The study of unexplored cobalt phosphide-catalyzed organic synthesis, like hydrogenation reaction, is of great interest and provides a potential option to realize sustainable chemical process.
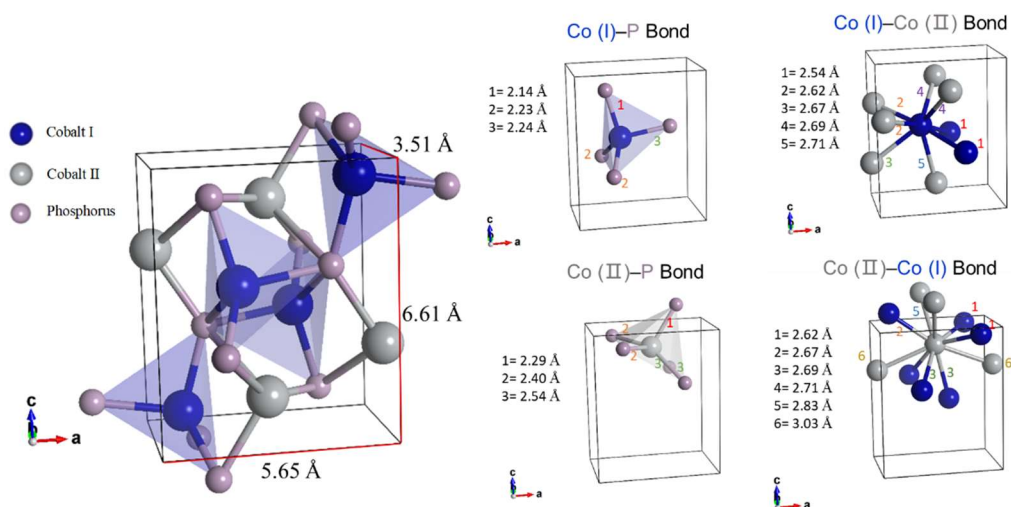
2.1. Structure of cobalt phosphide

There are several compositions of cobalt phosphide depends on the the ratio of cobalt and phosphorus. CoP and Co_2P are the most reported compositions and their crystal structures are shown in **Scheme 1-1** and **Scheme 1-2**, respectively.
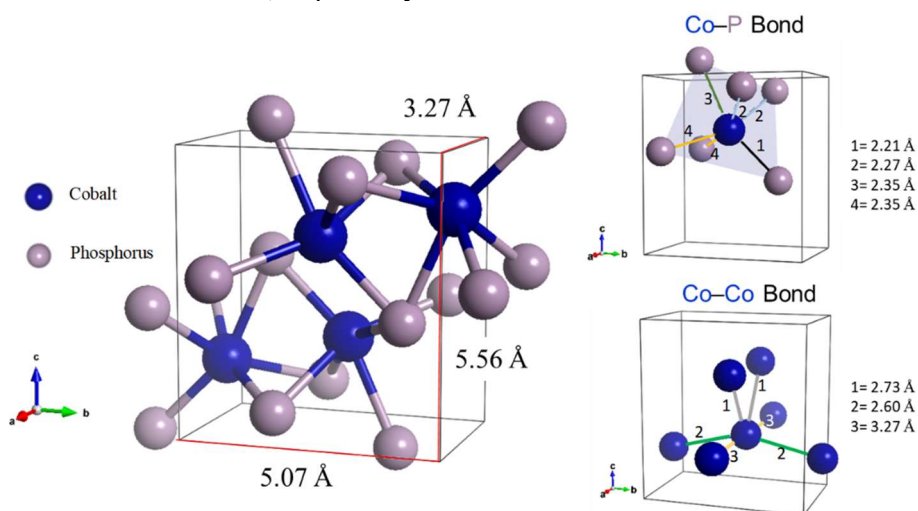
Scheme 1-1. Crystal structures of CoP.

CoP adopts the MnP structure type that six P atoms are coexistence with Co atom to give a distorted face-sharing CoP_6 octahedra configuration. In the meantime, P atom is arounded by six Co atoms to form a PCo_6 trigonal prism structure [26].

Scheme 1-2. Crystal structures of Co_2P.

Co$_2$P is reported to crystallize in the Co$_2$Si-type structure, containing CoP$_4$ tetrahedra and CoP$_5$ pentahedra that are edge-sharing to form nine-coordinate P atoms [27-28].

2.2.   Preparation of cobalt phosphide

Conventionally, cobalt phosphide is prepared by direct combination of elements at high reaction temperatures (> 900 °C) under an inert atmosphere with long annealing times (1-10 days) [29]. Because of the harsh reaction conditions and bulk size of obtained cobalt phosphide, other approaches that carried out under milder conditions to give nanosized products have been extensively desired.

2.2.1   Solution-phase synthesis

In 1997, Qian *et al.* reported a benzene-thermal method to prepare cobalt phosphide via the reaction of sodium phosphide (Na$_3$P) with the CoCl$_2$ in benzene in a Teflon-lined autoclave at 150 °C, giving a mixture of sphere-shaped Co$_2$P and spindle-shaped CoP nanocrystals in 90% yield [30]. In their subsequent work, high-quality and uniform Co$_2$P nanorods was firstly prepared by a one-pot solution-based synthesis through the reaction of CoCl$_2$ and yellow phosphorus in a Teleon-lined autoclave filled with aqueous ammonia at 220 °C [31]. In the case of ethylenediamine as a solvent, the plate-like Co$_2$P nanoparticles with 50 nm diameter could be obtained at temperature as low as 80 °C [32]. However, nanosized metal phosphides derived from these methods are generally polydispersed and the morphology is also not well controlled.

Since the successful conversion of iron salt with P(SiMe$_3$)$_3$ into the corresponding metal phosphides (FeP) by a low-temperature thermal decomposition method [33], phosphines have been regarded as versatile and attractive phosphorus sources. For example, cubic Co$_2$P nanorods were

synthesized via the decomposition of Co–TOP (TOP: tri-n-octylphosphine) complex at 300 °C, which is prepared by Co(acac)$_2$ (acac = acetylacetone) as metal precursor in presence with TOP, octyl ether (OE), and hexadecylamine (HDA) [34]. O'Brien *et al.* also prepared CoP nanowires by adding Co(acac)$_2$ and tetradecylphosphonic acid (TDPA) into a solution of tri-n-octylphosphine oxide (TOPO) and HDA via a 340 °C thermal deconmposition [35]. Overall, cobalt phosphide with high purity and crystallinity can be obtained through the above thermal decomposition methods. Furthermore, controllable synthesis of cobalt phosphide also can be realized by employing different combinations of metal precursor, phosphine source, and surfactant to give those in various sizes, shapes, and compositions, which are closely important to catalytic activity.

Other solution-phase synthesis methods such as photochemical deposition using UV-vis light irradiation [36], and electrochemical deposition in an electrolyte solution containing CoCl$_2$ and NaH$_2$PO$_2$ [37] are also utilized in some specific areas.

2.2.2 Gas-phase synthesis

PH$_3$ is efficient and active in direct phosphorization of metal precursors to metal phosphides through a gas-phase reaction, while it is extremely toxic and lethal even at a few ppm. Thus, hypophosphites (e.g. NH$_4$H$_2$PO$_2$ and NaH$_2$PO$_2$) are widely utilized as alternatives, which can in situ generate PH$_3$ by thermal decomposition at an elevated temperature. For example, CoP supported on carbon cloth (CC) was prepared by mixing Co(OH)F/CC and NaH$_2$PO$_2$ in a molar ratio of Co : P = 1:5 and then was heated at 300 °C for 60 min in Ar atmosphere to give a black CoP/CC product [38].

Another facile way for gas-phase synthesis of metal phosphide is the temperature-programmed reduction (TPR) method of phosphate compounds at high temperatures. Briefly, metal salt and phosphate source are deposited onto the support such as silica via aqueous impregnation with the following dry or/and calcination process. Then, the obtained sample is heated in a H$_2$ flow

condition to give the corresponding supported-metal phosphide. For instance, according to the synthesis report by Bussell *et al*. [39], after impregnation of the SiO_2 with $NH_4H_2PO_4$ and $Co(NO_3)_2$, Co_2P/SiO_2 with 5–20 nm particle sizes could be obtained under a flowing H_2 (300 mL/min) at 923 K. In general, silica is the most frequently used support for this method because of the strong tolerance for phosphidation. Other supports are prone to strongly interact with phosphorus to form undesired species, such as $AlPO_4$ in the case of Al_2O_3 [40]. Although TPR method has been employed in preparing various kinds of metal phosphides, the high preparation temperature (ca. 600 °C) and limited choices of supports have barriered their further applications.

2.3. Cobalt phosphide catalyzed gas-phase reaction

2.3.1. Hydrotreating reactions

Hydrotreating reaction (e.g. hydrodesulfurization (HDS), hydrodenitrogenation (HDN)) is an industrially acceptable process to refine the crude petroleum to the transportation fuels by removing heteroatoms like sulfur, oxygen, and nitrogen. Since the notable review by S.T. Oyama in 2003 [21], metal phosphides have been recognized as a kind of high active and stable catalysts for hydrodesulfurization (HDS) and hydrodenitrogenation (HDN) reactions.

In the early studies for the HDN of *o*-propylaniline, Co_2P was turned to be the least active catalyst among the other metal phosphides ($Co_2P < WP < Ni_2P < MoP$) [41]. As for HDS of dibenzothiophene (DBT) and HDN of quinoline, cobalt phosphide also exhibited an unattractive performance in an activity order of $Fe_2P < CoP < MoP < WP < Ni_2P$ [21]. Thus, cobalt phosphides did not receive enough attention as much as other metal phosphide competitors for the hydrotreating reactions

Burns *et al*. indicated that CoP/SiO_2 prepared by the conventional TPR method has nearly

four times higher activity than that of Co_2P/SiO_2 in the HDS of thiophene [39]. The similar result was also reported by Cecilia *et al* [42]. In their work, support plays an important role on the genaration of CoP or Co_2P supported on different supports by TPR of cobalt hydrogenphosphite. CoP phase is favored to be formed on MCM-41 and SiO_2 support, which could keep its activity for 48 h and the catalytic performance is similar to those of reported Ni_2P catalysts. In the case of γ-Al_2O_3, less active Co_2P phase was formed and the catalyst was rapidly deactivated after 3 hours under the same reaction condition. In a S analysis as shown in **Figure 1-1**, Co_xP_y/SiO_2 catalysts exhibited an apparent trend that the extent of S incorporation decreases as the catalyst surfaces are gradually P-rich, which explains the higher activity of CoP phase than Co_2P due to the superior durability.
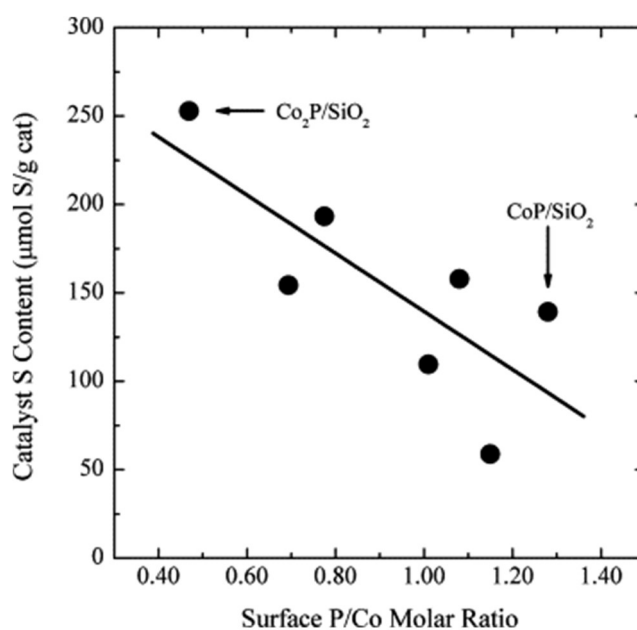
Figure 1-1. The function between the S content in Co_xP_y/SiO_2 catalysts and the P/Co molar ratio of the catalysts.

The preparation method of cobalt phosphide also influences the catalytic activity in HDS reaction. Zhou *et al.* prepared CoP and Co_2P catalysts by TPR of $Co(OH)_2$ and H_3PO_3 with stoichiometric P/Co ratios, which is different from conventional method using large excess of

phosphorus source [43]. The obtained CoP showed higher conversion of tested substrates including 1,2,3,4-tetrahydro-dibenzothiophene (TH-DBT), dibenzothiophene (DBT), and 1,2,3,4,4a,9b-hexahydro-dibenzothiophene (HH-DBT) compared to Co_2P, even outperforming the previous value obtained by Ni_2P, MoP, and WP (**Figure 1-2**). The reason for its high HDS activity could be explained by the less remined phosphorus after preparation, while the excess amount of phosphorus is well-known to have a negative influence for the activity of HDS catalysts.
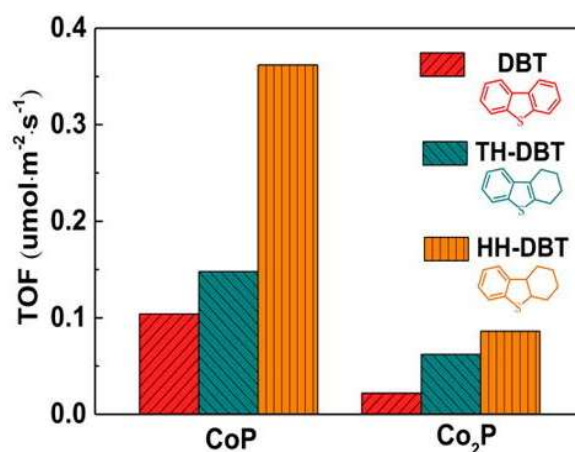
Figure 1-2.   Turnover frequencies of DBT, TH-DBT, and HH-DBT by using CoP, Co_2P, and WP catalysts.

Making full use of renewable biomass as a novel energy source is of vital importance to reduce the increasing consumption of fossil fuels and CO_2 emissions. Hydrodeoxygenation (HDO) of biomass is a promising substitute for fossil fuels through upgrading bio-oil via removal of oxygen-containing species. Metal phosphide catalysts are also applicable for HDO reaction. In the HDO of 2-methyltetrahydrofuran (2-MTHF), silica-supported metal phosphides was tested at 300 °C and 1 atm to give a catalytic activity order of Ni_2P > WP > MoP > CoP > FeP and indicated the type of metal also influences the product distribution [44].

As for cobalt phosphide catalyzed HDO reaction, the activities are strongly influenced by

the exposed active phase on the surface. In Rodríguez-Aguado`s report [45], Co_2P, CoP, and CoP_2 phase were formed by increasing the P/Co atomic ratio and found out the catalyst containing CoP as the main phase exhibited high activity in the HDO of phenol reaction. The comparison experiments of supported Ni_2P, Co_2P, and MoP catalysts prepared by TPR of the corresponding metal phosphate precursors were also carried out. Despite the high conversions of phenol, cyclohexanol was yielded as the main product in the case of Co_2P/Al-SBA-15 and Co_2P/m-Al_2O_3 due to their poor HDO performances. Moreover, there was a limit on the phenol conversion at 80%, which is caused by the catalyst deactivation during the reaction [46].

Mondal *et al.* report a $Co_xP@$ POP (POP: porous organic polymer) hybrid catalyst via phosphidation of the $Co_3O_4@POP$ nanohybrid with NaH_2PO_2 under a 300 °C, N_2 flow system [47]. In the HDO reaction of vanillin to 2-methoxy-4-methylphenol, $Co_xP@POP$ exhibited superior catalytic activity (~2-fold higher), selectivity, and stability than $Co_3O_4@POP$ that without phosphidation. These improvements are largely attributed to the modulation of the electronic properties of Co with the introduction of P. In addition, a higher H_2 consumption value of $Co_xP@POP$ could be observed in the H_2-TPR study, implying the better H_2 activation ability after phosphidation. Furthermore, the weaker interaction of vanillin with $Co_xP@POP$ surface was also demonstrated as another reason for its high activity proposed by IR studies, whereas the adsorption of vanillin was too strong in the case of $Co_3O_4@POP$ that slowed down the reaction.

A study about hydrodechlorination (HDC) of chlorobenzene using cobalt phosphide catalysts with different P contents revealed that, the catalyst with an initial P/Co atomic ratio = 2 was the most active one [48]. In the meantime, the lower Cl retention after reaction as well as the higher catalytic activity could be achieved with the increasement of P content, which means introduction of P brings an improved Cl-surface cleaning effect that is important for maintaining the activity in HDC
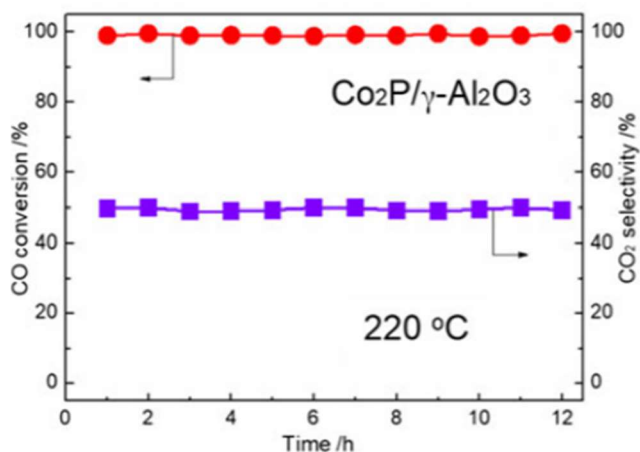
reaction.

As a result, the investigation and catalytic performance of cobalt phosphide catalysts in hydrotreating reactions are relatively fell behind those of other metal phosphide competitors (such as MoP, Ni_2P). All reported cobalt phosphide catalysts in these reactions are prepared by the gas-phase synthesis method. Moreover, the phosphorus-rich cobalt phosphides tend to exhibit higher durability, which is significantly associated with activity under hydrotreating conditions.

2.3.2. CO transformation

In Song and coworker`s report [49], silica-supported Co_xP catalysts with various Co/P molar ratios were prepared and evaluated in CO hydrogenation reaction. Unlike other Co based catalysts or conventional catalysts, the Co_xP/SiO_2 catalysts showed a high selectivity of C^{2+} oxygenates in 45%, which is attributed to the changes in electronic and adoption properties of the metallic cobalt after the phosphorus introduction. The $Co–Co_2P$ species were hypothesized to play an important role that CO dissociation and chain growth are catalyzed by metallic cobalt, while the $Co^{\delta+}$ species in Co_2P are responsible for nondissociative CO adsorption and subsequent CO insertion to form oxygenates.

Another example of CO transformation using cobalt phosphide catalyst was reported for a preferential CO oxidation (PROX) reaction [50]. $Co_2P/\gamma-Al_2O_3$ catalysts were active for PROX reaction and exhibited a similar result of widely-used $Pt/\gamma-Al_2O_3$ catalyst. The orthorhombic $AlPO_4$ phase was detected from XRD caused by the phosphidation of $\gamma-Al_2O_3$ support. The highest CO conversion and CO_2 selectivity were obtained by using $Co_2P/\gamma-Al_2O_3$ catalyst with 10 wt% Co loading (220 °C: 99.5% CO conversion, 49.7% CO_2 selectivity; 240 °C: 98.5% CO conversion, 48.0% CO_2 selectivity). Notably, the high CO conversion was unchanged for 12 h, which indicates the high stability of $Co_2P/\gamma-Al_2O_3$ catalyst (**Figure 1-3**).

Figure 1-3. Catalytic stability of the Co_2P/γ-Al_2O_3 catalyst in PROX reaction.

2.3.3. Ethane dehydrogenation

The outstanding performance and stability of cobalt phosphide catalyst at high temperature were also proved via ethane dehydrogenation (EDH) [51]. Among evaluated Co catalysts, SBA-15-supported Co–P materials improved ethylene selectivity apparently from 41% for monometallic Co/SBA-15 to 88%, attributing to the formation of $Co^{\delta+}$ sites that charge transfered with P. The further investigation found that overactive and lower coordination sites are blocked by the P species on the surface, increasing the selectivity of ethylene and the stability of catalyst. Furthermore, Co_2P/SBA-15 and CoP/SBA-15 catalyst both exhibited remarkable high temperature stability over Pt–Sn/SBA-15 that a well-studied Pt catalyst in EDH (**Figure 1-4**), demonstrating the tremendous potential of cobalt phosphide-based catalyst at high-temperature gas phase reaction.

13
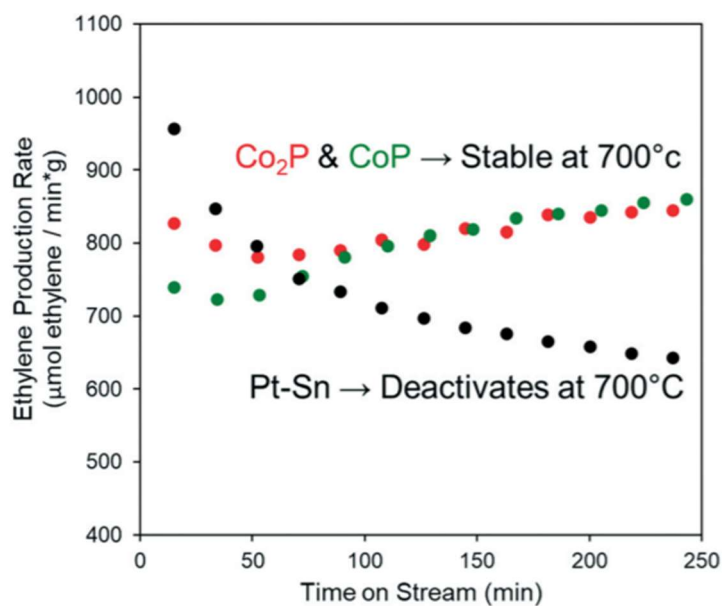
Figure 1-4. Ethylene production rate of EDH by Co_2P/SBA-15, CoP/SBA-15, and Pt–Sn/SBA-15.

2.4. Cobalt phosphide catalyzed liquid-phase reaction

Since the successes in hydrotreating and HER reactions, the catalysis of metal phosphide for liquid-phase reaction like organic synthesis is emerged as the next research fever.

2.4.1. Hydrogen generation by hydrolysis of boranes

Catalytic hydrolysis of ammonia borane (AB) and sodium borohydride is an attractive method for hydrogen generation, depending on their nontoxicity, hydrogen content, and stability.

Sun *et al.* reported CoP nanosheet supported on macroporous Ti mesh (CoP NA/Ti) can servers as an active catalyst for hydrolysis of AB for the first time [52]. The CoP NA/Ti provided a high initial TOF of 42.8 $mol_{H2} \cdot mol_{CoP}^{-1} \cdot min^{-1}$ and low activation energy. Furthermore, only 0.15% catalytic activity was lost after 10 cycles. These results are largely derived from its 3D nanoarray configuration structure that allows efficient diffusion and the exposes more active sites. Similarly,

CoP@CNF catalyst prepared by a Zn/Co MOFs exhibited the highest TOF value for hydrolysis of AB among the precious metal-free system at that time [53]. Because of conventional catalysts for hydrolysis of AB usually have troubles in aggregation and destabilization, these reports focused more attention to the structure of support material (e.g. high surface area, rich pore) or their influence for particle size of cobalt phosphide formed instead of the property of cobalt phosphide itself.

Furthermore, the hydrogen derived from hydrolysis of borane compounds can further be applied to reduction reaction. For example, self-assembled Co_2P nanowires were regarded as a bifunctional catalyst for both the reduction of 4-nitrophenol and hydrolysis of $NaBH_4$ [54]. Based on the XPS results, the P (δ-) species on the surface could act as a proton-acceptor, promoting the generation of the MH complex. In another borohydride-assisted reduction of 4-nitrophenol using Co_3O_4/CoP catalyst, CoP was proposed as the active site for both electron transfer and hydrogen atoms formation from BH_4^- [55].

Although new applications and insights about cobalt phosphide are obtained, the substrate or the reductant used is prone to cause waste problems, which is unacceptable from a Green Chemistry view and thus limited the utilization in a narrow field. However, the detail investigation about how cobalt phosphide activates hydrogen and the discussion about its hydrogenation ability are still lacked in these reports.

2.4.2. Hydrogenation

The catalytic hydrogenation is of vital importance for the modern chemical production and is existed in anywhere from the milligram-scale organic synthesis to the multiton-scale chemicals production. The hydrogenation with molecule hydrogen is the most atom-efficient way to produce desired saturated compounds.

Since the early work about the metal-rich dinickel phosphide for vapor phase reduction of nitrobenzene in 1958 [13], only a few researches about hydrogenation by metal phosphide catalyst have been reported. However, most of them emphases the applications in selective hydrogenation possibly because of their low activities [56-58].

Encouraged by the excellent performance in electrocatalysis, Queen et al. tried to discover the potential applicability of cobalt phosphide in thermally driven hydrogenation reaction. In 2017, they designed a cobalt phosphide/carbon nanocubes (Co_2P/CN_x nanocubes) catalyst from a metal-organic framework (MOF) material, which needs a high-temperature (>700 °C) phosphorization step via the pyrolysis treatment with red phosphorous [59]. The resulting Co_2P had an average 5 nm size and were uniformly distributed throughout the nanocube matrix. Importantly, Co_2P/CN_x nanocubes showed high catalytic performance for the hydrogenation of nitroarene reaction under 5.0 MPa H_2, 60 °C conditions, giving the desired anilines in high yields (13 substrates, 99%). Further reuse experiment also indicated its high stability and recyclability, which is essential to a heterogenous catalyst.

In 2019, Mayer et $al.$ provided the experimental estimates of cobalt phosphide about the thermochemistry for the first time [60]. Mesoscale CoP particles (CoP-M) was prepared by cobalt oxide and PH_3 after an acidic pretreatment, and another sample catlled colloidal CoP nanoparticles (CoP-NP) that derived from $CoCl_2$ and aminophosphine were used in this study. After introducing H_2,

reactive hydrogen was existed on both CoP samples with a ratio of ca. 0.2 H per CoP unit. In addition, the H_2 activation catalyzed by CoP−M was evaluated via hydrogenation of several kinds of hydrocarbons. Styrene and ethylbenzene were yielded after 2 days, which means CoP–M can activeate H_2 molecules and then moved to the substrates to give the hydrogenated products. The distribution of binding free energies was caculated by using hydrogen-atom transfer reagents and indicated that the value of H atoms on CoP was 51–66 kcal·mol^{-1}. Moreover, the XAS spectra confirm the possible incorporation of H in CoP–M and no obivious difference of the effective nuclear charge of Co was found under H_2 flow.

Above results suggest the great potential of cobalt phosphide-based catalyst as competitive candidate for hydrogenation reactions. In fact, the studies of hydrogenation reaction involved cobalt phosphide catalyst have been increased gradually during the last decades.

As for hydrogenation of levulinic-acid (LA) reaction, metal leaching is the most fatal problem due to the strong acid environment caused by the dissolved LA in aqueous solution. In this context, Zhao *et al.* found their solution by using an acid-resistant $CePO_4/Co_2P$ catalyst [61]. The $CePO_4/Co_2P$ was prepared by solvothermal evolution of the mixture of $Ce(NO_3)_3$, $Co(NO_3)_2$, and $(NH_4)_2HPO_4$ at 200 °C for 24 h combined with the further H_2 reduction at 800 °C for 3 h. The H_2-TPD measurements were performed and found the hydrogen adsorption–activation property of synthesized Co_2P was quite poor and much inferior to that of $CePO_4$, indicating hydrogen was more likely activated by $CePO_4$ during the reaction. Instead of hydrogen activation, Co_2P probably worked as the key component for the activation of LA due to the high strength of acid sites on Co_2P, which are conducive to the esterification and cyclization steps in this reaction. As a result, the cooperative catalysis between $CePO_4$ and Co_2P achieved the high TOF value of 0.61 s^{-1} for hydrogenation of LA to gamma-valerolactone (GVL), which is comparable to those of precious metal catalysts. In terms of the metal leaching problem, the leakage amount of Co in solution was fixed around 3.0 wt% due to the initial

oxidative Co species on the surface of Co_2P and did not increase any further with prolonged reaction time, implying its high acid-resistant feature.

Additionally, the acid catalysis of cobalt phosphide also was stressed in the hydrogenation of furfural (FA) reaction [62]. Based on the NH_3 pulse purge and pyridine-absorbed Fourier transform infrared (FTIR) spectra, the synthesized CoP had a stronger lewis acid property than Ni_2P (56.3 μmol/g vs. 43.2 μmol/g). Because of the well-adjusted synergistic effect of hydrogenation and acid catalysis of CoP, 1,2,5-pentanetriol was obtained as the main product in a high yield of 80.2% via a hydrogenative ring-opening route, while Ni_2P preferred to give cyclopentanol in 62.8% yield (**Figure 1-5**). Thus, besides the hydrogenation ability, cobalt phosphides also can server as an acid catalyst to some extent.
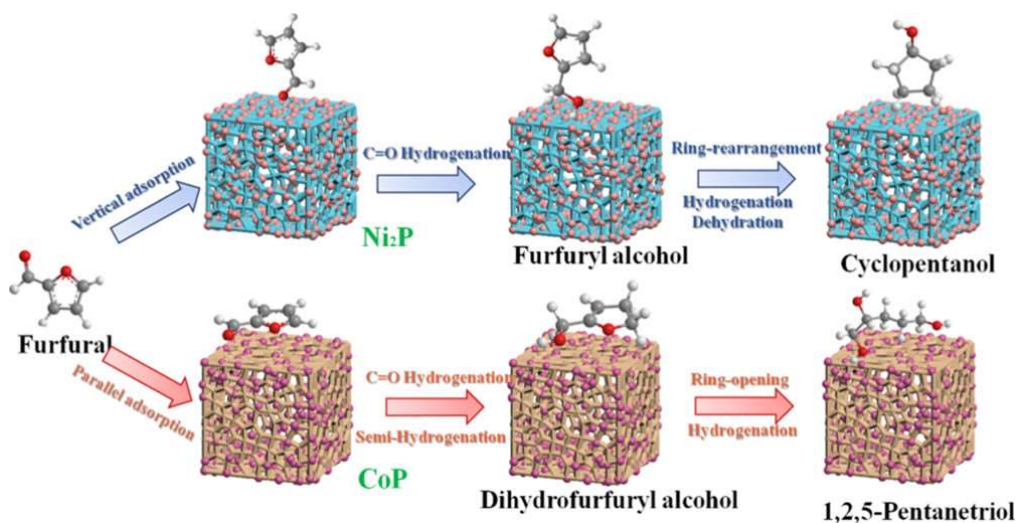
Figure 1-5. Reaction pathway of hydrogenation of furfural over Ni_2P and CoP catalyst.

On other hand, an active center discussion was raised in a study about P-modified Co/SiO_2 catalyst for the hydrogenation of dimethyl oxalate (DMO) to methyl glycolate (MG) reaction [63]. A series of Co_xP/SiO_2 catalyst (x= the molar ratio of cobalt-phosphorus) were synthesized by the impregnation method using $Co(NO_3)_2 \cdot 6H_2O$ and $NH_4H_2PO_4$ and additional TPR treatment at 923 K.

In sharp contrast to the 9.41% conversion and 33.1% selectivity achieved by Co/SiO$_2$ at 240 °C and

3.0 MPa H$_2$ conditions, the conversion and selectivity were increased to 31.4% and 90.5%,

respectively, after adding 0.35 wt% P into the Co/SiO$_2$ catalyst (Co$_{15}$P/SiO$_2$). According to XPS

spectra, a new peak at 778 eV that belongs to the Co^0 or Co$^{\delta+}$ ($0 < \delta < 1$) species appeared after P was

added and the peak intensity enhanced with the increasement of P amount. However, no Co$_2$P phase

was formed proved by XRD and TEM, indicating the active center is probably the P-modified Co^0 or

Co$^{\delta+}$ instead of the cobalt phosphide phase. On the contrary, the excess P resulted in the formation of

more Co$_2$P phase, reducing the number of active centers that led to a low conversion of DMO.

Support usually play an important role in improving the catalytic performance through the

metal-support interaction for supported catalysts, so do cobalt phosphide based-catalyst. In 2022,

Zhang *et al.* reported the strong metal-support interaction (SMSI) between metal phosphide NPs and

manganese phosphate support (noted as MnP-3) [64]. The Co$_3$O$_4$/Mn$_2$P$_2$O$_7$ formed by impregnation

method was treated under a high-temperature reduction in H$_2$ to give a MnP-3 supported Co$_2$P NPs

that has overlayer encapsulation (Co$_2$P$_L$/MnP-3) by one preparation step (**Figure 1-6**). Co$_2$P$_L$/MnP-3

showed significantly improved the capability against oxidation and acid with overlayer encapsulation
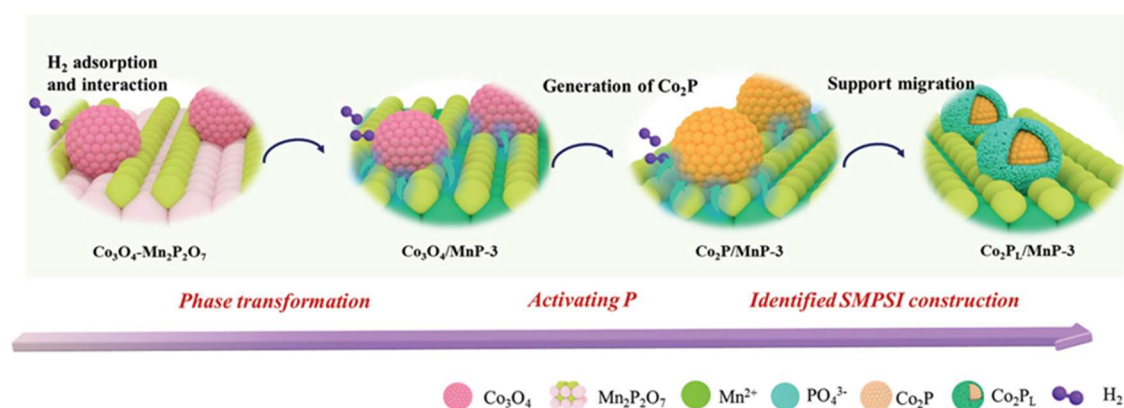
Figure 1-6. Preparation of Co$_2$P$_L$/MnP-3 catalyst.

and also facilitated hydrogenation of various kinds of olefin, aldehyde, carboxyl substrates

efficiently toward target saturated diacids with 100% selectivity. Although the electronic differences

between Co_2P_L/MnP-3 and Co_2P/MnP-3 were investigated by various analysis means (e.g. XPS, XAS) and all of them pointed out there was an electron transfer from the overlayer to Co_2P NPs in Co_2P_L/MnP-3, its higher activity than Co_2P/MnP-3 was explained by the superior stability in aqueous solution, which is more likely derived from the overlayer structure rather than the electronic changes. In consequence, this study broadens the possibility of cobalt phosphide catalyst in both activity and stability by combining the interaction with support.

3. Purpose of this thesis

Over the last century, catalysts have made incredible contribution to human beings as the great achievements benefited from catalyst in agricultural, energy technologies, and health care. In order to catch up nowadays growing needs and energy consumptions, traditional industrial processes that mainly focus on production efficiency and chemical yield have further aggravated the environmental problems, such as harmful pollutants and unnecessary waste of resources. To overcome above problems, the development of heterogenous catalysts based on earth abundant non-noble metal with high effiency and stability plays a pivotal role toward sustainable and cost-effective chemical processes.

For organic synthesis such as hydrogenation reaction, homogenous catalysts show high activity largely influenced by the ligand effect, which is generally derived from a phosphorus ligand complex, to stabilize and tune the electronic state of the central metal atom. On the other hand, heterogeneous catalysts are prone to exhibit high activity benefited from the unique property of nanosized metal particles (size effect). Thus, metal phosphide nanocrystals with both ligand effect from phosphorus and size effect are naturally regarded as a potential heterogeneous catalyst for organic
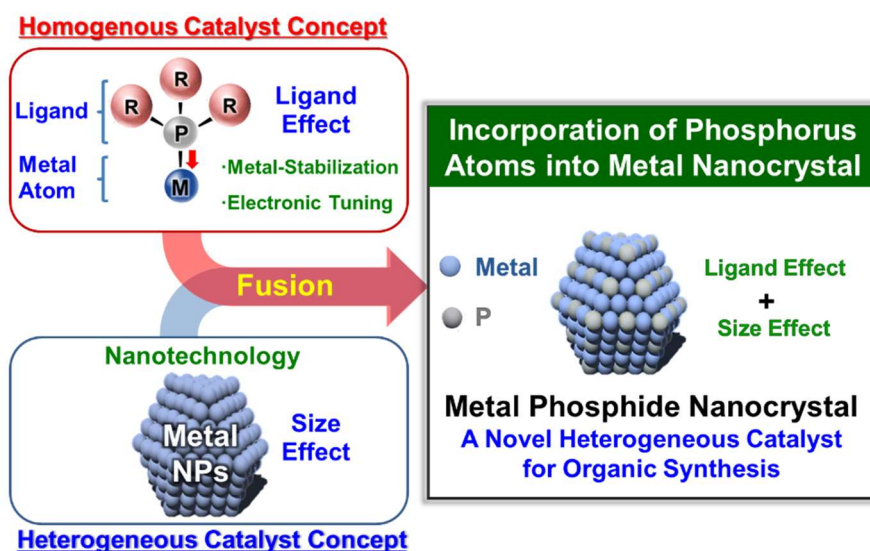
Figure 1-7. Metal phosphide nanocrystal possesses both homogenous and heterogeneous catalyst concepts.

synthesis (**Figure 1-7**).

Since the great successes have been achieved in hydrotreating and hydrogen evolution reactions, metal phosphides are severed as a novel metal catalyst for electrocatalysis, photocatalysis, and hydrotreating field and intensely studied. Despite of these achievements, the development of metal phosphide for liquid-phase organic synthesis still lags far behind and is rarely reported. Thus, a extensive and potential chemistry of metal phosphide remains to be explored and is of great interest.

The author paid attention to the investigation of non-noble metal phosphide, particularly cobalt phosphide, about its unique property and catalysis in liquid-phase organic synthesis like hydrogenation reactions, which can be regarded as a cutting-edge research.

The main purpose of this thesis is to develop efficient cobalt phosphide catalysts for sustainable liquid-phase reactions and figure out the origin of their high activities, providing potential candidate and beneficial insights to realize the next-generation green and sustainable chemical processes.

4. Outline of this thesis

The present thesis describes the development of cobalt phosphide catalysts for liquid-phase hydrogenation reactions.

In Chapter II, the author indicated that a well-defined cobalt phosphide nanocrystal (nano-Co_2P) was successfully prepared and efficient for the hydrogenation of nitriles to the desired primary amines under 1 bar H_2, which is firstly achieved by a non-precious metal catalyst under such mild condtions (**Scheme 1-3**). Furthermore, nano-Co_2P also provided a 20- to 500-fold greater TON (over 58000) than those of previous reports in nitrile hydrogenations, owing to the electron-rich Co species by introducing phosphorus atoms into Co nanoparticles.
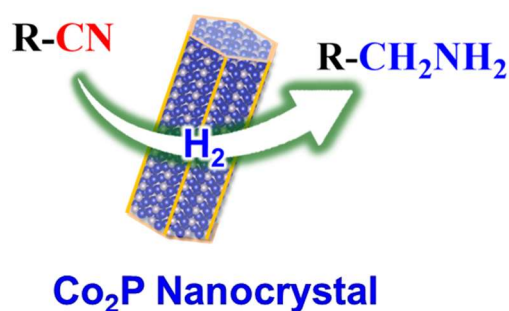
Scheme 1-3. Hydrogenation of nitriles to primary amines over nano-Co_2P catalyst.

In Chapter III, the author demonstrated an Al_2O_3-supported nano-Co_2P that can serve as a highly active catalyst for the selective hydrogenation of furfural derivatives (**Scheme 1-4**). Unlike the air-instable sponge metal catalysts with difficult and dangerous operations in industrial processes, nano-Co_2P is air-stable that realizes the easy and safe catalyst handlings in air. Based on the results from various analyses, the cobalt species in this catalyst showed an air-stable low-valence state even exposed to air, which is derived from the ligand effect of the phosphorus atoms.
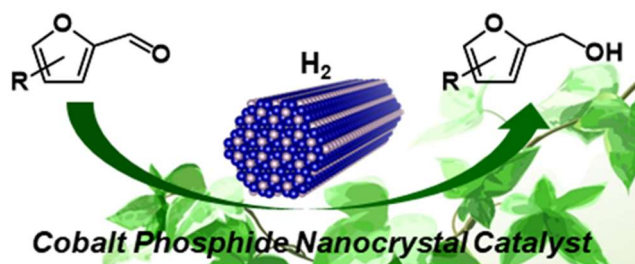
Scheme 1-4. Hydrogenation of nitriles to primary amines over nano-Co$_2$P catalyst.

The next chapter represents a novel single-crystal cobalt phosphide nanorods catalyst (Co$_2$P NRs) was synthesized for reductive amination of carbonyl compounds to primary amines (**Scheme 1-5**). In this Co$_2$P NRs catalystic system, various carbonyl compounds were transformed to the primary amine products in high yields under mild conditions like 1 bar H$_2$ or room temperature. Further analyzes indicated that the coordinatively unsaturated Co–Co sites are responsible for its high activity.
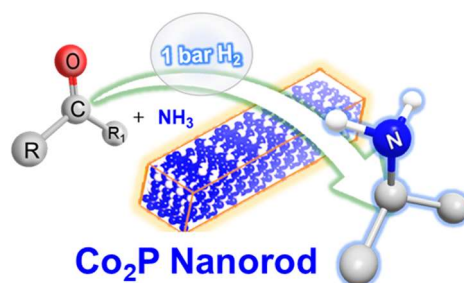
Scheme 1-5. Reductive amination of carbonyl compounds to primary amines by Co$_2$P NR catalyst.

The author mentions the hydrogenation of nitriles reaction can be efficiently catalyzed by a hydrotalcite-supported Co$_2$P NR catalyst (Co$_2$P NR/HT) in Chapter V (**Scheme 1-6**). Co$_2$P NR/HT exhibited an incredible substrate generality including aromatic, heteroaromatic, aliphatic nitriles, dinitriles, and sulfur-containing nitriles, giving the desired primary amines in high yields. Furthemore,

Co$_2$P NR/HT is the first example of non-precious metal catalyst for the selective hydrogenation of nitriles to primary amines under ammonia-free conditions. Spectroscopic analyses demonstrated that the combination of Co$_2$P NR and the support is of vital importance for the high activaty of the catalyst.
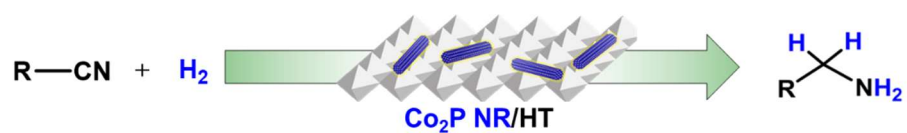
Scheme 1-6. Hydrogenation of nitriles to primary amines by hydrotalcite-supported Co$_2$P NR catalyst.

References

1. Berzelius, J. J. *Jahres–Bericht* **1835**, *14*, 237.

2. Zhou, Q. *Angew. Chem. Int. Ed.* **2015**, *55*, 5352–5353.

3. Haber, F.; Van Oordt, G. *Z. Anorg. Allg. Chem.* **1905**, *47*, 42–44.

4. Honkala, K.; Hellman, A.; Remediakis, I.; Logadottir, A.; Carlsson, A.; Dahl, S.; Christensen, C.; Nørskov, J. *Science* **2005**, *307*, 555–558.

5. Erisman, J. W.; Sutton, M. A.; Galloway, J.; Klimont, Z.; Winiwarter, W. *Nat. Geosci.* **2008**, *1*, 636–639.

6. Yentekakis, I.; Dong, F. *Frontiers in Environmental Chemistry* **2020**, *1*, 5.

7. Tundo, P.; Anastas, P.; Black, D.; Breen, J.; Collins, T.; Memoli, S.; Miyamoto, J.; Polyakoff, M.; Tumas, W. *Pure Appl. Chem*. **2000**, *72*, 1207–1228.

8. Anastas, P.; Zimmerman, J. *Env. Sci. and Tech.* **2003**, *37,* 94A–101A.

9. Bullock, R.M.; Chen, J.G.; Gagliardi, L.; Chirik, P.J.; Farha, O.K.; Hendon, C.H.; Jones, C.W.; Keith, J.A.; Klosin, J.; Minteer, S.D. *Science* **2020**, *369*, eabc3183.

10. Baturina, O.; Smirnova, A. *New and Future Developments in Catalysis* **2013**, 69–97.

11. Pelletier, B.; Pelletier, C.; Sédillot, J. *Mémoires et Observations de Chimie* **1798,** *2*, 42.

12. Von Schnering, H. G.; Hoenle, W. *Chem. Rev.* **1988**, *88*, 243.

13. Sweeny, N.; Rohrer, C.; Brown, O. *J. Am. Chem. Soc.* **1958**, *80*, 799.

14. Muetterties, E.; Sauer, J. *J. Am. Chem. Soc.* **1974**, *96*, 3410–3415.

15. Nozaki, F.; Adachi, R. *J. Catal.* **1975**, *40*, 166–172.

16. Alonso, F.; Yus, M. *Chem. Soc. Rev.* **2004**, *33*, 284–293.

17. Alonso, F.; Osante, I.; Yus, M. *Adv. Synth. Catal.* **2006**, *348*, 305–308.

18. Yus, M.; Alonso, F.; Osante, I. *Synlett* **2006**, *18*, 3017–3020.

19. Alonso, F.; Osante, I.; Yus, M. *Tetrahedron* **2007**, *63*, 93–102.

20. Robinson, W.; van Gestel, J.; Korányi, T.; Eijsbouts, S.; van der Kraan, A.; van Veen, J.; de Beer, V. *J. Catal.* **1996**, *161*, 539–550.

21. Oyama, S. *J. Catal.* **2003**, *216*, 343–352.

22. Liu, P.; Rodriguez, J. A. *J. Am. Chem. Soc.* **2005**, *127*, 14871–14878.

23. Popczun, E.; McKone, J.; Read, C.; Biacchi, A.; Wiltrout, A.; Lewis, N.; Schaak, R. *J. Am. Chem. Soc.* **2013**, *135*, 9267–9270.

24. Hong, L.; Guo, R.; Yuan, Y.; Ji, X.; Lin, Z.; Li, Z.; Pan, W. *ChemSusChem* **2020**, *14*, 539–557.

25. Shi, Y.; Zhang, B. *Chem. Soc. Rev.* **2016**, *45*, 1529–1541.

26. Miao, Y.; Li, F.; Zhou, Y.; Lai, F.; Lu, H.; Liu, T. *Nanoscale* **2017**, *9*, 16313–16320.

27. Ha, D.; Moreau, L.; Bealing, C.; Zhang, H.; Hennig, R.; Robinson, R. *J. Mater. Chem.* **2011**, *21*, 11498–11510.

28. Callejas, J.; Read, C.; Popczun, E.; McEnaney, J.; Schaak, R. *Chem. Mater.* **2015**, *27*, 3769–3774.

29. Bailer, J.C.; Emelius, H.J.; Nyholm, R.; Trotman-Dickenson, A.F. (Eds.), *Comprehensive Inorganic Chemistry*, vol. 2, Pergamon Press, Oxford, **1973**.

30. Qian, X.; Xie, Y.; Qian, Y.; Zhang, X.; Wang, W.; Yang, L. *Mater. Sci. Eng. B* **1997**, *49*, 135–137.

31. Hou, H.; Yang, Q.; Tan, C.; Ji, G.; Gu, B.; Xie, Y. *Chem. Lett.* **2004**, *33*, 1272–1273.

32. Xie, Y.; Su, H.; Qian, X.; Liu, X.; Qian, Y. *J. Solid State Chem.* **2000**, *149*, 88–91.

33. Perera, S.; Tsoi, G.; Wenger, L.; Brock, S. *J. Am. Chem. Soc.* **2003**, *125*, 13960–13961.

34. Park, J.; Koo, B.; Yoon, K.; Hwang, Y.; Kang, M.; Park, J.; Hyeon, T. *J. Am. Chem. Soc.* **2005**, *127*, 8433–8440.

35. Li, Y.; Malik, M.; O'Brien, P. *J. Am. Chem. Soc.* **2005**, *127*, 16020–16021.

36. Liu, Q.; Wang, M.; He, Y.; Wang, X.; Su, W. *Nanoscale* **2018**, *10*, 19100–19106.

37. Zhu, Y.; Liu, Y.; Ren, T.; Yuan, Z. *Adv. Funct. Mater.* **2015**, *25*, 7337–7347.

38. Tian, J.; Liu, Q.; Asiri, A.; Sun, X. *J. Am. Chem. Soc.* **2014**, *136*, 7587–7590.

39. Burns, A.; Layman, K.; Bale, D.; Bussell, M. *Appl Catal. A* **2008**, *343*, 68–76.

40. Stinner, C.; Tang, Z.; Haouas, M.; Weber, T.; Prins, R. *J. Catal.* **2002**, *208*, 456–466.

41. Stinner, C.; Prins, R.; Weber, T. *J. Catal.* **2001**, *202*, 187–194.

42. Cecilia, J.; Infantes-Molina, A.; Rodríguez-Castellón, E.; Jiménez-López, A. *Appl. Catal. B* **2009**, *92*, 100–113.

43. Zhou, X.; Li, X.; Prins, R.; Lv, J.; Wang, A.; Sheng, Q. *J. Catal.* **2021**, *394*, 167–180.

44. Bui, P.; Cecilia, J.; Oyama, S.; Takagaki, A.; Infantes-Molina, A.; Zhao, H.; Li, D.; Rodríguez-Castellón, E.; Jiménez López, A. *J. Catal.* **2012**, *294*, 184–198.

45. Rodríguez-Aguado, E.; Infantes-Molina, A.; Cecilia, J.; Ballesteros-Plata, D.; López-Olmo, R.; Rodríguez-Castellón, E. *Topics in Catalysis* **2017**, *60*, 1094–1107.

46. Berenguer, A.; Sankaranarayanan, T.; Gómez, G.; Moreno, I.; Coronado, J.; Pizarro, P.; Serrano, D. *Green Chem.* **2016**, *18*, 1938–1951.

47. Shit, S.; Koley, P.; Joseph, B.; Marini, C.; Nakka, L.; Tardio, J.; Mondal, J. *ACS Appl. Mater. Interfaces* **2019**, *11*, 24140–24153.

48. Cecilia, J.; Infantes-Molina, A.; Rodríguez-Castellón, E.; Jiménez-López, A. *J. Hazard. Mater.* **2013**, *260*, 167–175.

49. Song, X.; Ding, Y.; Chen, W.; Dong, W.; Pei, Y.; Zang, J.; Yan, L.; Lu, Y. *Energy Fuels* **2012**, *26*, 6559–6566.

50. Wang, S.; Cui, Y.; Shi, Y.; Yao, Z.; Liu, Q.; Sun, Y. *Phosphorus, Sulfur, and Silicon and the Related Elements* **2019**, *194*, 851–856.

51. Muhlenkamp, J.; LiBretto, N.; Miller, J.; Hicks, J. *Catal. Sci. Technol.* **2022**, *12*, 976–985.

52. Tang, C.; Qu, F.; Asiri, A.; Luo, Y.; Sun, X. *Inorg. Chem. Front.* **2017**, *4*, 659–662.

53. Hou, C.; Chen, Q.; Li, K.; Wang, C.; Peng, C.; Shi, R.; Chen, Y. *J. Mater. Chem. A* **2019**, *7*, 8277–8283.

54. Huang, X.; Wu, D.; Cheng, D. *J. Colloid Interface Sci.* **2017**, *507*, 429–436.

55. Liu, X.; Li, X.; Qin, L.; Mu, J.; Kang, S. *Appl. Surf. Sci.* **2018**, *434*, 967–974.

56. Muetterties, E.; Sauer, J. *J. Am. Chem. Soc.* **1974**, *5*, 3410–3415.

57. Wang, H.; Shu, Y.; Zheng, M.; Zhang, T. *Catal. Lett.* **2008**, *124*, 219–225.

58. Zhang, X.; Zhang, Q.; Guan, J.; He, D.; Hu, H.; Liang, C. *Asia-Pac. J. Chem. Eng.* **2009**, *4*, 574–580.

59. Yang, S.; Peng, L.; Oveisi, E.; Bulut, S.; Sun, D.; Asgari, M.; Trukhina, O.; Queen, W. *Chem. Eur. J.* **2018**, *24*, 4234–4238.

60. Delley, M.; Wu, Z.; Mundy, M.; Ung, D.; Cossairt, B.; Wang, H.; Mayer, J. *J. Am. Chem. Soc.* **2019**, *141*, 15390–15402.

61. Feng, H.; Li, X.; Qian, H.; Zhang, Y.; Zhang, D.; Zhao, D.; Hong, S.; Zhang. N. *Green Chem.* **2019**, *21*, 1743–1756.

62. Tong, Z.; Li, X.; Dong, J.; Gao, R.; Deng, Q.; Wang, J.; Zeng, Z.; Zou, J.; Deng, S. *ACS Catal.* **2021**, *11*, 6406–6415.

63. Zhuang, Z.; Li, Y.; Chen, F.; Chen, X.; Li, Z.; Wang, S.; Wang, X.; Zhu, H.; Tan, Y.; Ding, Y. *Chem. Commun.* **2022**, *58*, 1958–1961.

64. Chen, Z.; Zeng, X.; Li, X.; Lv, Z.; Li, J.; Zhang, Y. *Adv.Mater.* **2022**, *34*, 2106724.

Chapter II.

Air-stable and Highly Active Cobalt Phosphide Nanoparicle Catalyst

for Nitrile Hydrogenation

1. Introduction

Primary amines are an important class of chemicals and are vital intermediates and precursors for synthesis of agrochemicals, pharmaceuticals, and polymers [1-3]. Conventionally, primary amines are obtained by reduction of nitriles with stoichiometric amounts of metal hydrides like LiAlH$_4$ and NaBH$_4$, which is poor atom efficiency and produces large amount of wastes [4-6]. On the other hand, the hydrogenation of nitriles using inexpensive molecule hydrogen as the green reducing agent offers a sustainable method for primary amine synthesis. Co and Ni based catalysts (Raney or sponge metal catalysts), prepared from the corresponding metal-Al alloy, are commonly used for nitrile hydrogenation in industry due to their cost-efficiency [7, 8]. In order to activate the catalyst, they have to go through a base (e.g. sodium hydroxide solution) treatment at a specific temperature to remove the aluminium part. Despite of the excess base, dissolved aluminate wastes, and the following tedious washing process, these catalysts have fatal problem in air-instability (flammability). Specifically, they must be operated under strict air-free conditions and stored in water or alcohol, resulting in difficult catalyst handling and complicate processes. Moreover, these catalysts exhibit activity often at the expenses of high catalyst loadings and require severe reaction conditions like high H$_2$ pressures (200–400 bar) [8-10]. Therefore, the development of highly efficient with air stability catalysts represent an emerging frontier and is of great interest.

In this context, notable progress has been made to overcome these limitations during the last decade. The Beller and Milstein groups developed iron [11-13], cobalt [14, 15], and manganese [16-18] complex catalysts for nitrile hydrogenation under an H$_2$ pressure of 30–60 bar. Fout and co-workers also reported that a bench-stable cobalt precatalyst enables this transformation under an H$_2$ pressure of 4 bar [19]. However, these homogeneous catalysts inevitably have problems in catalyst recovery and reuse as well as the contamination risk of solved metals [11-19]. On the other hand, stable and nonprecious metal-based heterogeneous catalysts for nitrile hydrogenation also have been

reported [20-24]. The Beller group reported stable Co nanoparticles derived from metal-nitrogen complexes [20, 21] and metal–organic framework [22], which efficiently promote this transformation. These nano-structured materials are stable and serve as reusable nonprecious metal catalysts for the nitrile hydrogenation under an H_2 pressure of 2.5–30 bar. However, these state-of-the-art catalysts still require pressurized H_2 and suffer from low activity. Hence, there is still a strong demand for the development of a high active catalyst for this transformation.

In this chapter, the author developed a well-defined cobalt phosphide nancrystal (nano-Co_2P) catalyst and exhibit high catalytic activity for hydrogenation of a wide range of nitriles to the desired primary amines even under just 1 bar H_2 pressure conditions, representing the first example of a non-precious metal catalyst for ambient pressure nitrile hydrogenation. Nevertheless, nano-Co_2P catalyst is recovered easily and can be reused without loss any activity, proving a new and green sustainable method for the production of a wide range of primary amines from nitriles.

2. Experimental section

2.1. General

All precursors and solvents were used as received, without further purification. CoCl$_2$·6H$_2$O and 1-octadecene (technical grade 90%) were purchased from Nacalai Tesque, INC., and Sigma-Aldrich. Co. Hexadecylamine and triphenyl phosphite were purchased from Tokyo Chemical Industry Co., Ltd. Hydrotalcite (AD 500NS) was purchased from Tomita Pharmaceutical Co., Ltd. Al$_2$O$_3$ was purchased from Sumitomo Chemical. TiO$_2$ (JRC TIO-9) was provided by the Catalysis Society of Japan as a reference catalyst. SiO$_2$ (Q-9) was purchased from Fuji Silysia Chemicals Ltd. All nitriles were commercially available. Tokyo Chemical Industry Co., Ltd.: valeronitrile (>98%), decanenitrile (>98%), phenylacetonitrile (>98%), anisonitrile (>98%), 4-(trifluoromethyl)benzonitrile (>98%), methyl-4cyanobenzoate (>98%), adiponitrile (>98%), sebaconitrile (98%), isophthalonitrile (>98%). FUJIFILM Wako Pure Chemical: 1-adamantanecarbonitrile (97%), benzonitrile (>98%), 3-cyanopridine (>98%), 4-cyanopridine (>98%), 2-furancarbonitrile (98%), 5-cyanopridine (96%), 4-acetylbenzonitrile (>98%), terephthalonitrile (>95%). Sigma-Aldrich: cyclohexanecarbonitrile (98%), 4-bromobenzonitrile (99%).

Gas chromatography (GC-FID) and GC-mass spectrometry (GC-MS) were performed using a Shimadzu GC-2014 instrument equipped with an InertCap for amines (30 m × 0.32 mm i.d.) and a GCMS-QP2010 SE instrument equipped with an InertCap WAX-HT capillary column (30 m × 0.25 mm i.d.). The oven temperature was programmed as follows: 120 °C starting temperature, kept for 3 min, temperature ramp at 10 °C/min to 260 °C, then at −20 °C/min to 120 °C. Other conditions were as follows: 2.44 mL/min column flow rate, 10.0 split ratio; vaporization chamber temperature of 250 °C; detector temperature of 260 °C. ^{1}H and ^{13}C nuclear magnetic resonance (NMR) spectra were recorded using a JEOL JNM-ESC400 spectrometer. Transmission electron microscopy (TEM) observations were carried out using a JEM-ARM200F instrument operated at 200 kV. Scanning

transmission electron microscopy (STEM) images with elemental maps were collected using a FEI

Titan Cubed G2 60-300 instrument operated at 300 kV, and equipped with a Super-X energy-dispersive

X-ray spectroscopy (EDX) detector. Elemental mapping based on quantification analysis of EDX

spectra was carried out using Esprit. The TEM sample and STEM sample were deposed without any

pretreatment on a holey carbon supported Cu-grid (167 mesh. 30μm thickness) and transferred to the

microscope. Co K-edge X-ray absorption spectra were recorded at room temperature at the BL01B1

and BL14B2 lines, using a Si (311) or Si (111) monochromator, at SPring-8, Japan Synchrotron

Radiation Research Institute (JASRI), Harima, Japan. Data analysis was performed using the REX

2000 program, ver. 2.5.7 (Rigaku). Fourier-transform infrared (FT-IR) spectra were recorded using a

JASCO FT-IR 4100 spectrometer equipped with a mercury cadmium telluride detector. X-ray

photoelectron spectroscopy (XPS) analyses were performed on an ESCA1700R system equipped with

a dual Mg/Al X-ray source and a hemispherical analyzer operating in fixed analyzer transmission

mode. Spectra were obtained using a pass energy of 58.7 eV; an AlKα X-ray source was operated at

350 W and 14 kV. Excess charges on the samples were neutralized by argon ion sputtering. The

analysis area was 0.8×2 mm. The working pressure in the analyzing chamber was less than 1×10^{-7}

Pa. Spectra were acquired in the Co 2p, P 2p, O 1s, C 1s, and Si 2p regions. The C 1s peak at a binding

energy (BE) of 285 eV was taken as an internal reference.

2.2. Preparation of catalysts

Synthesis of nano-metal phosphides: All reactions were carried out under an argon atmosphere using

standard Schlenk line techniques. In a typical synthesis, $CoCl_2 \cdot 6 H_2O$ (1.0 mmol) and 2.4 g (10 mmol)

of hexadecylamine were combined with 10.0 mL of 1-octadecene and 2.6 mL (10 mmol) of triphenyl

phosphite in a Schlenk flask. The mixture was heated to 150 °C under argon flow and maintained for

1 h. The temperature was then increased to 300 °C and kept at this temperature for 2 h, which yielded

a black colloidal solution. The mixture was then cooled in air to room temperature. The obtained colloid was isolated by precipitation with acetone, and the redispersion and precipitation cycles continued using a chloroform and acetone mixed solvent (chloroform: acetone = 1:1) until the supernatant liquid was transparent. The obtained powder was dried in vacuum overnight at room temperature to give nano-Co_2P. The other nano-sized metal phosphides were prepared in a similar way to nano-Co_2P by using the corresponding metal precursors (Ni: $NiCl_2 \cdot 6H_2O$, Cu: $CuCl_2 \cdot 2H_2O$, Fe: $Fe(CO)_5$).

Preparation of nano-Co_2P/support: Typically, nano-Co_2P (0.04 g) was dispersed in hexane (50 mL) and stirred with hydrotalcite (1.0 g) for 2 h at room temperature. The obtained powder was dried in a vacuum overnight at room temperature to give nano-Co_2P/HT as a gray powder. The same procedure was used to prepare other nano-Co_2P/support catalysts (support = Al_2O_3, TiO_2 and SiO_2).

Synthesis of nano-CoP: In a typical synthesis, under a flow of argon, $Co(acac)_2$ (1 mmol), 1-octadecene (5 mL, 15.6 mmol) and oleylamine (10 mL, 30.4 mmol) were placed in a Schlenk flask. The mixture was stirred and heated to 120 °C and kept at this temperature for 1 h. Then, triphenylphosphine (5 mL, 11 mmol) was added to the above solution and heated to 340 °C for 4 h. Afterwards, the mixture was allowed to cool in air to room temperature. To remove as much organics as possible, redispersion and precipitation cycles continued until the supernatant liquid was transparent using a hexane and ethanol mixed solvent (hexane: ethanol = 1:1). The obtained powder was dried at room temperature in vacuum overnight. The corresponding EDX spectrum revealed the atomic ratio between Co and P was close to 1:1.

Preparation of CoO_x: All reactions were carried out under an argon atmosphere using standard

Schlenk line techniques. Tri-n-octylphosphine oxide (0.1 g) and 0.09 g (0.32 mmol) of oleic acid were dissolved with 12 mL of 1,2-dichlorobenzene in a Schlenk flask. The mixture was heated to 180 °C under argon flow and maintained for 10 min. 0.52 g (1.52 mmol) of $Co_2(CO)_8$ dissolved in 4 mL of 1,2-dichlorobenzene was quickly injected and stirred for 4 min. Afterwards, the mixture was allowed to cool in air to room temperature. The obtained powder was purified by ethanol and centrifuged. Then the supernatant was removed and the powder was redispersed in hexanes. The precipitation/redispersion process was performed twice overall.

2.3. Reaction procedure

A typical reaction procedure for the hydrogenation of nitrile using nano-Co_2P/HT was as follows. nano-Co_2P/HT powder (0.1 g) was placed in a 50-mL stainless-steel autoclave with a Teflon inner cylinder, followed by addition of nitrile (0.5 mmol), 2-propanol (3 mL) and NH_3 aq. (25%, 1.2 mL). The reaction mixture was stirred vigorously at 130 °C under 40 bar of H_2. After the reaction, the reaction solution was analyzed by GC to determine the conversion and the yield using biphenyl as an internal standard. After reaction, to obtain the hydrochloride salts, the crude reaction mixture was filtered to remove the catalyst and the ammonia was removed under vacuum conditions. The mixture was then added to a hydrogen chloride solution (1.25 M, 1,4-dioxane). The solvent was removed leaving behind the corresponding salt, giving the pure hydrochloride salts, which were subjected to NMR analysis.

2.4. Product identification

***n*-Pentylamine hydrochloride**
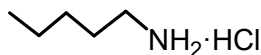
CAS registry No. [142-65-4]. ^{1}H NMR (DMSO, 400 MHz): δ = 7.95 (s, 3H), 2.73 (t, *J* = 7.3, 2H), 1.56 (m, 2H), 1.33-1.26 (m, 4H), 0.88 (t, *J* = 6.8, 3H). ^{13}C NMR (DMSO, 100 MHz): 38.7, 27.9, 26.5, 21.5, 13.6.

1-Cyclohexylmethanamine hydrochloride
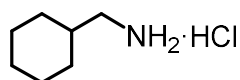
CAS registry No. [50877-01-5]. ^{1}H NMR (DMSO, 400 MHz): δ = 7.84 (s, 3H), 2.62 (d, *J* = 6.4, 2H), 1.69 (m, 4H), 1.53 (m, 2H), 1.16 (m, 3H), 0.91 (m, 2H). ^{13}C NMR (DMSO, 100 MHz): 44.3, 35.3, 29.6, 25.5, 25.0.

Decylamine hydrochloride
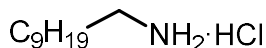
CAS registry No. [143-09-9]. ^{1}H NMR (DMSO, 400 MHz): δ = 7.75 (s, 3H), 2.75 (t, *J* = 8.5, 2H), 1.51 (m, 2H), 1.25 (m, 14H), 0.86 (t, *J* = 7.6, 3H). ^{13}C NMR (100 MHz, DMSO): 38.7, 31.2, 28.8, 28.7, 28.6, 28.4, 26.9, 25.7, 22.0, 13.9.

1-Adamantylmethylamine hydrochloride
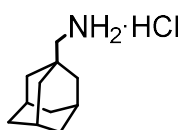
CAS registry No. [1501-98-0]. ^{1}H NMR (DMSO, 400 MHz): δ = 7.76 (s, 3H), 2.48 (s, 2H), 1.96 (s, 3H), 1.68 (d, *J* = 11.9, 3H), 1.59 (d, *J* = 11.4, 3H), 1.50 (s, 6H). ^{13}C NMR (DMSO, 100 MHz): 49.9, 38.7, 36.0, 30.5, 27.4.

Benzylamine hydrochloride
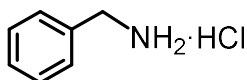
CAS registry No. [3287-99-8]. ^{1}H NMR (DMSO, 400 MHz): δ = 8.05 (s, 3H), 7.30 (m, 5H), 3.01 (s, 2H). ^{13}C NMR (DMSO, 100 MHz): 134.0, 128.9, 128.5, 128.3, 42.1.

2-Phenylethylamine hydrochloride

CAS registry No. [156-28-5]. ^{1}H NMR (DMSO, 400 MHz): δ = 8.07 (s, 3H), 7.36-7.23 (m, 5H), 3.10-
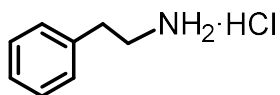
2.82 (m, 4H). ^{13}C NMR (DMSO, 100 MHz): 137.4, 128.53, 128.52, 126.6, 39.8, 32.9.

3-Picolylamine hydrochloride
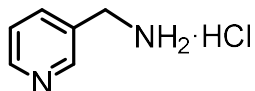
CAS registry No. [84359-15-9]. ^{1}H NMR (DMSO, 400 MHz): δ = 8.78(s, 1H), 8.72-8.43 (m, 4 H), 8.10 (d, J = 5.7, 1H), 7.60 (t, J = 8.0, 1H), 4.21 (s, 2H). ^{13}C NMR (DMSO, 100 MHz): 66.3, 38.6, 28.6, 28.4, 26.8, 25.7.

4-Picolylamine hydrochloride
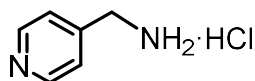
CAS registry No. [64460-41-9]. ^{1}H NMR (DMSO, 400 MHz): δ = 8.61 (s, 2H), 7.52 (d, 2H, J = 4.4), 4.19 (s, 2H). ^{13}C NMR (DMSO, 100 MHz): 149.6, 143.8, 123.2, 41.2.

Furan-2-ylmethanamine hydrochloride
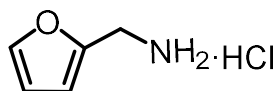
CAS registry No. [4753-68-8]. ^{1}H NMR (DMSO, 400 MHz): δ =8.50 (sbr, 3H), 7.73 (m, 1H), 6.54–6.56 (m, 1H), 6.48–5.51 (m, 1H), 4.06 (m, 2H). ^{13}C NMR (DMSO, 100 MHz): 147.6, 143.8, 110.9, 110.2, 34.8.

(1H-indol-5-yl)methanamine monohydrochloride
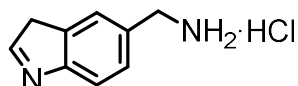
CAS registry No. [865878-77-9]. ^{1}H NMR (DMSO, 400 MHz): δ = 10.88 (s, 1H), 8.82 (s, 3H), 7.95 (s, 1H), 7.37 (t, J = 2.8, 1H), 7.31 (dd, J = 8.4, 1.7, 1H), 7.32−7.16 (m, 2H), 4.08 (s, 2H). ^{13}C NMR (DMSO, 100 MHz): 135.6, 127.4, 126.1, 121,9, 120.8, 111.3, 100.8.

4-Methoxybenzylamine hydrochloride

CAS registry No. [17061-61-9]. ^{1}H NMR (DMSO, 400 MHz): δ = 8.18 (s, 3H), 7.47-7.30 (m, 2H),
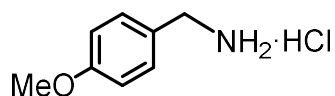
7.04-6.89 (m, 2H), 3.93 (s, 2H), 3.75 (s, 3H). ^{13}C NMR (DMSO, 100 MHz): 157.8, 129.4, 128.7, 113.5, 55.0, 44.0.

4-Bromobenzylamine hydrochloride
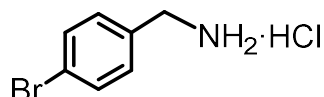
CAS registry No. [26177-44-6]. ^{1}H NMR (DMSO, 400 MHz): δ = 8.49 (s, 3H), 7.61 (d, J = 7.9, 2H), 7.48 (d, J = 7.8, 2H), 3.98 (s, 2H). ^{13}C NMR (DMSO, 100 MHz): 133.4, 131.3, 131.2, 121.6, 41.3.

4-Trifluoromethylbenzylamine hydrochloride
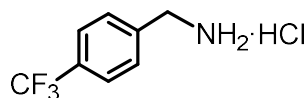
CAS registry No. [3047-99-2]. ^{1}H NMR (DMSO, 400 MHz): δ = 8.71 (s, 3H), 7.85-7.60 (m, 4H), 4.12 (s, 2H). ^{13}C NMR (DMSO, 100 MHz): 138.8, 129.7, 128.6, 125.2, 122.7, 41.5.

1-[4-(Aminomethyl)phenyl]ethan-1-one hydrochloride
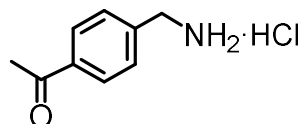
CAS registry No. [66522-66-5]. ^{1}H NMR (DMSO, 400 MHz): δ = 8.51 (s, 3H), 7.97 (d, J = 8.5, 2H), 7.66 (d, J = 8, 2H), 4.09 (s, 2H), 2.58 (s, 3H). ^{13}C NMR (DMSO, 100 MHz): 197.6, 139.1, 136.5, 129.0, 128.2, 41.6, 26.8.

4-(Aminomethyl)benzoic acid methyl ester hydrochloride
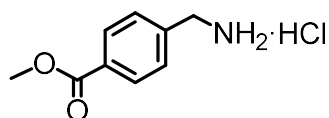
CAS registry No. [6232-11-7]. ^{1}H NMR (DMSO, 400 MHz): δ = 8.46 (s, 3H), 8.00 (d, J = 8.4, 2H), 7.63 (d, J = 8.0, 2H), 4.11 (s, 2H), 3.86 (s, 3H). ^{13}C NMR (DMSO, 100 MHz): 165.8, 129.3, 129.1, 129.0, 128.2, 52.2, 41.7.

1,6-Diaminohexane dihydrochloride
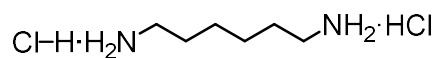
CAS registry No. [6055-52-3]. ^{1}H NMR (DMSO, 400 MHz): δ = 7.82 (s, 6H), 2.83-2.58 (m, 4H), 1.67-1.46 (m, 4H), 1.37-1.22 (m, 4H). ^{13}C NMR (DMSO, 100 MHz): 38.4, 26.6, 25.2.

1,10-Diaminodecane dihydrochloride
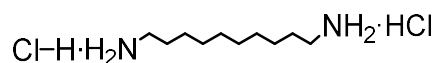
CAS registry No. [7408-92-6]. ^{1}H NMR (DMSO, 400 MHz): δ = 8.08 (s, 6H), 2.71 (m, 4H), 1.55 (m, 4H), 1.26 (m, 12H). ^{13}C NMR (DMSO, 100 MHz): 38.6, 28.6, 28.4, 26.8, 25.7.

1,4-Bis(aminomethyl)benzene dihydrochloride
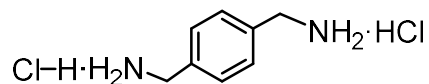
CAS registry No. [3057-45-2]. ^{1}H NMR (DMSO, 400 MHz): δ = 8.48 (s, 6H), 7.50 (s, 4H), 4.01 (s, *4*H). ^{13}C NMR (DMSO, 100 MHz): 134.2, 128.6, 41.8.

m-Xylylenediamine dihydrochloride
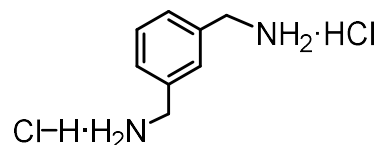
CAS registry No. [51964-30-8]. ^{1}H NMR (DMSO, 400 MHz): δ = 8.66 (s, 6H), 7.61 (d, *J* = 1.9 Hz, 1H), 7.55 (dd, *J* = 7.4, 1.8 Hz, 2H), 7.45 (dd, *J* = 8.4, 6.9 Hz, 1H), 3.99 (s, 4H). ^{13}C NMR (DMSO, 100 MHz): 134.3, 129.6, 128.8, 128.6, 41.9.

N,N,N′,N′-Tetrakis(3-aminopropyl)-1,4-butanediamine
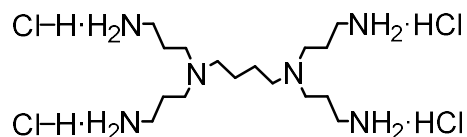
CAS registry No. [120239-63-6]. 1H NMR (CDCl$_3$, 400 MHz): δ = 2.83 (t, 8H), 2.62 (t, 8H), 2.41 (m, 4H), 1.78(t, 8H), 1.60(m, 4H), 1.48(m, 8H). ^{13}C NMR (CDCl$_3$, 100 MHz): 53.6, 51.4, 40.3, 31.4, 24.5.

3. Results and discussion

3.1. Characterization of nano-Co₂P

Prepared cobalt phosphide was firstly analysed by X-ray diffraction (XRD) as shown in **Figure 2-1** (a), which is in constant with the peaks attributed to the di-cobalt phosphide (Co₂P). The lower and wider peaks of XRD also demonstrated the nano-size of the fabricated Co₂P. Transmission electron microscopy (TEM) images of the obtained Co₂P confirm the 20×9 nm (length×width) rod morphology with a hexagonal phase observed from the vertical view (**Figures 2-1** (b-c)). Scanning transmission electron microscopy (STEM) with elemental mapping indicated cobalt and phosphorus as the constituent elements were homogeneously distributed within each nano-Co₂P (**Figures 2-1** (d-f)).
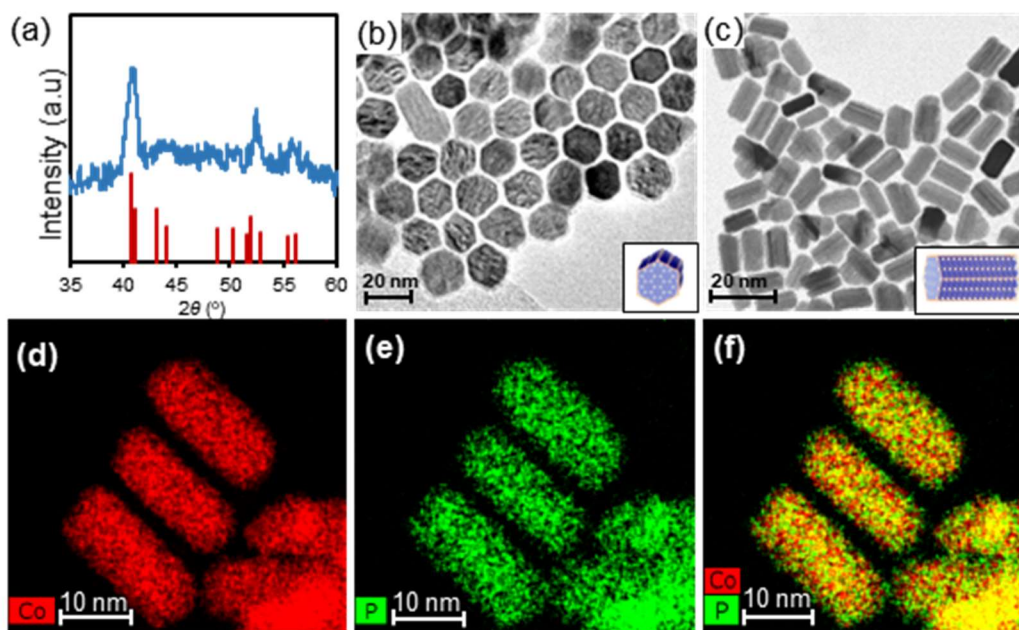
Figure 2-1. (a) The XRD pattern of the prepared cobalt phosphide. (b) TEM image of nano-Co₂P in top view showing the hexagonal phase structure. (c) TEM image of nano-Co₂P in side view showing a nanorod morphology. Elemental mapping images of (d) Co and (e) P. (f) Composite overlay image formed from (d) and (e).

The porosity analysis of prepared nano-Co_2P by N_2 adsorption was also carried out. The results are shown in **Figures 2-2**. N_2 adsorption and desorption isotherm linear plot revealed that the shape of the curve of nano-Co_2P is the type IV isotherm shape, indicating the existence of meso pore. Furthermore, BJH adsorption dV/dlog(D) pore volume of nano-Co_2P showed that the average pore size of nano-Co_2P is 17 nm, which is close to the length of nano-Co_2P as shown in **Figures 2-1**. These results showed that the pore with a mean diameter of 17 nm exists not in nano-Co_2P but within the aggregated nano-Co_2P nanoparticles.
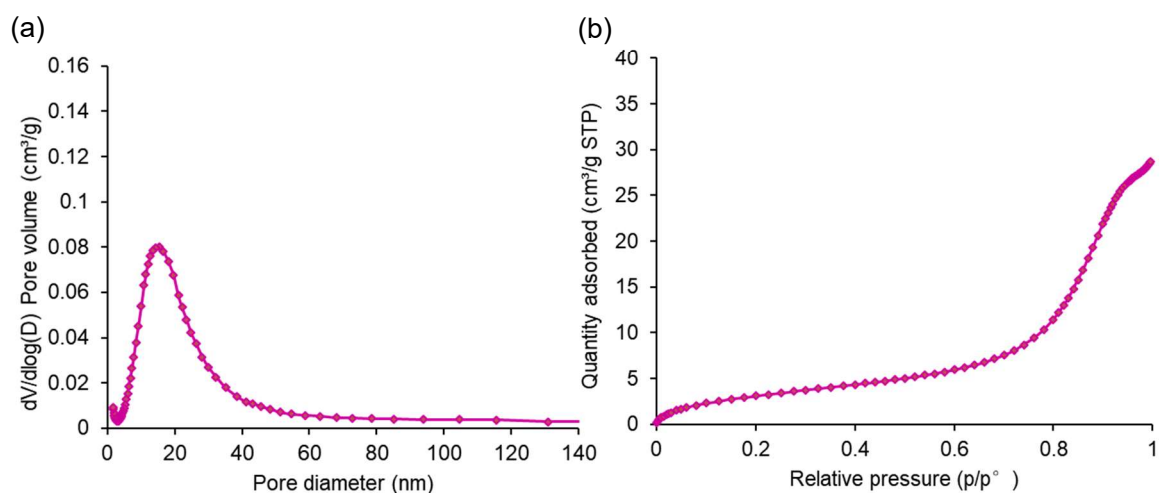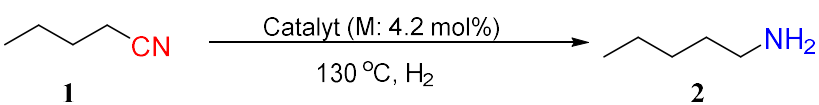
Figure 2-2. (a) The BJH Adsorption dV/dlog(D) pore volume of nano-Co_2P. (b) The N_2 adsorption and desorption isotherm linear plot of nano-Co_2P.

3.2. Catalytic activity in hydrogenation of nitriles

The catalytic performance of nano-Co_2P was investigated in the hydrogenation of valeronitrile (**1**) as the model reaction under 40 bar H_2 pressure, 130 °C condtions. Notably, nano-Co_2P showed high activity and gave the corresponding amine (**2**) in 62% yield (**Table 2-1**, entry 1). nano-CoP also promoted the reaction and a lower yield of **1** in 40% was obtained (entry 3).

Table 2-1. Hydrogenation of valeronitrile (**1**) over virous catalyst.[a]

Entry	Catalyst	H_2 (bar)	Time (h)	Yield (%)[b]
1	nano-Co_2P	40	1	62
2	nano-Co_2P/HT	40	1	94
3	nano-CoP	40	1	40
4	nano-Ni_2P	40	1	0
5	nano-Fe_2P	40	1	0
6	nano-Cu_3P	40	1	0
7	CoO_x NP	40	1	0
8	Co_2P (bulk)	40	1	2
9	nano-Co_2P/Al_2O_3	40	1	89
10	nano-Co_2P/TiO_2	40	1	78
11	nano-Co_2P/SiO_2	40	1	64
12[c]	nano-Co_2P/HT	5	20	89
13[c]	nano-Co_2P/HT	1	20	85

[a]Reaction conditions: catalyst (0.04 g, 0.1 g for supported catalyst), substrate (0.5 mmol), 2-propanol (3 mL), 130 $^\circ$C, NH_3 aq.(1.2 mL). [b]Determined by GC using biphenyl as standard. [c]150 $^\circ$C.

While other non-pricious metal-based metal phosphides (nano-CoP, nano-Ni_2P, nano-Fe_2P, and nano-Cu_2P), conventional Co nanoparticles (NPs) (CoO_x NP), and bulk Co_2P were inactive (entries 4-8) under the same conditions, strongly emphasizing the specific behavior of nano-Co_xP by the incorporation of phosphorus atoms into cobalt species. To evaluate the support effects on the

catalyst activity, nano-Co$_2$P on different supports were evaluated in the hydrogenation of **1** (entries 2, 9–11). All of them showed an improved activity in the yield of **2** compared to nano-Co$_2$P, owing to the increase of surface area of nano-Co$_2$P. The type of supports did not significantly affect the activity and nano-Co$_2$P/HT gave the highest yield of **2** in 94% among tested supported-catalysts (entry 2).

Remarkably, the high performance of this catalyst was further demonstrated by the hydrogenation of **1** when the H$_2$ pressure was decreased to 5 bar, giving **2** with 89% yield (entry 12). More importantly, nano-Co$_2$P gave a high yield of **2** under an H$_2$ pressure of just 1 bar (entry 13), which is the first example of non-precious metal-based catalyst to promote the hydrogenation of nitrile under an atmospheric H$_2$ pressure.

Moreover, 5.2 g of **1** to was also smoothly transformed into **2** with a 20- to 500-fold greater TON (over 58,000) than those of the state-of-the-art homogeneous and heterogeneous non-precious catalysts (**Table 2-2**). This result confirms again the superior activity of nano-Co$_2$P/HT catalyst as well as the high stability under the elevated temperature (**Scheme 2-1**).
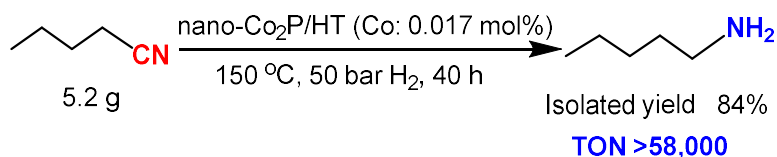
Scheme 2-1. Gram scale experiment of hydrogenation of **1** by nano-Co$_2$P/HT catalyst.

Table 2-2. Comparison of activity between nano-Co$_2$P and reported nonprecious metal catalysts for nitrile hydrogenation.

Entry	Catalyst	Active metal	Reaction condition	TON	reference
1	nano-Co$_2$P/HT	Co	0.017 mol% catalyst, NH$_3$ aq., 50 bar, 150 °C, 40 h.	58800 (5000 based on total cobalt atoms)	This work
2	{Fe(H)(HBH$_3$)(CO)[(CH$_3$)N((CH$_2$CH$_2$)P(CH(CH$_3$)$_2$)$_2$)$_2$]}	Fe	0.5−1 mol% catalyst, 30 bar H$_2$, 70−130 °C, 3−6 h.	174	*Nat. Commun.* 54111 (2014)
3	Fe(PNP)Br$_2$ Complex	Fe	1−5 mol% catalyst, 1−5 mol% NaHBEt$_3$, 3−15 mol% KHMDS, 60 bar H$_2$, 140 °C, 19−48 h.	100	*Chem. Commun.* **52**, 1812–1815 (2016)
4	Fe(PNP^{Cy})	Fe	0.5−1 mol% catalyst, 30 bar H$_2$, 40−70 °C, 2−3 h.	190	*Catal. Sci. Technol.* **6**, 4768–4772 (2016)
5	Co PNNH Pincer Complex	Co	2 mol% catalyst, 2 mol% NaEt$_3$BH, 4.4 mol% KOtBu, 30 bar H$_2$, 135°C, 36−60 h.	100	*J. Am. Chem. Soc.* **137**, 8888–8891 (2015)
6	(^{Mes}CCC)-CoCl$_2$py Catalyst Precursor	Co	4 mol % catalyst, 8 mol % NaHBEt$_3$, 12 mol % KOtBu, 4 bar, 115°C, 8 h.	25	*J. Am. Chem. Soc.* **139**, 13554–13561 (2017)
7	Co(acac)$_3$ + Tetradentate phosphine	Co	4 mol% Co(acac)$_3$, 4.4 mol% tetradentate phosphine, 10 mol% KOtBu, 30 bar H$_2$, 80−120°C, 18 h.	25	*ChemSusChem* **10**, 842–846 (2017)
8	CoBr$_2$ with NaHBEt$_3$ + HN-(CH$_2$CH$_2$P^{i}Pr$_2$)$_2$ (^{iPr}PN^{H}P)	Co	2 mol% CoBr$_2$, 6 mol% NaHBEt$_3$, 20 or 40 bar H$_2$, 110 or 130 °C, 4−24 h.	48	*ACS Catal.* **8**, 9125–9130 (2018)
9	Zr$_{12}$-TPDC-Co	Co	0.5 mol% catalyst, 40 bar H$_2$, 110 °C, 42 h.	200	*J. Am. Chem. Soc.* **139**, 7004–7011 (2017)
10	Co(OAc)$_2$/Phen@ α-Al$_2$O$_3$	Co	4−6 mol% catalyst, 5−40 bar H$_2$, 85−130 °C, 2−24 h.	25	*J. Am. Chem. Soc.* **138**, 8781–8788 (2016)
11	Cobalt-terephthalic acid MOF@C-800	Co	3.8 mol% catalyst, 25 bar H$_2$, 5 bar NH$_3$, 120 °C, 16 h.	25	*Chem. Sci.* **9**, 8553–8560 (2018)
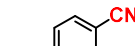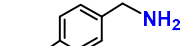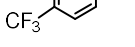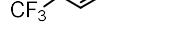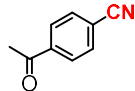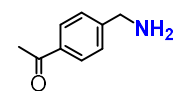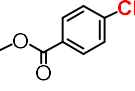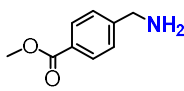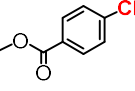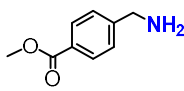
12	Co$_3$O$_4$/ NGr@CeO$_2$	Co	1.6−5 mol% catalyst, aqueous NH$_3$, 30−50 bar H$_2$, 120 °C, 8−15 h.	62	*Catal.Sci.Tech nol.***8,** 499–507 (2018)
13	Manganese Pincer Complexes	Mn	3 mol% catalyst, *t*-BuONa, 50 bar H$_2$, 120 °C, 24 h.	33	*J. Am. Chem. Soc.* **138,** 8809–8814 (2016)
14	*Fac*-[(CO)$_3$Mn(di ppe)(OTf)]	Mn	3 mol% catalyst, 10 mol% KO*t*Bu, 7-35 bar H$_2$, 90 °C, 15−30 min.	31	*ACS Catal.* **9,** 392–401 (2019)
15	Bisphosphine Mn(I) Complex	Mn	2 mol % catalyst, 20 mol % *t*-BuOK, 100 °C, 50 bar H$_2$, 18 h.	48	*Org. Lett.* **20,** 7212–7215 (2018)
16	MC/Ni Catalyst	Ni	13 mol % MC/Ni catalyst, NH$_3$ aq. (36 wt. %), 2.5 bar H$_2$, 80°C, 6−18 h.	8	*ChemSusChem* **12,** 1–11 (2019)
17	Ni nanoparticles embedded in imidazolium based ionic liquids	Ni	0.7 mol% based on the Ni precursor, 20−30 bar H$_2$, 90°C, 22 h.	1021 (143 based on total nickel atoms)	*New J. Chem.,* **41,** 9594–9597 (2017)
18	Ni/Al$_2$O$_3$-600	Ni	20 mg catalyst, 2.5 bar H$_2$, NH$_3$·H$_2$O (36.5 wt%), 60 °C, 6 h.	8	*New J. Chem.,* **44,** 549-555 (2020)
19	Ni-phen@SiO$_2$	Ni	45 mg catalyst (4.5 mol % Ni), 50 bar H$_2$, 100°C, 7 M NH$_3$/MeOH, 20 h.	22	*Sci. Adv.* **4,** eaat0761, (2018)
20	Cu/SiO$_2$ with H$_2$ pretreatmen t	Cu	6 mol % catalyst, 13−40 bar H$_2$, 110−130°C, 9−20 h.	12	*Applied Catalysis A: General* **494,** 41–47 (2015)

The general applicability of nano-Co$_2$P/HT-catalyzed reaction was further investigated through using various (hetero)aromatic and aliphatic nitriles as substrate (**Table 2-3**). Except for valeronitrile, other kinds of aliphatic nitriles underwent hydrogenation smoothly to produce the corresponding primary amines up to 99% yield (entries 2-7). In addition, heteroaromatic nitriles containing nitrogen and oxygen atoms also exhibited high reactiviy, converting to the desired primary amines with good yields (entries 8-12). On the other hand, aromatic substrate like benzonitrile and those bearing an electron-withdrawing group (–CF$_3$, –Br) or electron donating group (–OCH$_3$)

afforded high yields of the corresponding primary amine products (entries 13-21). Moreover, selective hydrogenation of nitrile in the presence of a ketone or ester group could also be realized, which is a challenging issue because of its low functional group tolerance (entries 22-24). nano-Co₂P /HT also gave excellent yields of primary amines even when decrease the H_2 pressure to 1 bar (entries 2, 4, 6, 12, 14, 17, 19, 21, and 24), demonstrating its high activity.

Table 2-3. Hydrogenation of various nitriles over nano-Co₂P/HT catalyst.[a]

$$R\!-\!CN \xrightarrow[\text{H}_2]{\text{nano-Co}_2\text{P/HT (Co: 4.2 mol\%)}} R\diagup NH_2$$

Entry	Substrate	H_2 (bar)	Temp. (°C)	Time (h)	Product	Yield (%)[b]
1	(CN)	40	130	1	(NH₂)	94
2		1	130	24		85
3	cyclohexyl-CN	40	130	2	cyclohexyl-CH₂NH₂	99
4		1	150	20		87
5	C₈H₁₇-CN	40	130	4	C₉H₁₉-NH₂	88
6		1	150	20		90
7	adamantyl-CN	40	150	4	adamantyl-CH₂NH₂	91
8	pyridin-3-yl-CN	40	130	1	pyridin-3-yl-CH₂NH₂	93
9[c]	pyridin-4-yl-CN	40	130	5	pyridin-4-yl-CH₂NH₂	92
10	furan-2-yl-CN	40	130	4	furan-2-yl-CH₂NH₂	95
11	indole-5-CN (NC)	40	130	2	(H₂N)indole	93
12[e]		1	150	20		85
13	benzonitrile (CN)	40	130	1	benzylamine (NH₂)	99
14		1	150	20		94
15	phenyl-CH₂CN	40	130	2	phenyl-C₂H₄NH₂	92
16	MeO-C₆H₄-CN	40	130	1	MeO-C₆H₄-CH₂NH₂	93
17[e]		1	150	20		87
18	Br-C₆H₄-CN	20	130	2	Br-C₆H₄-CH₂NH₂	92
19		1	150	16		86

Entry	Substrate	H_2 (bar)	Temp. ($^{\circ}$C)	Time (h)	Product	Yield (%)[b]
20		40	130	2		90
21		1	150	20		81
22		30	130	2		94
23[c]		40	130	5		88
24[f]		1	150	20		89

[a]Reaction conditions: catalyst (0.1 g), substrate (0.5 mmol), 2-propanol (3 mL), NH_3 aq. (1.2 mL). [b]Determined by GC using biphenyl as standard. [c]0.4 mL NH_3 aq. [d]5 mL NH_3 aq. [e]0.6 ml NH_3 aq. [f]Catalyst (0.2 g), 0.6 mL NH_3 aq.

Furthermore, multinitriles were also hydrogenated successfully by nano-Co_2P/HT catalyst to give the valuable products. For instance, 1,6-hexamethylenediamine, an important precursors of nylon-6,6 [25], was effectively yielded via the nano-Co_2P/HT-catalyzed hydrogenation of adipodinitrile. Sebaconitrile and aromatic dinitriles like terephthalonitrile and isophthalonitrile were sufficiently converted to the corresponding diamines over 85% yields. In addition, 3, 3′, 3″, 3‴-(butane-1,4-diylbis(azanetriyl))tetrapropanenitrile as a tetra-nitrile was efficiently hydrogenated that all the end CN groups were transformed to the amine moieties (**Scheme 2-2**).
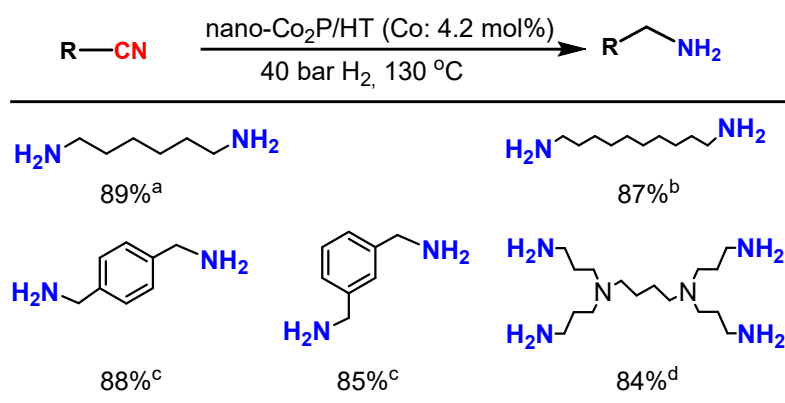
Scheme 2-2. Hydrogenation of multinitriles using nano-Co_2P catalyst. Reaction conditions: nano-Co_2P (0.1 g), substrate (0.5 mmol), 2-propanol (3 mL), NH_3 aq. (1.2 mL), yield determined by GC using biphenyl as standard. [a]NH_3 aq. (0.6 mL), 4 h. [b]4 h. [c]10 h. [d]Substrate (0.07 mmol), 100 $^{\circ}$C, 50 bar H_2, 3 h and yield determined by NMR using biphenyl as standard.

After the reaction, nano-Co_2P/HT was easily recovered by filtration and ready to be reused without any catalyst pretreatment [23]. The high activity and selectivity of nano-Co_2P/HT was retained even after 7th reuse (**Figure 2-3** (a)), revealing the high durability of nano-Co_2P. Hot filtration experiment was carried out by removing nano-Co_2P/HT from the reaction mixture at 35% yield. The recovered reaction mixture was further treated under the same reaction conditions, but no additional amine products could be observed, which indicated the hydrogenation proceeded heterogeneously on the Co_2P surface (**Figure 2-3** (b)).
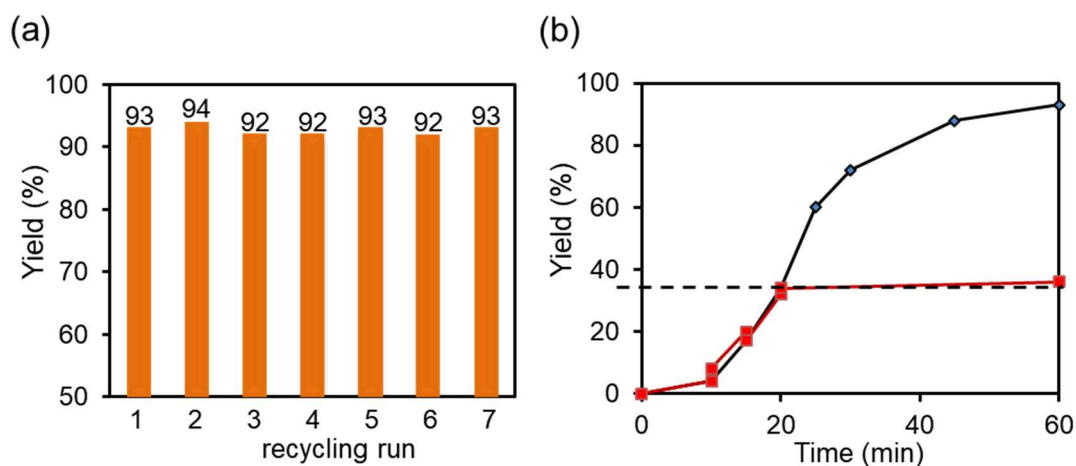
Figure 2-3. (a) Reuse experiments of nano-Co_2P/HT in hydrogenation of **1**. (b) Hot filtration experiment of nano-Co_2P/HT in hydrogenation of **1**. Reaction condition: catalyst (0.1 g), **1** (0.5 mmol), 2-propanol (3 mL), NH_3 aq. (0.8 mL), 130 °C, 40 bar H_2, 1 h.

3.3. The origin of high performance of nano-Co_2P

In order to figure out the actual electronic state of nano-Co_2P, the Co K-edge X-ray absorption near edge structure (XANES) spectrum of nano-Co_2P was performed under air atmosphere. As shown in **Figure 2-4** (a), the absorption edge energy of nano-Co_2P was found to be close to that of Co foil but much lower than that of CoO, which suggested that the Co species in nano-Co_2P existed in metallic states [26]. The similar result was observed for nano-CoP. Fourier transformation (FT) of the k^3-weighted extended X-ray adsorption fine structure (EXAFS) in **Figure 2-4** (b) indicated that

nano-Co_2P has two main peaks around 1.8 and 2.3 Å, which are attributed to those from Co-P and Co-Co scattering, respectively [27]. The formation of the metal-metal bond also implied a metallic nature [28] of nano-Co_2P and its intensity was higher than that of nano-CoP, which accounts for the superior activity of nano-Co_2P.
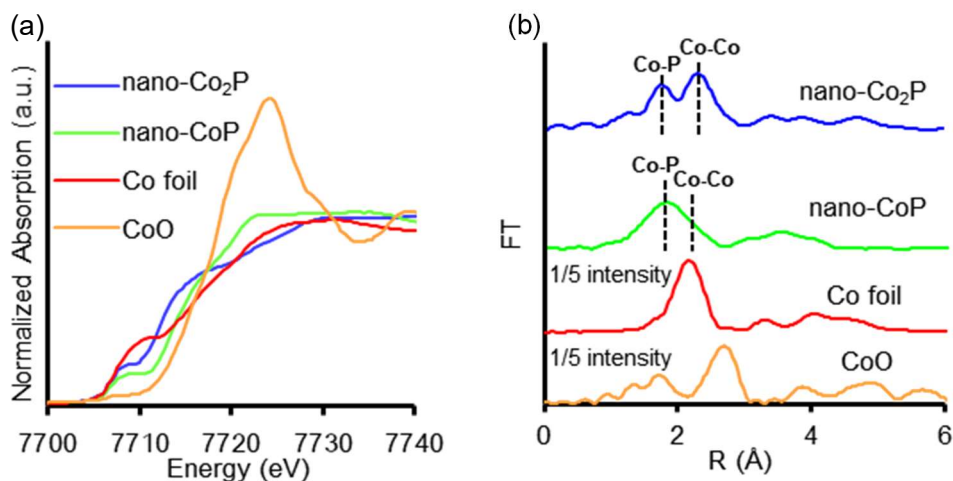
Figure 2-4. (a) Co *K*-edge XANES spectra of nano-Co_2P, nano-CoP, Co foil, and CoO. (b) Fourier transformation of the k^3-weighted EXAFS of nano-Co_2P, nano-CoP, Co foil, and CoO.

The X-ray photoelectron spectroscopy (XPS) of nano-Co_2P exhibited peaks located at 777.7 eV and 792.9 eV, respectively, which are similar to those of metallic Co $2p_{3/2}$ (777.9 eV) and $2p_{1/2}$ (793.5 eV) [29] (**Figure 2-5** (a)). Notably, the lower binding energy demonstrated that there were partially negatively charged Co species ($Co^{\delta-}$) on the nano-Co_2P. On the other hand, an asymmetric peak could be observed in the XPS spectrum of P 2p, which can be split into two peaks attributed to element P located at 129.0 and 130.0 eV [30]. In the meantime, another peak could be split to two peaks located at 133.3 and 134.4 eV derived from phosphate species, which are caused by the surface oxidation [31] (**Figure 2-5** (b)).
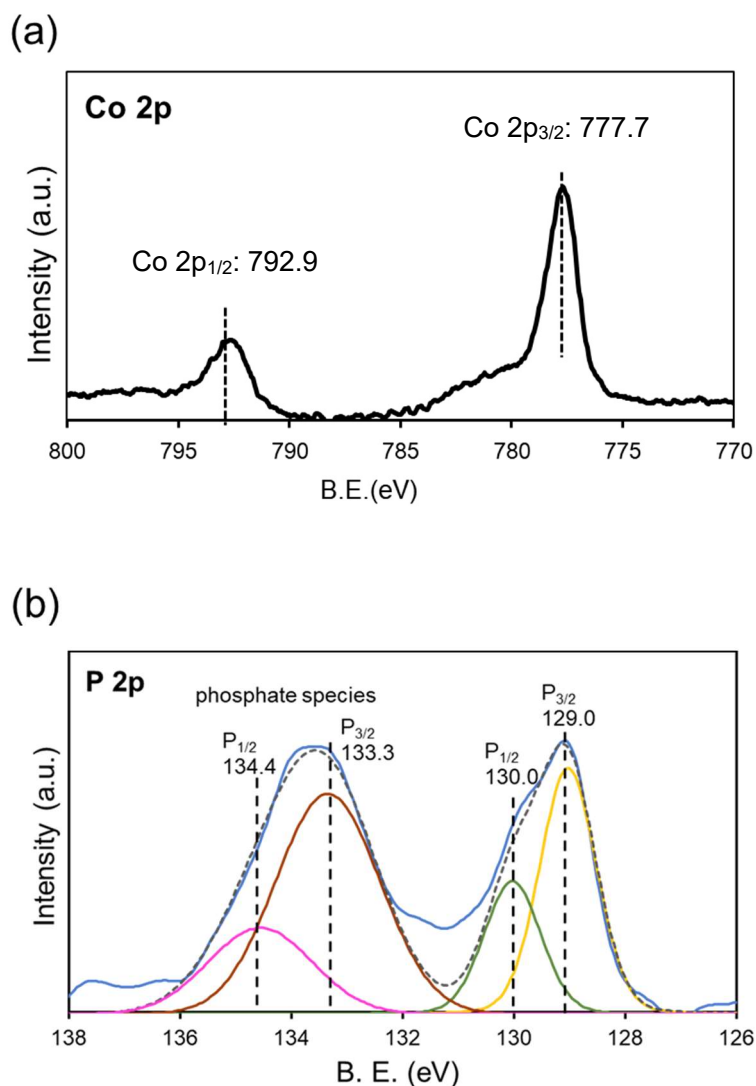
Figure 2-5. (a) Co 2p XPS spectrum and (b) P 2p XPS spectrum of nano-Co$_2$P.

The electronic state of Co was also investigated by FT-IR spectroscopy of CO adsorption as shown in **Figure 2-6**. FT-IR spectrum of CO chemisorption on nano-Co$_2$P showed a much lower absorption band at 2056 cm^{-1} than that of gaseous CO (2143 cm^{-1}) [32], indicating a linearly adsorbtion of CO on the electron-populated cobalt center that leads a strong back-donation to the $2\pi^*$ antibonding molecular orbital of CO.
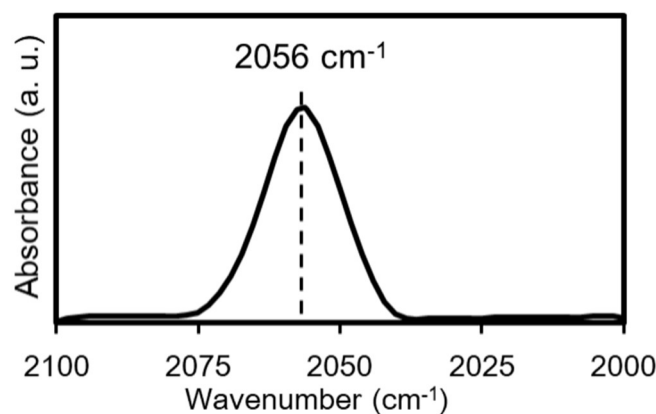
Figure 2-6. *In situ* FT-IR spectroscopy of CO adsorption on nano-Co_2P.

Above results clearly illustrate that nano-Co_2P processes a electron-riche low-valent cobalt ($Co^{\delta-}$), which is significantly different from the conventional non-precious metals (0) requring a high-temperature H_2 pre-treatment before reaction.

At last, the density functional theory (DFT) calculations was performed to clarify the structure–activity relationship of nano-Co_2P. The projected density of states (PDOS) of *d*-orbitals in Co_2P (0001) surfaces, bulk Co, and bulk Co_2P as well as their differences were summarized in **Figure 2-7**. Notably, these calculation results demonstrated that there are larger amplitudes of the *d*-orbital PDOS around the Fermi level of Co atoms at the Co_2P surface than those in the bulk Co and in bulk Co_2P [33]. While the *d*-electrons around the Fermi level are prone to donate electrons to the lowest unoccupied molecular orbital (LUMO) of nitrile [34], the Co species with increased *d*-electrons in nano-Co_2P would provide a stronger back-donation to the π* orbital of nitrile to activate the C≡N bond, resulting in the high activity of nano-Co_2P catalyst.
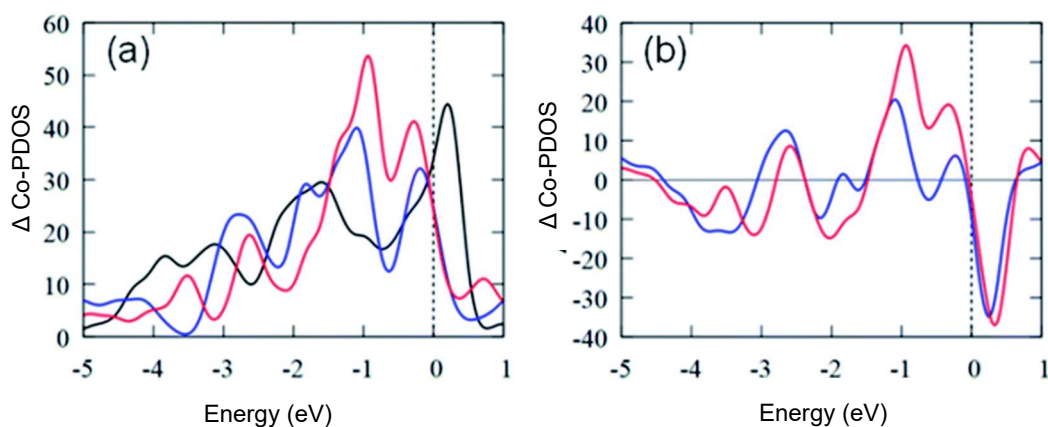
Figure 2-7. (a) Projected density of states of the Co atom (Co-PDOS) in bulk Co (black), bulk Co_2P (blue) and on the Co_2P surface (red). (b) Differences of Co-PDOSs (ΔCo-PDOS) between bulk Co and bulk Co_2P (blue) and between the bulk Co and Co_2P surface (red).

4. Conclusion

This chapter describes a well-defined nano-Co_2P can serve as a efficient catalyst for hydrogenation nitriles under conditions as mild as 1 bar H_2 pressure, which is firstly achieved by a non-pricious metal-based catalyst under such mild condition. After reaction, nano-Co_2P catalyst can be recovered easily and reused without loss any activity. XAFS and DFT calculations confirm that nano-Co_2P possess Co species with high *d*-electron density, which accelerates the activation of nitrile via the enhanced back-donation and thus leads to the high activity. This study provides a milestone attempt for developing metal phosphides as highly efficient catalyst for organic synthesis.

References

1   Legras, J. L.; Chuzel, G.; Arnaud, A.; Galzy, P. *World J. Microbiol. Biotechnol*. **1990**, *6*, 83–108.

2   Lawrence, S. A. *Amines: Synthesis Properties, and Application*; Cambridge University Press: Cambridge, **2006**.

3   Roughley, S. D.; Jordan, A. M. *J. Med. Chem*. **2011**, *54*, 3451–3479.

4   J. Seyden-Penne, *Reduction by Alumino- and Borohydrides in Organic Synthesis*, Wiley, New York, **1997**.

5   Anderson, P. G.; Munslow, I. J. *Modern Reduction Methods*, Wiley-VCH, Weinheim, **2008**.

6   Werkmeister, S.; Junge, K.; Beller, M. *Org. Process Res. Dev*. **2014**, *18*, 289–302.

7   Mérel, D. S.; Do, M. L. T.; Gaillard, S.; Dupau, P.; Renaud, J.-L. *Coord. Chem. Rev*. **2015**, *288*, 50–68.

8   Roose, P.; Eller, K.; Henkes, E.; Rossbacher, R.; Höke, H. *Amines, Aliphatic. Ullmann's Encyclopedia of Industrial Chemistry*; Wiley-VCH, New York, **2015**.

9   Nishimura, S. *Handbook of Heterogeneous Catalytic Hydrogenation for Organic Synthesis*, Wiley-VCH, New York, **2001**.

10   Ertl, G.; Knözinger, H.; Weitkamp, J. *Preparation of Solid Catalysts*, Wiley-VCH, New York, **1999**.

11   Bornschein, C.; Werkmeister, S.; Wendt, B.; Jiao, H.; Alberico, E.; Baumann, W.; Junge, H.; Beller, M. *Nat. Commun*. **2014**, *5*, 4111.

12   Chakraborty, S.; Leitus, G.; Milstein, D. *Chem. Commun*. **2016**, *52*, 1812–1815.

13   Lange, S.; Elangovan, S.; Cordes, C.; Spannenberg, A.; Jiao, H.; Junge, H.; Bachmann, S.; Scalone, M.; Topf, C.; Junge, K.; Beller, M. *Catal. Sci. Technol*. **2016**, *6*, 4768–4772.

14   Adam, R.; Bheeter, C.; Cabrero-Antonino, J.; Junge, K.; Jackstell, R.; Beller, M. *ChemSusChem*. **2017**, *10*, 842–846.

15 Mukherjee, A.; Srimani, D.; Chakraborty, S.; Ben-David, Y.; Milstein, D. *J. Am. Chem. Soc.* **2015**, *137*, 8888–8891.

16 Elangovan, S.; Topf, C.; Fischer, S.; Jiao, H.; Spannenberg, A.; Baumann, W.; Ludwig, R.; Junge, K.; Beller, M. *J. Am. Chem. Soc*. **2016**, *138*, 8809–8814.

17 Garduño, J.; García, J. *ACS Catal.* **2019**, *9*, 392−401.

18 Weber, S.; Stöger, B.; Kirchner, K. *Org. Lett.* **2018**, *20*, 7212−7215.

19 Tokmic, K.; Jackson, B.; Salazar, A.; Woods, T.; Fout, A. *J. Am. Chem. Soc.* **2017**, *139*, 13554–13561.

20 Chen, F.; Topf, C.; Radnik, J.; Kreyenschulte, C.; Lund, H.; Schneider, M.; Surkus, A.; He, L.; Junge, K.; Beller, M. *J. Am. Chem. Soc.* **2016**, *138*, 8781–8788.

21 Ferraccioli, R.; Borovika, D.; Surkus, A.; Kreyenschulte, C.; Topf, C.; Beller, M. *Catal. Sci. Technol.* **2018**, *8*, 499 –507.

22 Murugesan, K.; Senthamarai, T.; Sohail, M.; Alshammari, A.; Pohl, M.; Beller, M.; Jagadeesh, R. *Chem. Sci.* **2018**, *9*, 8553–8560.

23 Zhang, Y.; Yang, H.; Chi, Q.; Zhang, Z. *ChemSusChem.* **2019**, *12*, 1–11.

24 Wang, J.; Tang, Q.; Jin, S.; Wang, Y.; Yuan, Z.; Chi, Q.; Zhang, Z. *New J. Chem.* **2020**, *44*, 549–555.

25 Schaffer, S.; Haas, T. *Org. Process Res. Dev.* **2014**, *18*, 752–766.

26 Liu, K.; Zhang, C.; Sun, Y.; Zhang, G.; Shen, X.; Zou, F.; Zhang, H.; Wu, Z.; Wegener, E.; Taubert, C.; Miller, J.; Peng, Z.; Zhu, Y. *ACS Nano* **2018**, *12*, 158–167.

27 Zhou, L.; Zhu, C.; Edmonds, L.; Yang, H.; Cui, W.; Li, B. *RSC Adv.* **2014**, *4*, 43220–43226.

28 Cotton, F. A. G. *Progress in Inorganic Chemistry: Metal–Metal Bonds in Transition Metal Compounds*, Wiley-VCH, New York, **1968**.

29 Wagner, C. D.; Riggs, W. M.; Davis, L. E.; Moulder J. F.; Muilenberg, G. E. *Handbook of X-*

Ray Photoelectron Spectroscopy, Perkin-Elmer, Eden Prairie, **1979**.

30   Cao, S.; Chen, Y.; Hou, C.; Lv, X.; Fu, W. *J. Mater. Chem. A* **2015**, *3*, 6096–6101.

31   Wang, J.; Zhu, L.; Dharan, G.; Ho, G. *J. Mater. Chem. A* **2017**, *5*, 16580–16584.

32   Khassin, A.; Yurieva, T.; Kaichev, V.; Bukhtiyarov, V.; Budneva, A.; Paukshtis, E.; Parmon, V. *J. Mol. Catal. A: Chem.* **2001**, *175*, 189–204.

33   Liang, Z.; Zhong, X.; Li, T.; Chen, M.; Feng, G. *ChemElectroChem* **2019**, *6*, 260–267.

34   La Pierre, H.; Arnold, J.; Bergman, R.; Dean Toste, F. *Inorg. Chem.* **2012**, *51*, 13334–13344.

Chapter III.

Selective Hydrogenation of Furfural Derivatives

by Cobalt Phosphide Catalyst

1. Introduction

With the increasing consumption of nonrenewable fossil resources to meet nowadays development of humanity, the deterioration of the environment and energy problems are gradually getting worse [1, 2]. For this reason, renewable and abundant biomass is regarded as a promising alternative for the sustainable production of valuable chemicals and fuels. Among the key chemicals produced from biomass, furfural derivative is one of the most important platform chemicals with an annual production volume of more than 200,000 tons [3-6]. The selective hydrogenation is considered to be an effective method for high-value conversion of furfural derivatives to furfural alcohol products (**Scheme 3-1**), which serves as an important intermediate for synthesizing polymers, fibers, and fine chemicals. Since the aromatic structure are widely exist in pharmaceutical synthesis [7], the selective hydrogenation of the carbonyl group without the destruction of aromaticity of furfural derivative is an attractive issue but also challenging.
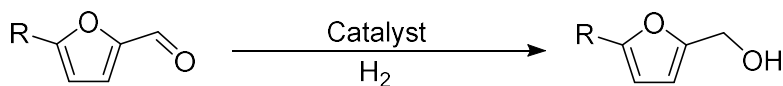
Scheme 3-1. Selective hydrogenation of furfural derivatives.

Although precious metals are usually selected as the active component for hydrogenation reaction, these catalysts with high hydrogenation activity are prone to cause selectivity problems due to the over hydrogenation and/or decarbonylation in the hydrogenation of furfural derivative [8, 9]. Some successful examples have also been reported [10-13], like Taylor *et al.* indicated that the hydrogenation of furfural can be achieved by a supported platinum catalyst through controlling the reaction temperature as low as 50 °C, giving furfuryl alcohol with 99% selectivity [10]. On the other hand, the component metals in them are of high cost and low reservation, which limit their extensive application.

To overcome above problems, much effort has been devoted to the development of

nonprecious metal catalysts for selective hydrogenation of furfural derivatives [14-19]. However, high reaction temperature and/or high H_2 pressure are usually required to achieve a good performance because of their poor activity. For example, Prakruthi *et al.* reported that a maximum 87% yield of furfuryl alcohol was obtained by loading Cu (15 wt%) on dealuminated layered double hydroxides at 220 °C [14]. Trupti *et al.* also developed a Ni/CN catalyst gave 96% conversion of furfuryl and 95% selectivity of furfuryl alcohol under 200 °C [15]. Furthermore, all reported nonprecious metal catalysts to date for furfural hydrogenation are susceptible to air (air instability), resulting in complicate catalyst handlings under strictly anaerobic conditions or a high-temperature pre-treatment with H_2 before use [16-19]. Therefore, the development of non-noble metal catalysts with both air stability and high efficiency is strongly desired but also challenging.

In this chapter, the author demonstrated an Al_2O_3-supported Co_2P nanocrystal (nano-Co_2P/Al_2O_3) can server as a highly efficien catalyst for the selective hydrogenation of furfural derivatives. In sharp contrast to conventional non-precious metal catalysts, Co_2P nanocrystal bearing a unique air-stable property enabling easy and safe catalyst handling. FT-IR and DFT studies confirmed that the high activity of this catalyst is benefited from the strong backdonation from the Co *d*-electrons to π^* orbital to activate the carbonyl moiety in furfural derivatives.

2. Experimental section

2.1. General

All precursors and solvents were used as received, without further purification. $CoCl_2 \cdot 6H_2O$, and 1-octadecene (technical grade 90%) were purchased from the Nacalai Tesque, INC. and Sigma-Aldrich, respectively. Hexadecylamine and triphenyl phosphite were purchased from Tokyo Chemical Industry Co., Ltd. Acetone, chloroform, n-hexane, methanol, 2-propanol, 1,4-dioxane, and NaOH were purchased from FUJIFILM Wako Pure Chemical Corporation. Al_2O_3 was obtained from Sumitomo Chemical Co., Ltd. Hydroxyapatite was purchased from FUJIFILM Wako Pure Chemical Corporation. ZrO_2 (JRC ZRO-8) and MgO (JRC-MGO-3 1000A) were provided by the Catalysis Society of Japan as reference catalysts. Bulk Co_2P was purchased from Mitsuwa Chemicals. 5-Hydroxymethylfurfural (HMF) was purchased from FUJIFILM Wako Pure Chemical Corporation. Furfural, 5-methylfurfural and 5-acetoxymethylfurfural were purchased from Tokyo Chemical Industry Co., Ltd. HMF and 5-acetoxymethylfurfural were used as received, without further purification. Furfural and 5-methylfurfural were purified by distillation before use.

Inductively coupled plasma-atomic emission spectroscopy (ICP-AES) was performed using a Perkin Elmer Optima 8300 instrument. ^1H and ^{13}C nuclear magnetic resonance (NMR) spectra were recorded using a JEOL JNM-ESC400 spectrometer and chemical shifts (δ) are reported in ppm relative to tetramethylsilane. Transmission electron microscopy (TEM) observations were carried out using a FEI Tecnai G2 20ST instrumentoperated at 200 kV. Scanning transmission electron microscopy (STEM) images with elemental maps were collected using a FEI Titan Cubed G2 60-300 instrument operated at 300 kV and equipped with Super-X energy-dispersive X-ray spectroscopy (EDX) detector. Elemental mapping based on quantification analysis of EDX spectra was carried out using Esprit. Co K-edge X-ray absorption spectra were recorded at room temperature at the BL01B1 and BL14B2 lines, using a Si (111) monochromator at SPring-8, Japan Synchrotron Radiation Research Institute (JASRI),

Harima, Japan. Data analysis was performed using the xTunes software. XRD studies were conducted on a Philips X′Pert-MPD diffractometer with Cu-Ka radiation (45 kV, 40 mA). Fourier-transform infrared (FT-IR) spectra were recorded using a JASCO FT-IR 4100 spectrometer equipped with a mercury cadmium telluride detector. A thin disk of the sample was prepared by pressing the pure sample onto a stainless-steel grid. The sample disk was then placed inside an IR cell to enable thermal treatment in a controlled atmosphere. The sample pellet was treated under vacuum (< 1 mmHg) at 130 °C for 1 h before the introduction of probe molecules. XPS analysis was performed on a Kratos AXIS 165 X-ray photoelectron spectrometer equipped with a monochromatic Al X-ray source. The spectra were obtained at a pass energy of 80.0 eV with an Al Kα X-ray source operating at 12 mA and 15 kV. The working pressure in the analysis chamber was less than 5.0×10^{-9} mmHg. The C 1s peak at a binding energy of 284.5 eV was used as the internal reference. TPO was carried out on a BELCAT-II instrument. Prior to the experiment, 20 mg of nano-Co_2P was treated under a flow of He (50 cm^3/min) at 300 °C for 1 h and then cooled to room temperature. After flushing with 5% O_2 in He (50 cm^3/min) at 30 °C, TPO was performed using 5% O_2 in a flow of He (50 cm^3/min) and by raising the temperature from 30 to 500 °C at 10 °C/min.

2.2.   Preparation of catalysts

Synthesis of nano-Co_2P: All reactions were carried out under an argon atmosphere using standard Schlenk line techniques. In a typical synthesis, 1.0 mmol of $CoCl_2·6H_2O$ and 10.0 mmol of hexadecylamine were combined with 10.0 mL of 1-octadecene and 10.0 mmol of triphenyl phosphite in a Schlenk flask. The system was heated to 150 °C to remove low-boiling-point impurities. The temperature was then increased to 290 °C and maintained for 2 h. Afterward, the mixture was cooled to room temperature. The black product was isolated by precipitation with acetone. To remove as

much organics as possible, redispersion and precipitation cycles using chloroform and acetone were continued until the supernatant liquid was transparent. The obtained powder was dried in vacuum overnight.

Preparation of nano-Co₂P/support: Typically, 37.2 mg of nano-Co$_2$P was dispersed in 100 mL *n*-hexane and stirred with 1.0 g of Al$_2$O$_3$ at room temperature. The obtained powder was dried in vacuum overnight to give nano-Co$_2$P/Al$_2$O$_3$ as a gray powder. The same procedure was used to prepare the other nano-Co$_2$P/support catalysts.

Preparation of CoO$_x$/Al$_2$O$_3$ by impregnation method: CoCl$_2$·6H$_2$O (0.5 mmol) was dissolved in acetone (50 mL). Al$_2$O$_3$ (1.0 g) was added, and the mixture was stirred for 30 min at room temperature. Acetone was removed by evaporation under reduced pressure, and the obtained powder was dried at 110 °C overnight. The dried powder was calcined in air at 500 °C for 3 h to give CoO$_x$/Al$_2$O$_3$.

Preparation of CoO$_x$/Al$_2$O$_3$ by deposition-precipitation method: Al$_2$O$_3$ (1.0 g) was soaked in 50 mL of an aqueous solution of CoCl$_2$ (10 mM). The pH was then adjusted to 8.5 with a solution of NaOH (0.1 M). After stirring the mixture for 6 h at room temperature, the obtained solid was filtered, washed with deionized water, and dried in vacuum at room temperature, giving CoO$_x$/Al$_2$O$_3$.

2.3. Reaction procedure

The typical reaction procedure for the hydrogenation of HMF to BHMF using nano-Co$_2$P/Al$_2$O$_3$ was as follows. nano-Co$_2$P/Al$_2$O$_3$ powder was placed in a 50-mL stainless steel autoclave with a Teflon inner cylinder. HMF (0.25 mmol) and distilled water (3 mL) were subsequently added. The reaction mixture was stirred vigorously at 130 °C under 4 MPa of H$_2$. After the reaction, dimethyl sulfone (internal standard) and MeOH were added to the reaction mixture, and then, the catalyst was separated by centrifugation. The reaction solution was analyzed by GC-MS to determine the

conversion and yield.

2.4. Recycling experiments

After the reaction, nano-Co$_2$P/Al$_2$O$_3$ was removed by centrifugation, and the yield was determined by GC-MS analysis. The spent catalyst was washed with water and 2-propanol for the reuse experiments without any other pre-treatments.

2.5. Gram-scale reaction

The gram-scale reaction of HMF was performed in a 300-mL stainless steel autoclave with a Teflon inner cylinder at 130 °C under 4 MPa of H$_2$ for 4 h. After the reaction, nano-Co$_2$P/Al$_2$O$_3$ was filtered to separate the liquid phase from the solid catalyst. The solvent was evaporated, and the residue was subjected to silica gel column chromatography (chloroform/methanol = 93/7) to give isolated BHMF, which was identified by GC-MS and ^{1}H and ^{13}C NMR.

2.6. Product identification

Bis(2,5-hydroxymethyl)furan (BHMF)

CAS registry No. [1883-75-6]. ^{1}H NMR (DMSO, 400 MHz): δ = 6.18 (s, 2H), 5.13 (t, J = 5.7 Hz, 2H), 4.35 (d, J = 6.0 Hz, 4H). ^{13}C NMR (DMSO, 100 MHz): δ = 154.7, 107.3, 55.7.

Furfuryl alcohol

CAS registry No. [98-00-0]. ^{1}H NMR (CDCl$_3$, 400 MHz): δ = 7.40 (d, J = 1.5 Hz, 1H), 6.35–6.33 (m, 1H), 6.29 (d, J = 3.2 Hz, 1H), 4.61 (s, 2H), 1.79 (brs, 1H). ^{13}C NMR (CDCl$_3$, 100 MHz): δ = 154.0, 142.7, 110.3, 107.7, 57.5.

5-Methylfurfuryl alcohol

CAS registry No. [3857-25-8]. ^{1}H NMR (CDCl$_3$, 400 MHz): δ = 6.16 (d, J = 2.8 Hz, 1H), 5.91–5.90 (m, 1H), 4.54 (s, 2H), 2.29 (s, 3H). ^{13}C NMR (CDCl$_3$, 100 MHz): δ = 152.4, 152.3, 108.7, 106.2, 57.5, 13.5.

2,5-Furandimethanol monoacetate

CAS registry No. [89630-82-0]. ^{1}H NMR (CDCl$_3$, 400 MHz): δ = 6.35 (d, J = 3.4 Hz, 1H), 6.26 (d, J = 2.7 Hz, 1H), 5.03 (s, 2H), 4.63 (s, 2H), 2.08 (s, 3H). ^{13}C NMR (CDCl$_3$, 100 MHz): δ = 170.6, 154.8, 149.5, 111.4, 108.5, 58.1, 57.5, 20.8.

3. Results and discussion

3.1. Characterization of nano-Co$_2$P

The X-ray diffraction (XRD) patterns of prepared cobalt phosphide are shown in **Figure 3-1** (a). The results exhibit the diffraction peaks at 2θ angle of 40.8°, 43.5°, 52.3°, and 55.8°, attributing to the (121), (211), (002), and (320) planes of the orthorhombic Co$_2$P, respectively. The transmission electron microscopy (TEM) image of nano-Co$_2$P is displayed in **Figure 3-1** (b). It can be seen that a uniform nano-rod structure with an average length* width = 32 nm* 18 nm of nano-Co$_2$P is formed. The high-angle annular dark-field scanning transmission electron microscopy (HAADF-STEM) image and elemental mapping images using energy-dispersive X-ray spectroscopy (EDX) confirm the presence of cobalt and phosphorus as the constituent elements and are homogeneously dispersed within each nano-rod (**Figures 3-1** (d-g)). In addition, elemental analysis results based on EDX indicates that the Co/P atomic ratio of nano-Co$_2$P is nearly 2 (**Figure 3-1** (h)). All these results point out that a nano-sized Co$_2$P was successful synthesized. After immobilized on Al$_2$O$_3$, the size and morphology of nano-Co$_2$P are remained and is of high dispersion (**Figure 3-1** (c)).
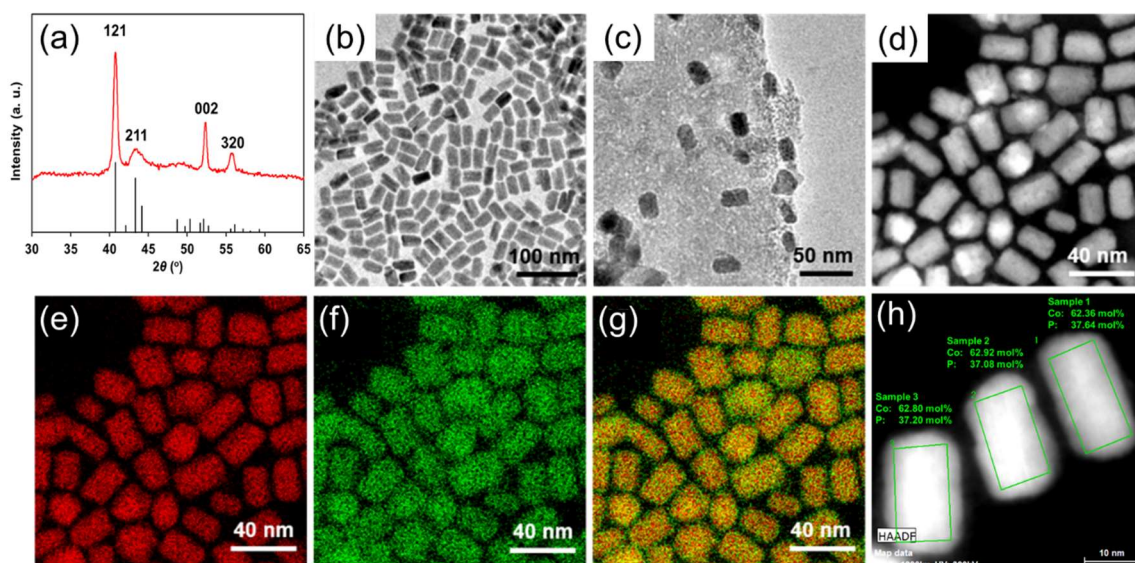
Figure 3-1. (a) The XRD pattern of the prepared cobalt phosphide. (b) TEM image of nano-Co_2P. (c) TEM image of nano-Co_2P/Al_2O_3. (d) HAADF-STEM image of nano-Co_2P. Elemental mapping images of (d) Co and (e) P. (f) Composite overlay image formed from (d) and (e). (h) Elemental analysis of nano-Co_2P.

Then, the X-ray absorption fine structure (XAFS) analysis was carried out under air to investigate the electronic states and local structures of Co species in nano-Co_2P (**Figure 3-2**). The Co K-edge X-ray absorption near edge structure (XANES) spectrum show that the absorption edge energy of nano-Co_2P is close to that of Co foil, suggesting the Co species in Co_2P are in metallic state. As for Al_2O_3-supported nano-Co_2P, the spectral feature is slightly changed but no characteristic peak from Co oxides is observed, indicating the influence of Al_2O_3 on the electronic states and/or local structure of nano-Co_2P. On the other hand, a conventional Al_2O_3-supported cobalt catalyst prepared via impregnation method (CoO_x/Al_2O_3) exhibit a higher absorption edge energy than those of nano-Co_2P and Co foil, but is similar with Co_3O_4, suggesting the presence of the di- and trivalent Co species. These results demonstrate that the Co species in nano-Co_2P/Al_2O_3 are air-stable zero-valent, while Co metal in air is easily oxidized. Thus, the chemical properties of Co species in nano-Co_2P are significantly different from zero-valent cobalt metal and conventional cobalt oxide due to the

65

integration of phosphorus (P-alloying).
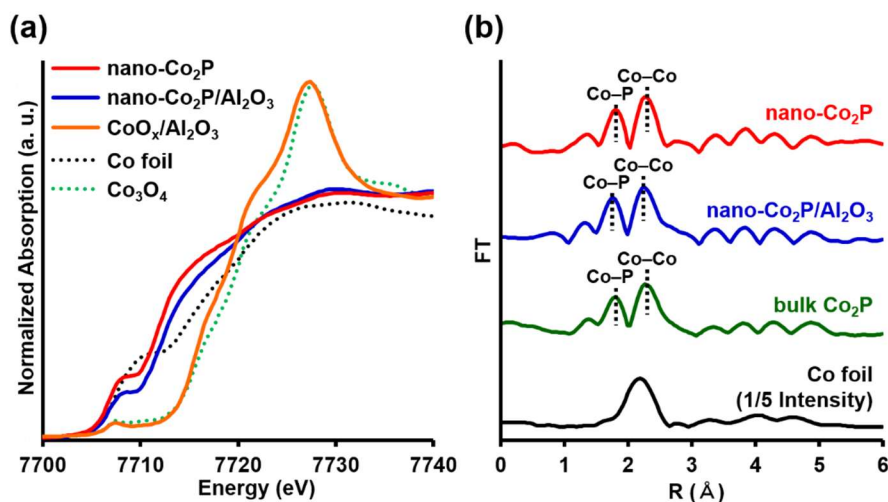
Figure 3-2. (a) Co K-edge XANES spectra of nano-Co$_2$P, nano-Co$_2$P/Al$_2$O$_3$, and CoO$_x$/Al$_2$O$_3$ with Co foil and Co$_3$O$_4$ as references. (b) Fourier transform (FT) of the k^3-weighted EXAFS spectra of nano-Co$_2$P and nano-Co$_2$P/Al$_2$O$_3$ with bulk-Co$_2$P and Co foil as references.

The Fourier-transform extended X-ray absorption fine structure (FT-EXAFS) spectra show the existence of peaks at 1.6–2.0 and 2.0–2.5 Å, respectively, in nano-Co$_2$P, nano-Co$_2$P/Al$_2$O$_3$, and bulk Co$_2$P, corresponding to Co–P and Co–Co bonds [20]. In contrast, no peaks attributed to the Co–O bond is observed in nano-Co$_2$P and nano-Co$_2$P/Al$_2$O$_3$, confirming the metallic state without oxidation which is also indicated in the XANES analysis [21].
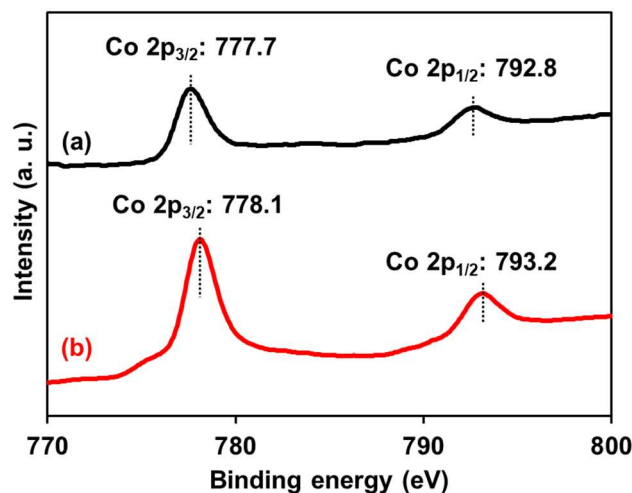
Figure 3-3. Co 2p XPS spectra of (a) nano-Co_2P and (b) nano-Co_2P/Al_2O_3.

The interaction between nano-Co_2P and Al_2O_3 is also confirmed by X-ray photoelectron spectroscopy (XPS) as shown in **Figure 3-3**. As for nano-Co_2P, the binding energy peaks at Co $2p_{3/2}$ (777.7 eV) and Co $2p_{1/2}$ (792.8 eV) are very close to those of metallic cobalt (Co $2p_{3/2}$: 777.9 eV, Co $2p_{1/2}$: 793.5 eV), which are consistent with the results from XANES spectra [22]. After immobilization on Al_2O_3, Co $2p_{3/2}$ and $2p_{1/2}$ peaks of nano-Co_2P shift to 778.1 and 793.2 eV, respectively, suggesting the presence of electronic interaction with Al_2O_3.

3.2. Catalytic activity in hydrogenation of HMF

The catalytic activity of nano-Co_2P/Al_2O_3 was evaluated using 5-hydroxymethylfurfural (HMF) as model substrate using water as solvent under 130 °C, 4 MPa H_2 conditions for 1 h without any pre-treatments. The results are summarized in **Table 3-1**. An unsupported nano-Co_2P catalyst promoted the selective hydrogenation of HMF to provide the corresponding 2,5-bis(hydroxymethyl)furan (BHMF) in 14% yield (entry 1). Notably, the activity of nano-Co_2P was significantly improved after immobilization on Al_2O_3 (nano-Co_2P/Al_2O_3) and BHMF was obtained in 54% yield with >99% selectivity because of the high dispersion of nano-Co_2P on Al_2O_3 (entry 2). After

prolonging the reaction time to 4 h, BHMF could be obtained in a quantitative yield (entry 3). Moreover, nano-Co_2P/Al_2O_3 also exhibit high activity even under milder reaction conditions (80 °C, 2 MPa H_2 pressure), yielding >99 % BHMF with high selectivity (entry 4). nano-Co_2P dispersed on other metal oxide supports also promoted the hydrogenation of HMF efficiently (entries 5–7) and found that hydrogenation efficiency does not significantly affect by the type of support. On the contrary, conventional cobalt nanoparticle (CoO_x/Al_2O_3) catalysts synthesized by impregnation and deposition-precipitation methods showed no activity in this reaction (entries 8 and 9). In addition, Co_2P with bulk size was also ineffective (entry 10). As a result, not only the introducing of P atom into Co but also the nano-sizing effect are the key reasons for the high activity of nano-Co_2P for hydrogenation.

Table 3-1. Hydrogenation of 5-hydroxymethylfurfural (HMF) to 2,5-bis(hydroxymethyl)furan (BHMF) using Co catalysts[a]
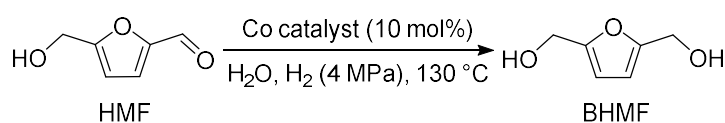
entry	catalyst	time (h)	conv.[b] (%)	sel.[b] (%)
1	nano-Co_2P	1	15	96
2	nano-Co_2P/Al_2O_3	1	54	>99
3	nano-Co_2P/Al_2O_3	4	>99	>99
4[c]	nano-Co_2P/Al_2O_3	12	>99	>99
5	nano-Co_2P/ZrO_2	1	50	95
6	nano-Co_2P/hydroxyapatite	1	40	>99
7	nano-Co_2P/MgO	1	28	92
8[d]	CoO_x/Al_2O_3	1	0	-
9[e]	CoO_x/Al_2O_3	1	0	-
10	bulk Co_2P	1	6	0

[a]Reaction conditions: HMF (0.25 mmol), H_2O (3 mL). [b]Determined by gas chromatography-mass spectrometry (GC-MS) using an internal standard technique. [c]H_2 (2 MPa), 80 °C. [d]Catalyst prepared by impregnation method. [e]Catalyst prepared by deposition-precipitation method.

After filtering out nano-Co$_2$P/Al$_2$O$_3$ at 50 % conversion of HMF, the recovered filtrate was further treated under the same reaction conditions. However, the yield of BHMF was unchanged and no other product was yielded, confirming the hydrogenation was occurree on nano-Co$_2$P/Al$_2$O$_3$ heterogeneously (**Scheme 3-2**). Then, the recycling experiments were carried out to identify the catalyst durability. The used nano-Co$_2$P/Al$_2$O$_3$ was recovered easily from the reaction mixture by centrifugation and reusable even after the fifth recycling experiment without changing its catalytic activity and selectivity (**Figure 3-4**). The initial reaction rate at short reaction time (1 h) was also investigated (white diamonds in **Figure 3-4**) and similar yields of BHMF was obtained with the reused and fresh catalysts, revealing the high reusability of catalyst. Moreover, inductively coupled plasma–atomic emission spectrometry (ICP-AES) of the catalyst before and after the reaction showed almost the same loading amounts of Co and P in nano-Co$_2$P/Al$_2$O$_3$ (befor, Co: 1.96 wt%, P: 0.68 wt%; after, Co: 2.04 wt%, P: 0.74 wt%), which are highly consistent with the recycling experiment results.
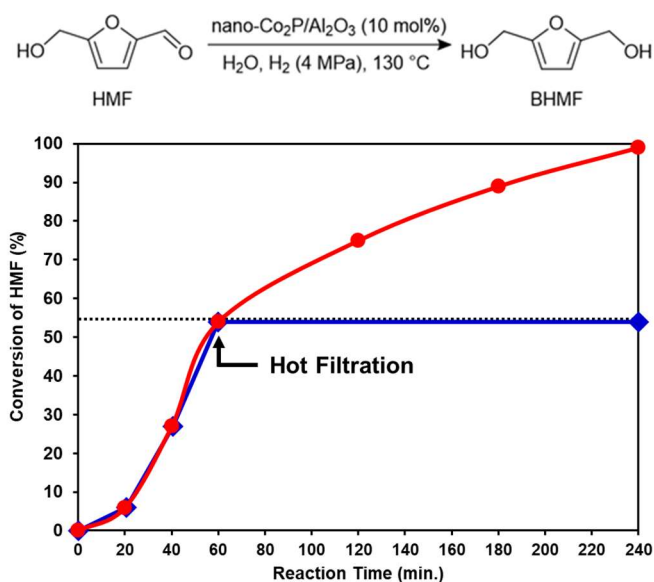
Scheme 3-2. Hot filtration experiment of nano-Co$_2$P/Al$_2$O$_3$ in hydrogenation of HMF to BHMF.
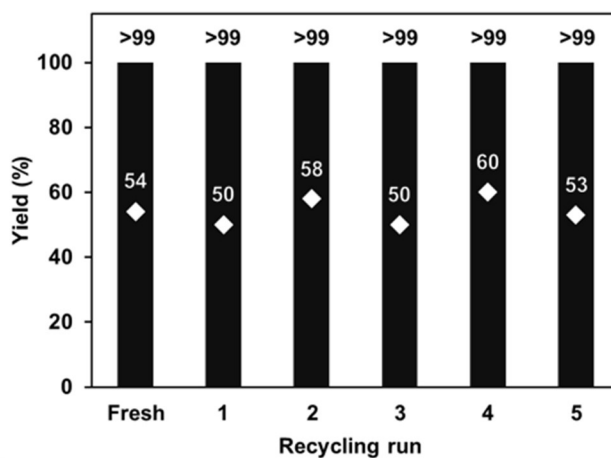
Figure 3-4. Reuse experiments of nano-Co$_2$P/Al$_2$O$_3$ in the hydrogenation of HMF to BHMF. Reaction conditions: nano-Co$_2$P/Al$_2$O$_3$ (10 mol%), HMF (0.25 mmol), H$_2$O (3 mL), H$_2$ (4 MPa), 130 °C. Reaction time: 4 h (black bars), 1 h (white diamonds).

Furthermore, the air stability of nano-Co$_2$P was envaulted by exposing the catalyst to air for settled time and the catalyst was then tested in the hydrogenation of HMF. Notably, the catalytic activity was remained even after 72 h exposure time (**Figure 3-5**), confirming the unique air-stable feature of nano-Co$_2$P.
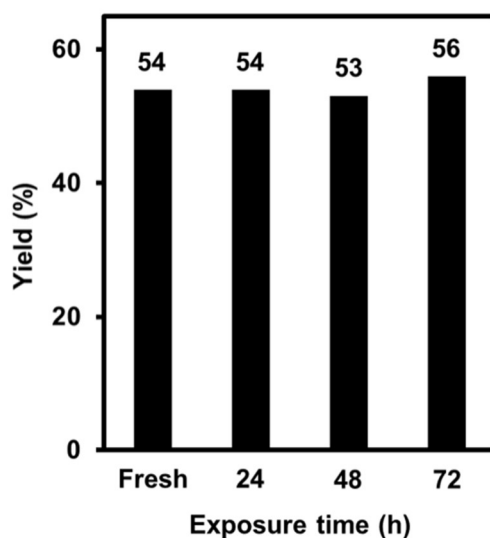
Figure 3-5. Air stability tests of nano-Co$_2$P/Al$_2$O$_3$ in the hydrogenation of HMF to BHMF. Reaction conditions: nano-Co$_2$P/Al$_2$O$_3$ (10 mol %), HMF (0.25 mmol), H$_2$O (3 mL), H$_2$ (4 MPa), 130 °C, 1 h.

The air stability of nano-Co_2P was further investigated by temperature programmed oxidation (TPO) as shown in **Figure 3-6**. The TPO profile showed that O_2 consumption begins to increase from about 130 °C and finishes at 425 °C (**Figure 3-6** (a)). CO_2 gas was also evolved during the TPO experiment, as shown in **Figure 3-6** (b), with the mass signal of CO_2 (m/z = 44) appearing in the 220–440 °C range. The carbon source of the produced CO_2 might originate from residual organic contaminants, such as a surfactant on the surface of nano-Co_2P. From these results, O_2 consumption in the TPO experiment is likely caused by the oxidation of nano-Co_2P and the combustion of residual organics on the surface of nano-Co_2P. The TPO profile clearly showed that nano-Co_2P is not oxidized by O_2 below 130 °C, which demonstrates that nano-Co_2P is air-stable under ambient conditions (catalyst handling conditions). The air stability significantly distinguishes nano-Co_2P from conventional metallic cobalt nanoparticles which are easily oxidized by O_2 even at -50° C [23].
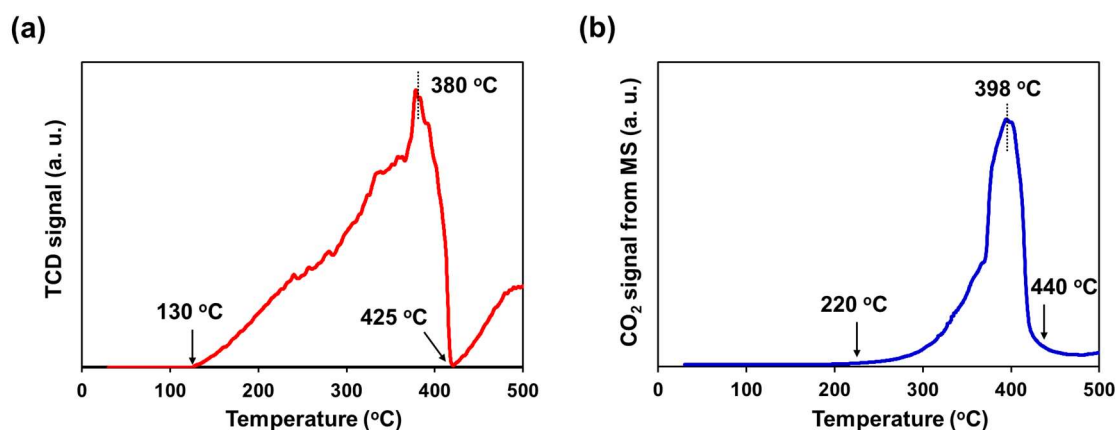
Figure 3-6. (a) TPO profile and (b) evolution of CO_2 during a TPO experiment with nano-Co_2P.

nano-Co_2P/Al_2O_3 was also able to applied in gram-scale expriment: 1.0 g of HMF was soomthly converted into the dirseired product BHMF with high isolated yield (85%, 0.86 g) (**Scheme 3-3**).
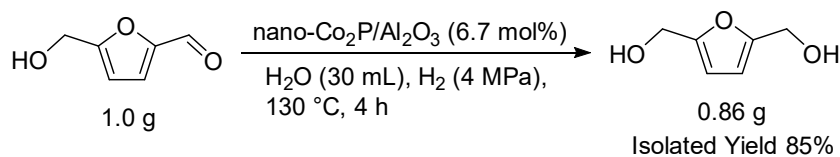
Scheme 3-3. Gram-scale reaction of 5-hydroxymethylfurfural using nano-Co_2P/Al_2O_3.

Encouraged by the high performance of nano-Co_2P/Al_2O_3, the application was studied by using other biomass-derived furfurals. The hydrogenation results of furfural, 5-methylfurfural, and 5-acetoxymethylfurfural in different solvents were summarized in **Table 3-2**.

Table 3-2. Hydrogenation of biomass-derived furfurals using nano-Co_2P/Al_2O_3 catalyst[a]

entry	substrate	solvent	conv.[b] (%)	sel.[b] (%)
1		H_2O	76	71
2		MeOH	85	99
3		1,4-dioxane	29	93
4		H_2O	90	77
5		MeOH	91	99
6		1,4-dioxane	36	92
7[c]		H_2O	54	>99
8[c]		MeOH	31	89
9[c]		1,4-dioxane	5	80
10[d]		H_2O	>99[e]	<1[e,f]
11[d]		MeOH	>99[e]	<1[e,f]
12[d]		1,4-dioxane	>99[e]	82[e]

[a]Reaction conditions: nano-Co_2P/Al_2O_3 (6.7 mol%), substrate (0.25 mmol), solvent (3 mL), H_2 (4 MPa), 130 °C, 2 h. [b]Determined by GC-MS using an internal standard technique. [c]nano-Co_2P/Al_2O_3 (10 mol%), 1 h. [d]H_2 (5 MPa), 150 °C, 12 h. [e]Determined by ^1H NMR using an internal standard technique. [f]BHMF was detected as the main product.

Under the optimized conditions, the carbonyl groups of all tested substrates were selectively coverted to the desired alcohol products in high yields without the formation of any byproduct from furan-ring hydrogenation [24, 25] nor hydrodeoxygenation [26, 27].

3.3. The origin of high performance of nano-Co₂P/Al₂O₃

To clarify the reason for high performance of nano-Co_2P/Al_2O_3, the investigation by Fourier-transform infrared (FT-IR) was carried out as show in **Figure 3-7**. Delightfully, the carbonyl bond stretching vibration peak derived from furfural was observed at 1665 cm^{-1} in the case of furfural-treated nano-Co_2P/Al_2O_3, which is far lower than that on Al_2O_3 (Δ25 cm^{-1}) and furfural vapor (Δ55 cm^{-1}) (**Figures 3-7** (b, c)) [28], revealing the strong activation of the C=O bond of furfural by nano-Co_2P.
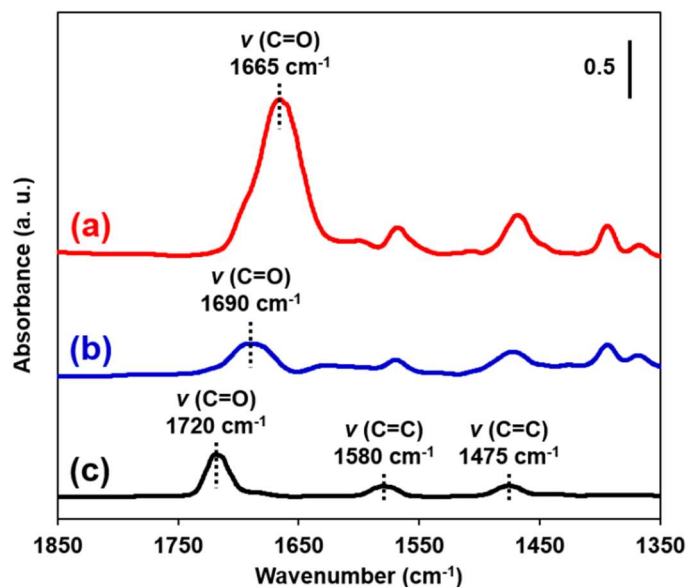
Figure 3-7. FT-IR spectra of (a) furfural-treated nano-Co_2P/Al_2O_3, (b) furfural-treated Al_2O_3, and (c) pure furfural vapor.

The density functional theory (DFT) calculations were employed to figure out the detailed activation states of furfural on the Co_2P surface. Briefly, the adsorption structures can be classified into the following groups: parallel adsorption of both the C=O bond and furan ring on the surface (group A), adsorption of the O atom in C=O and a C-O bond in the furan ring on the surface (group B), and adsorption of only C=O on the surface (group C). The adsorption energies, $\Delta E = E(Co_2P\text{-furfural}) - E(Co_2P) - E(\text{furfural})$, of each group are calculated that A, B, and C are -67.7, -42.7, and -33.6 kcal/mol, respectively. Since a more negative energy means more stable adsorption, thus, group A is the more acceptable adsorption structure during the reaction. In the most stable adsorption structure as shown in **Figure 3-8** (a), the C=O bond length of the furfural molecule elongated from 1.23 to 1.37 Å on the hollow site of nano-Co_2P. In the meantime, the 0.16 electrons from nano-Co_2P transferred to furfural, leading to the decrease of d-electrons on the nano-Co_2P surface around the Fermi level (**Figure 3-8** (b)). Based on these results, strong activation of the carbonyl moiety of furfural was occurred through enhancing the backdonation of d-electrons on the nano-Co_2P to its π^* orbital to activate the C=O bond, which is consistent with the results from the IR study.
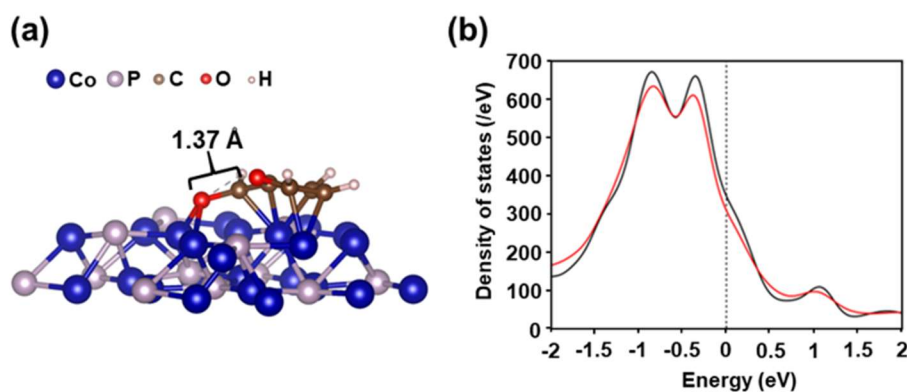
Figure 3-8. (a) Optimized structure of furfural adsorbed on the Co_2P surface and (b) projected density of states of d-electrons on the Co_2P surface (i.e., the first layer) with (red) and without (black) furfural.

4. Conclusion

This chapter describes the unique catalysis of a supported cobalt phosphide nanoalloy for the selective hydrogenation of furfural derivatives for the first time. The air-stable metallic nature of nano-Co$_2$P catalyst enables its easy-handling and is ready to use unlike conventional catalyst requiring H$_2$ pretreatment. The catalyst shows high activity in this reaction and can be reused without significant activity or selectivity loss. IR studies and DFT calculations reveal that C═O group of substrate is activated by nano-Co$_2$P catalyst through the strong backdonation of electrons from cobalt species to the π^* orbital of the C═O group, thereby facilitating the hydrogenation reaction.

References

1   Nong, D.; Escobar, N.; Britz, W.; Börner, J. *J. Cleaner Prod.* **2020**, *272*, 122738.

2   Troiano, D.; Orsat, V.; Dumont, M. J. *ACS Catal.* **2020**, *10*, 9145–9169.

3   Dheskali, E.; Koutinas, A. A.; Kookos, I. K. *Chem. Eng. Res. Des.* **2020**, *163*, 273–280.

4   Alonso, D. M.; Bond, J. Q.; Dumesic, J. A. *Green Chem.* **2010**, *12*, 1493–1513.

5   Nakagawa, Y.; Tamura, M.; Tomishige, K. *ACS Catal.* **2013**, *3*, 2655–2668.

6   Chen, S.; Wojcieszak, R.; Dumeignil, F.; Marceau, E.; Royer, S. *Chem. Rev.* **2018**, *118*, 11023–11117.

7   Villaverde, M.; Bertero, N.; Garetto, T.; Marchi, A. *Catal. Today* **2013**, *213*, 87–92.

8   Pushkarev, V.; Musselwhite, N.; An, K.; Alayoglu, S.; Somorjai, G. *Nano Lett.* **2012**, *12*, 5196–5201.

9   An, K.; Musselwhite, N.; Kennedy, G.; Pushkarev, V.; Robert Baker, L.; Somorjai, G. *J. Colloid Interface Sci.* **2013**, *392*, 122–128.

10   Taylor, M.; Durndell, L.; Isaacs, M.; Parlett, C.; Wilson, K.; Lee, A.; Kyriakou, G. *Appl. Catal. B* **2016**, *180*, 580–585.

11   Chen, J.; Lu, F.; Zhang, J.; Yu, W.; Wang, F.; Gao, J.; Xu, J. *ChemCatChem* **2013**, *5*, 2822–2826.

12   Chatterjee, M.; Ishizaka, T.; Kawanami, H. *Green Chem.* **2014**, *16*, 4734–4739.

13   Tamura, M.; Tokonami, K.; Nakagawa, Y.; Tomishige, K. *Chem. Commun.* **2013**, *49*, 7034–7036.

14   Prakruthi, H.R.; Chandrashekara, B.M.; Jai, P.B.S.; Bhat, Y.S. *J. Ind. Eng. Chem.* **2018**, *62*, 96–105.

15   Kotbagi, T.; Gurav, H.; Nagpure, A.; Chilukuri, S.; Bakker, M. *RSC Adv.* **2016**, *6*, 67662–67668.

16   Zhu, Y.; Kong, X.; Yin, J.; You, R.; Zhang, B.; Zheng, H.; Wen, X.; Zhu, Y.; Li, Y.-W. *J. Catal.* **2017**, *353*, 315–324.

17   Ma, Y.; Xu, G.; Wang, H.; Wang, Y.; Zhang, Y.; Fu, Y. *ACS Catal.* **2018**, *8*, 1268–1277.

18 Watari, R.; Matsumoto, N.; Kuwata, S.; Kayaki, Y. *ChemCatChem* **2017**, *9*, 4501–4507.

19 Zhu, Y.; Kong, X.; Zheng, H.; Ding, G.; Zhu, Y.; Li, Y.-W. *Catal. Sci. Technol.* **2015**, *5*, 4208–4217.

20 Zhou, L.; Zhu, C.; Edmonds, L.; Yang, H.; Cui, W.; Li, B. *RSC Adv.* **2014**, *4*, 43220–43226.

21 Cotton, F. A. G. *Progress in Inorganic Chemistry: Metal–Metal Bonds in Transition Metal Compounds*, Wiley-VCH, New York, **1968**.

22 Wagner, C. D.; Riggs, W. M.; Davis, L. E.; Moulder J. F.; Muilenberg, G. E. *Handbook of X-Ray Photoelectron Spectroscopy*, Perkin-Elmer, Eden Prairie, **1979**.

23 H. F. J. van't Blik et al., *J. Catal.* **1986**, *97*, 188–199.

24 Zhu, Y.; Kong, X.; Zheng, H.; Ding, G.; Zhu, Y.; Li, Y.-W. *Catal. Sci. Technol.* **2015**, *5*, 4208–4217.

25 Alamillo, R.; Tucker, M.; Chia, M.; Pagán-Torres, Y.; Dumesic, J. *Green Chem.* **2012**, *14*, 1413–1419.

26 Kong, X.; Zhu, Y.; Zheng, H.; Dong, F.; Zhu, Y.; Li, Y.-W. *RSC Adv.* **2014**, *4*, 60467–60472.

27 Kumalaputri, A. J.; Bottari, G.; Erne, P. M.; Heeres, H. J.; Barta, K. *ChemSusChem* **2014**, *7*, 2266–2275.

28 Khassin, A. A.; Yurieva, T. M.; Kaichev, V. V.; Bukhtiyarov, V. I.; Budneva, A. A.; Paukshtis, E. A.; Parmon, V. N. *J. Mol. Catal. A: Chem.* **2001**, *175*, 189–204.

Chapter I V.

Reductive Amination of Carbonyl Compounds to Primary Amines

by Cobalt Phosphide Nanorod Catalyst

1. Introduction

Primary amines are important fine chemicals and central intermediates for the producing pharmaceuticals, surfactants, and solvents [1-3]. The reaction of carbonyl compounds with ammonia and reducing agent, called reductive amination, is extensively employed to the primary amine synthesis in laboratories and industries [4, 5]. Particularly, catalytic reductive aminations using molecular hydrogen represents one of the most atom-efficient and sustainable methods for s due to the carbonyl compounds and reagents are inexpensive, diversely available starting materials and only water is theoretically formed as by-product [6, 7] (**Scheme 4-1**). Commonly, this transformation is regarded as a challenging reaction because of the low selectivity caused by the over-alkylation and directly hydrogenation of carbonyl compounds to the corresponding alcohols. Therefore, the development of highly active and selective catalyst is of central importance and continues to attracting attentions in both academic and industrial fields.
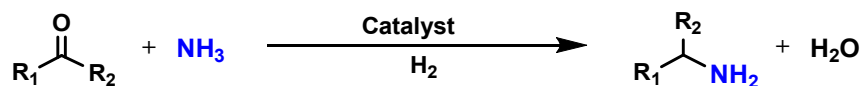
Scheme 4-1. Catalytic reductive amination of carbonyl compounds to primary amines with molecule hydrogen.

Impressive progress has been made in developing catalysts based on earth-abundant metal-based heterogeneous catalysts for reductive amination [8-14]. Conventional Ni or Co sponge metals, also named Raney catalysts, are commonly used for industrial reductive amination reactions [15-17]. Unfortunately, sponge metal catalysts are of high air-sensitivity and have low activity, requiring harsh reaction conditions, e.g., high H_2 pressures. Therefore, the development of air-stable and efficient catalyst for the reductive amination to primary amines is highly demanded but also challenging.

During the past decades, there is a "Nitrogen-doping strategy" to develop air-stable non-noble-metal catalysts through the pyrolysis treatment of the metal-N complex precursor, resulting a

kind of nanostructured non-pricious metal nanoparticles (NPs) coating with nitrogen-doped materials. These catalysts exhibit notable catalysis in heterogeneous reactions fields, including the stability derived from the encapsulation structure with N-doped carbon layers [8-12, 15-22]. Up to now, several Ni, Co, and Fe-based NPs prepared by this method are also reported to be air-stable and reusable catalyst for reductive amination reaction (**Figure 4-1** (a)) [8-12]. However, those catalytic systems still need flammable ammonia gas and/or high H_2 pressures to achieve this reaction. Moreover, their N-doped carbon layers inevitably shields the active sites on the surface, which partly decreases the activities. In other words, their air stability and activity are in a trade-off relationship. Thus, the development of novel, efficient, and green non-noble-metal NPs catalyst for reductive amination is highly desired. Herein, we newly prepare a cobalt phosphide nanorods (Co_2P NRs) catalyst based on the "P-alloying strategy", which can overcome above problems and serve as smart catalyst in the reductive amination reaction (**Figure 4-1** (b)).
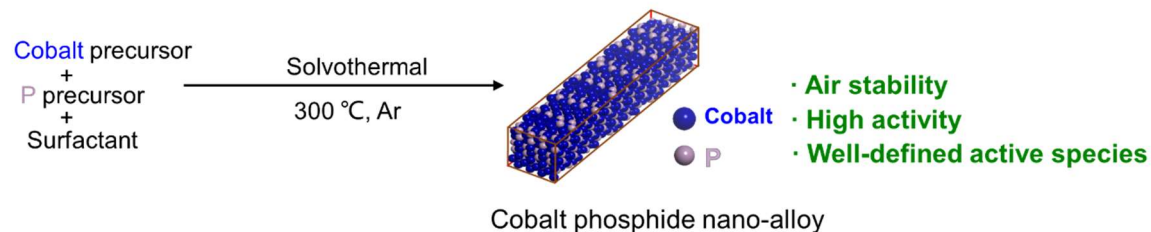
Figure 4-1. Air-stable non-precious metal catalysts for reductive amination based on (a) an N-doping strategy and (b) a P-alloying strategy.

This chapter represents a novel and well-defined Co_2P NR is synthesized for reductive amination of a wide range of carbonyl compounds to primary amines in high yields. The high activity of Co_2P NR eables this reaction processed under mild conditons (1 bar H_2/room temperature), which represents the first example of a non-pricious metal catalyst for reductive amination under ambient condition. Furthermore, Co_2P NR is easily recovered from the reaction mixture and can be reused without any loss of activity.

2. Experimental section

2.1. General

All the organic reagents were obtained commercially and the purity of each reagent was checked before use.

Co(acac)$_2$ was purchased from Mitsuwa Pure Chemicals. 1-Octadecene (technical grade; 90%) was purchased from Sigma-Aldrich. Co. Hexadecylamine and triphenyl phosphite were purchased from Tokyo Chemical Industry Co., Ltd. SiO$_2$ (Q-9) was procured from Fuji Silysia Chemicals Ltd. Raney Co (about 48%) was purchased from FUJIFILM Wako Pure Chemical. All the substrates were commercially available.

Benzaldehyde (>98%), p-anisaldehyde (>99%), 2,3-dimethoxybenzaldehyde (>98%), biphenyl-4-carboxaldehyde (>98%), 4-acetamidobenzaldehyde (>98%), 5-hydroxymethyl-2-furaldehyde (>95%), 4-(4,4,5,5-tetramethyl-1,3,2-dioxaborolan-2-yl)benzaldehyde (>97%), 5-methylfurfural, cyclohexanecarbaldehyde, heptanal (98%), 4'-(methylsulfonyl)acetophenone (>98%), 4-acetylpyridine (>97%), benzophenone (>99%), 1-indanone (>98%), 2-adamantanone (>98%), 2-octanone (>98%), 2-dodecanone (>98%), cyclohexanone (>99%), and estrone (>98%) were obtained from Tokyo Chemical Industry Co., Ltd. p-Tolualdehyde (97%), p-chlorobenzaldehyde (>98%), acetophenone, 1-(4-methoxyphenyl)ethanone (>98%), p-chloroacetophenone (>95%), p-bromoacetophenone (98%), 4-(N-acetylamino)acetophenone (96%), and haloperidol (>98%) were obtained from FUJIFILM Wako Pure Chemical.

^{1}H and ^{13}C nuclear magnetic resonance (NMR) spectra were recorded on a JEOL JNM-ESC400 spectrometer. Transmission electron microscopy (TEM) observations were conducted using a JEM-ARM200F instrument operated at 200 kV. Scanning transmission electron microscopy (STEM) images with elemental maps were collected using a FEI Titan Cubed G2 60-300 instrument, operated at 300 kV, and equipped with a Super-X energy-dispersive X-ray

spectroscopy (EDX) detector. Elemental mapping based on quantification analysis of EDX spectra was carried out using Esprit.

Co K-edge X-ray absorption spectra were recorded at room temperature using a Si (311) or Si (111) monochromator at the BL01B1 and BL14B2 lines, SPring-8, Japan Synchrotron Radiation Research Institute (JASRI), Harima, Japan. XRD was performed using a Philips X′Pert-MPD diffractometer with Cu-Kα radiation. XPS analysis was performed on an ESCA1700R system equipped with a dual Mg/Al X-ray source and a hemispherical analyzer operating in fixed-analyzer transmission mode. The spectra were obtained using a pass energy of 58.7 eV and an Al-K X-ray source operated at 350 W and 14 kV. Excess charges on the samples were neutralized by argon ion sputtering. The analysis area was 0.8 mm × 2 mm. The working pressure in the analysis chamber was less than 1×10^{-7} Pa. Spectra were acquired in the Co 2p, O 1s, C 1s, and Si 2p regions. The C 1s peak at a binding energy (BE) of 285 eV was used as an internal reference.

Fourier-transform infrared (FT-IR) spectra were recorded on a JASCO FT-IR 4100 spectrometer equipped with a mercury cadmium telluride detector.

2.2. Preparation of catalysts

Preparation of Co₂P NRs

All the reactions were carried out in argon atmosphere using standard Schlenk line techniques. In a typical synthesis, Co(acac)$_2$ (1.0 mmol) and 2.4 g (10.0 mmol) of hexadecylamine were combined with 10.0 mL of 1-octadecene and 2.6 mL (10.0 mmol) of triphenyl phosphite in a Schlenk flask. The mixture was heated to 150 °C under argon flow and maintained for 1 h. The temperature was then increased to 300 °C and maintained for 2 h, yielding a black colloidal solution. The mixture was then cooled in air to room temperature. The obtained colloid was isolated by precipitation with acetone, and the redispersion and

precipitation cycles were continued using a chloroform-acetone mixed solvent (chloroform:acetone = 1:1) until the supernatant liquid was transparent. The obtained powder was dried overnight in vacuum at room temperature to produce Co_2P NRs.

Preparation of CoP NPs

In a typical synthesis, under a flow of argon, $Co(acac)_2$ (1 mmol), 1-octadecene (5.0 mL, 15.6 mmol) and oleylamine (10 mL, 30.4 mmol) were placed in a Schlenk flask. The mixture was stirred and heated to 120 °C, and this temperature was maintained for 1 h. Then, triphenylphosphine (5.0 mL, 11 mmol) was added to the above solution and heated to 340 °C for 4 h. Afterwards, the mixture was allowed to cool in air to room temperature. To remove as much organics as possible, redispersion and precipitation cycles were continued until the supernatant liquid was transparent using a hexane-ethanol mixed solvent (hexane:ethanol = 1:1). The obtained powder was dried at room temperature in vacuum overnight.

Preparation of Co/SiO$_2$

Co/SiO_2 was prepared as follows. SiO_2 was soaked in an aqueous solution of $Co(NO_3)_2$. After stirring for 10 min, the pH was adjusted to 10.0 with an aqueous NaOH solution and the mixture stirred at room temperature in air for 6 h. The resulting slurry was filtered. The recovered solid was washed with deionized water and then dried at room temperature in vacuo to generate Co/SiO_2. Co/SiO_2 was then treated under H_2 at atmospheric pressure and 250 °C for 2 h to provide Co/SiO_2-Red.

2.3. Reaction procedure

A typical reaction procedure for the reductive amination using Co_2P NR was as follows.

The synthesis of primary amine from aldehyde and aq. NH_3

The Co_2P NRs (4.0 mg) were placed in a 50-mL stainless-steel autoclave with a Teflon inner cylinder, followed by addition of benzaldehyde (**1a**) (0.5 mmol) and aq. NH_3 (3.0 mL). The reaction mixture was stirred vigorously at 100 °C under 5 bar of H_2. The reaction solution was then analyzed by GC–MS to determine the conversion and yield using an internal standard method.

The yields of primary and imine are calculated as follows:

$$\text{Yield (\%) of primary amine} = \frac{\text{the mol of primary amine product}}{\text{the initial mol of substrate}} \times 100\%$$

$$\text{Yield (\%) of imine} = \frac{\text{the mol of imine product}}{\text{the initial mol of substrate}} \times 2 \times 100\%$$

After reaction, to obtain the hydrochloride salts, the crude reaction mixture was filtered to remove the catalyst and the ammonia was removed under vacuum conditions. The mixture was then added to a hydrogen chloride solution (1.25 M, 1,4-dioxane). The solvent was removed leaving behind the corresponding salt, giving the pure hydrochloride salts, which were subjected to NMR analysis.

The synthesis of primary amine from ketone and NH_4OAc

The Co_2P NRs (4.0 mg) were placed in a 50-mL stainless-steel autoclave with a Teflon inner cylinder, followed by adding ketone, ethanol (3 mL) and NH_4OAc (0.20 g). The reaction mixture was stirred vigorously at 100 °C under 10 bar of H_2. The reaction solution was then analyzed by GC–MS to determine the conversion and yield using an internal standard method. The calculation of conversion of substrate and yield of primary amine and imine are similar to these mentioned in the case of aldehyde. After reaction, to obtain the hydrochloride salts, the crude reaction

mixture was filtered to remove the catalyst and the ammonia was removed under vacuum conditions. The mixture was then added to a hydrogen chloride solution (1.25 M, 1,4-dioxane). The solvent was removed leaving behind the corresponding salt, giving the pure hydrochloride salts, which were subjected to NMR analysis.

2.4. Recycling experiment

After the reaction, Co_2P NRs were recovered by filtration. The catalyst was washed with water and dried at room temperature in vacuo without further purification or reactivation before reuse.

2.5. Product identification
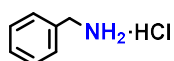
benzylamine hydrochloride

^{1}H NMR (400 MHz, DMSO-d_6): δ = 8.49 (s, 3H), 7.50 (d, J = 6.8 Hz, 2H), 7.44–7.34 (m, 3H), 4.01 (s, 2H) ppm. ^{13}C NMR (100 MHz, DMSO-d_6): δ = 134.05, 128.84, 128.47, 128.29, 42.09 ppm.
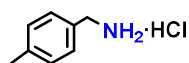
p-tolylmethanaminium hydrochloride

^{1}H NMR (400 MHz, DMSO-d_6): δ = 8.25 (s, 3H), 7.37 (d, J = 8.20 Hz, 2H), 7.21 (d, J = 8.20 Hz, 2H), 3.93 (s, 2H), 2.30 (s, 3H) ppm. ^{13}C NMR (100 MHz, DMSO-d_6): δ = 137.69, 131.53, 129.11, 128.91, 42.08, 20.82 ppm.
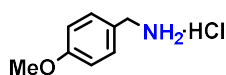
(4-methoxyphenyl)methanaminium hydrochloride

^{1}H NMR (400 MHz, DMSO-d_6): δ = 8.18 (s, 3H), 7.40 (d, J = 7.80 Hz, 2H), 6.97 (d, J = 7.80 Hz, 2H), 3.94 (s, 2H), 3.76 (s, 3H) ppm. ^{13}C NMR (100 MHz, DMSO-d_6): δ = 159.20, 130.61, 126.22, 113.79, 55.20, 41.64 ppm.
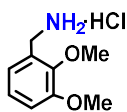
2,3-dimethoxybenzylamine hydrochloride

^{1}H NMR (400 MHz, DMSO-d_6): δ = 8.60 (s, 3H), 7.12–7.08 (m, 3H), 3.97 (s, 2H), 3.83 (s, 3H), 3.80 (s, 3H) ppm. ^{13}C NMR (100 MHz, DMSO-d_6): δ = 152.24, 146.75, 127.10, 124.17, 121.12, 113.68, 60.59, 55.70, 36.79 ppm.
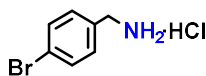
(4-bromophenyl)methanaminium hydrochloride

^{1}H NMR (400 MHz, DMSO-d_6): δ = 8.49 (s, 3H), 7.61 (d, J = 7.92 Hz, 2H), 7.48 (d, J = 7.83 Hz, 2H), 3.98 (s, 2H) ppm. ^{13}C NMR (100 MHz, DMSO-d_6): δ = 133.48, 131.30, 131.27, 121.59, 41.37 ppm.
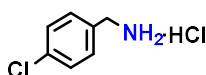
(4-chlorophenyl)methanaminium hydrochloride

^{1}H NMR (400 MHz, DMSO-d_6): δ = 8.65 (s, 3H), 7.56 (d, J = 8.20 Hz, 2H), 7.47 (d, J = 8.20 Hz, 2H), 3.98 (s, 2H). ^{13}C NMR (100 MHz, DMSO-d_6): δ = 133.19, 133.11, 131.11, 128.50, 41.40 ppm.
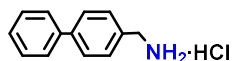
(1,1'-biphenyl)-4-methanaminium hydrochloride

^{1}H NMR (400 MHz, DMSO-d_6): δ = 8.27 (s, 3H), 7.70 (m, 4H), 7.56 (m, 2H), 7.48 (m, 2H), 7.39 (m, 1H), 4.08 (s, 2H) ppm. ^{13}C NMR (100 MHz, DMSO-d_6): δ = 140.30, 139.55, 133.28, 129.58, 129.02, 127.71, 126.81, 126.72, 41.89 ppm.
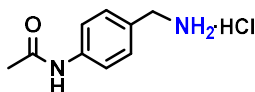
(4-acetamidophenyl)methanaminium hydrochloride

^{1}H NMR (400 MHz, DMSO-d_6): δ = 10.28 (s, 1H), 8.49 (s, 3H), 7.64 (d, J = 8.80 Hz, 2H), 7.42 (d, J = 8.80 Hz, 2H), 3.93 (s, 2H), 2.09 (s, 3H) ppm. ^{13}C NMR (100 MHz, DMSO-d_6): δ = 168.48, 139.56,

130.37, 129.51, 118.88, 41.85, 23.98 ppm.
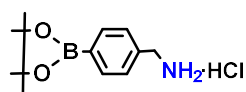
(4-(4,4,5,5-tetramethyl-1,3,2-dioxaborolan-2-yl)phenyl)methanaminium hydrochloride

^{1}H NMR (400 MHz, DMSO-d_6): δ = 8.72 (s, 3H), 7.80 (d, J = 8.22 Hz, 2H), 7.60 (d, J = 8.22 Hz, 2H),

4.15 (s, 2H), 1.36 (s, 12H) ppm. ^{13}C NMR (100 MHz, DMSO-d_6): δ = 134.59, 134.33, 129.97, 128.36,

83.73, 42.10, 24.72 ppm.
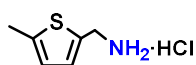
(5-methylthien-2-yl)methylamine hydrochloride

^{1}H NMR (400 MHz, methanol-d_4): δ = 6.77 (d, J = 3.62 Hz, 1H), 6.49 (d, J = 3.62 Hz, 1H), 3.99 (s,

2H), 2.31 (s, 2H), 2.23 (s, 3H) ppm. ^{13}C NMR (100 MHz, methanol-d_4): δ = 144.38, 132.85, 128.46,

127.60, 39.69, 16.02 ppm.
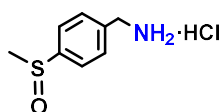
(4-(methylsulfinyl)phenyl)methanamine hydrochloride

^{1}H NMR (400 MHz, methanol-d_4): δ = 7.85 (d, J = 8.04 Hz, 2H), 7.77 (d, J = 8.42, 2H), 4.29 (s, 2H),

2.87 (s, 3H) ppm. ^{13}C NMR (100 MHz, methanol-d_4): δ = 148.10, 138.78, 132.15, 126.53, 44.63, 44.47

ppm.
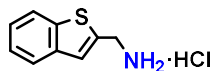
Benzo[b]thiophen-2-yl methanamine hydrochloride

^{1}H NMR (400 MHz, methanol-d_4): δ = 7.99 (d, J = 9.20 Hz, 1H), 7.94 (d, J = 8.98, 1H), 7.61 (s, 1H),

7.53–7.46 (m, 2H), 4.55 (s, 2H) ppm. ^{13}C NMR (100 MHz, methanol-d_4): δ = 142.60, 141.61, 137.19,

127.97, 127.27, 126.80, 125.95, 124.24, 40.32 ppm.
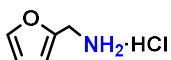
Furan-2-ylmethanamine hydrochloride

^{1}H NMR (400 MHz, DMSO-d_6): δ= 8.50 (sbr, 3H), 7.73 (m 1H), 6.56–6.54 (m, 1H), 6.48–5.51 (m, 1H), 4.06 (m, 2H) ppm. ^{13}C NMR (100 MHz, DMSO-d_6): δ = 147.40, 143.54, 110.87, 110.26, 34.93 ppm.
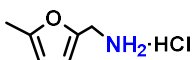
5-methyl-2-furanylmethanamine hydrochloride

^{1}H NMR (400 MHz, DMSO-d_6): δ = 8.38 (s, 3H), 6.43 (d, J =3.20 Hz, 1H), 6.12 (d, J =3.20 Hz, 1H), 4.01 (s, 2H), 2.29 (s, 3H) ppm. ^{13}C NMR (100 MHz, DMSO-d_6): δ = 152.13, 145.94, 111.11, 106.89, 34.96, 13.24 ppm.
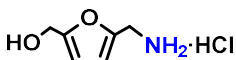
5-aminomethylfurfuryl alcohol hydrochloride

^{1}H NMR (400 MHz, methanol-d_4): 6.54 (d, J = 3.13 Hz, 1H), 6.48 (d, J =3.13 Hz, 1H), 4.68 (s, 2H), 4.18 (s, 2H) ppm. ^{13}C NMR (100 MHz, methanol-d_4): δ = 156.80, 155.35, 109.30, 107.57, 57.59, 39.52 ppm.
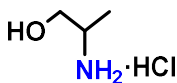
DL-2-amino-1-propanol hydrochloride

^{1}H NMR (400 MHz, methanol-d_4): 3.79 (dd, J = 16.0, 7.2 Hz, 1H), 3.59 (dd, J = 18.4, 2.8 Hz, 1H), 3.45–3.36 (m, 1H), 1.35 (d, J = 6.4 Hz, 3H) ppm. ^{13}C NMR (100 MHz, methanol-d_4): δ = 65.16, 51.38, 16.34 ppm.
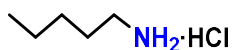
pentan-1-aminium hydrochloride

^{1}H NMR (400 MHz, DMSO-d_6): δ = 7.95 (s, 3H), 2.73 (t, J = 7.32 Hz, 2H), 1.56 (m, 2H), 1.33–1.26 (m, 4H), 0.88 (t, J = 6.84 Hz, 3H) ppm. ^{13}C NMR (100 MHz, DMSO-d_6): δ = 38.65, 27.86, 26.51, 21.53, 13.63 ppm.
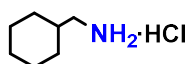
cyclohexanemethanamine hydrochloride

^{1}H NMR (400 MHz, DMSO-d_6): δ = 7.84 (s, 3H), 2.62 (d, J = 6.45 Hz, 2H), 1.69–1.51 (m, 6H), 1.18–1.15 (m, 3H), 0.93–0.88 (m, 2H) ppm. ^{13}C NMR (100 MHz, DMSO-d_6): δ = 44.35, 35.33, 29.60, 25.52, 24.95 ppm.
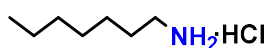
hexylamine hydrochloride

^{1}H NMR (400 MHz, DMSO-d_6): δ = 7.78 (s, 3H), 2.78–2.71 (m, 2H), 1.57–1.47 (m, 8H), 0.90– 0.84 (m, 3H) ppm. ^{13}C NMR (100 MHz, DMSO-d_6): δ = 38.71, 31.08, 28.24, 26.90, 25.87, 22.02, 13.95 ppm.
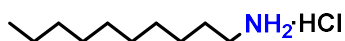
1-decylamine hydrochloride

^{1}H NMR (400 MHz, DMSO-d_6): δ = 7.75 (s, 3H), 2.82–2.62 (m, 2H), 1.54–1.48 (m, 2H), 1.30–1.22 (m, 14H), 0.93–0.78 (m, 3H) ppm. ^{13}C NMR (100 MHz, DMSO-d_6): δ = 38.74, 31.16, 28.77, 28.73, 28.58, 28.42, 26.88, 25.70, 21.99, 13.87 ppm.
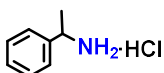
1-phenylethanaminium hydrochloride

^{1}H NMR (400 MHz, DMSO-d_6): δ = 8.68 (s, 3H), 7.58–7.52 (m, 2H), 7.44–7.34 (m, 3H), 4.40–4.34

(m, 1H), 1.54 (d, J = 6.82 Hz, 3H) ppm. ^{13}C NMR (100 MHz, DMSO-d_6): δ = 139.53, 128.68, 128.34, 126.89, 50.06, 20.87 ppm.
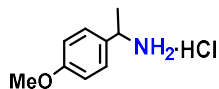
1-(4-methoxyphenyl)ethanaminium hydrochloride

^{1}H NMR (400 MHz, DMSO-d_6): δ = 8.56 (s, 3H), 7.48 (d, J = 6.81 Hz, 2H), 6.96 (d, J = 8.45 Hz, 2H), 4.35–4.30 (m, 3H), 1.52 (d, J = 6.41 Hz, 3H) ppm. ^{13}C NMR (100 MHz, DMSO-d_6): δ = 159.24, 131.28, 128.47, 114.11, 55.52, 49.74, 20.80 ppm.
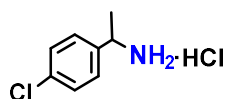
1-(4-chlorophenyl)ethanaminium hydrochloride

^{1}H NMR (400 MHz, DMSO-d_6): δ = 7.63 (d, J = 7.62, 2H), 7.48 (d, J = 8.43 Hz, 2H), 4.44–4.39 (m, 1H), 1.54 (d, J = 6.41 Hz, 3H) ppm. ^{13}C NMR (100 MHz, DMSO-d_6): 138.50, 132.76, 129.04, 128.52, 49.37, 20.85 ppm.
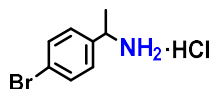
1-(4-bromophenyl)ethanamine hydrochloride

^{1}H NMR (400 MHz, DMSO-d_6): δ = 8.35 (s, 3H), 7.46 (d, J = 8.62 Hz, 2H), 7.26 (d, J = 8.25 Hz, 2H), 4.24–4.19 (m, 1H), 1.44 (d, J = 6.53 Hz, 3H) ppm. ^{13}C NMR (100 MHz, DMSO-d_6): δ = 138.91, 131.61, 129.37, 121.64, 49.49, 20.66 ppm.

1-(4-acetamidophenyl)ethanaminium hydrochloride

^{1}H NMR (400 MHz, DMSO-d_6): δ = 10.22 (s, 1H), 8.54 (s, 3H), 7.63 (d, J = 8.04 Hz, 2H), 7.44 (d, J = 8.04 Hz, 2H), 4.36–4.27 (m, 1H), 2.06 (s, 3H), 1.51 (d, J = 7.65 Hz, 3H) ppm. ^{13}C NMR (100 MHz,

DMSO-d_6): δ = 168.54, 139.51, 133.65, 127.32, 119.06, 49.46, 20.62 ppm.
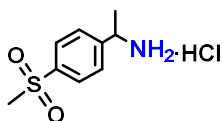
1-(4-(methylsulfonyl)phenyl)ethanaminium hydrochloride

^{1}H NMR (400 MHz, DMSO-d_6): δ = 8.95 (s, 3H), 8.02 (d, J = 6.80 Hz, 2H), 7.87 (d, J = 6.80 Hz, 2H), 4.55–4.51 (m, 1H), 3.32 (s, 3H), 1.62 (d, J = 6.45 Hz, 3H) ppm. ^{13}C NMR (100 MHz, DMSO-d_6): δ = 145.32, 140.84, 128.35, 127.52, 50.14, 44.03, 20.94 ppm.
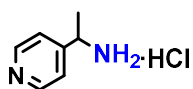
1-(pyridin-4-yl)ethanaminium hydrochloride

^{1}H NMR (400 MHz, DMSO-d_6): δ = 9.30 (s, 3 H), 8.97 (s, 2H), 8.27–8.17 (m, 2H), 4.68 (q, J = 6.44 Hz, 1H), 1.56 (d, J = 7.03 Hz, 3H) ppm. ^{13}C NMR (100 MHz, DMSO-d_6): δ = 157.53, 143.26, 125.33, 49.46, 20.50 ppm.
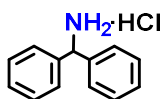
diphenylmethanaminium hydrochloride

^{1}H NMR (400 MHz, DMSO-d_6): δ = 9.00 (s, 3H), 7.53–7.34 (m, 10H), 5.64 (s, 1H) ppm. ^{13}C NMR (100 MHz, DMSO-d_6): δ = 138.52, 129.20, 128.75, 127.58, 57.40 ppm.
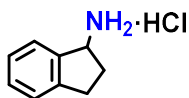
2,3-dihydro-1H-inden-1-aminium hydrochloride

^{1}H NMR (400 MHz, DMSO-d_6): δ = 8.71 (s, 3H), 7.71–7.67 (m, 1H), 7.33–7.22 (m, 3H), 4.70–4.61 (m, 1H), 3.12–3.01 (m, 1H), 2.91–2.80 (m, 1H), 2.49–2.39 (m, 1H), 2.08–1.95 (m, 1H) ppm. ^{13}C NMR (100 MHz, DMSO-d_6): δ = 143.98, 139.48, 128.93, 126.60, 125.21, 124.87, 54.63, 30.33, 29.90 ppm.
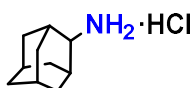
adamantan-2-aminium hydrochloride

^{1}H NMR (400 MHz, DMSO-d_6): δ = 8.39 (s, 3H), 3.25–3.20 (m, 1H), 2.09–1.48 (m, 14H) ppm. ^{13}C NMR (100 MHz, DMSO-d_6): δ = 54.76, 36.88, 36.23, 29.95, 29.53, 26.47, 26.38 ppm.
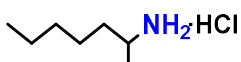
heptan-2-amine hydrochloride

^{1}H NMR (400 MHz, DMSO-d_6): δ = 8.01 (s, 3H), 3.15–3.05 (m, 1H), 1.65–1.35 (m, 2H), 1.35–1.20 (m, 6H), 1.17 (d, J = 7.23 Hz, 3H), 0.90–0.84 (m, 3H) ppm. ^{13}C NMR (100 MHz, DMSO-d_6): δ = 46.80, 34.09, 31.00, 24.46, 21.92, 18.16, 13.87 ppm.
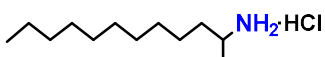
2-dodecylamine hydrochloride

^{1}H NMR (400 MHz, DMSO-d_6): δ = 7.95 (s, 3H), 3.16–3.05 (m, 1H), 1.64–1.17 (m, 18H), 1.07 (d, J = 6.44 Hz, 3H), 0.88–0.83 (m, 3H) ppm. ^{13}C NMR (100 MHz, DMSO-d_6): δ = 47.06, 34.42, 31.58, 29.32, 29.27, 29.18, 29.10, 29.04, 25.08, 22.39, 18.44, 14.29 ppm.
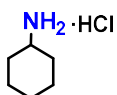
cyclohexylamine Hydrochloride

^{1}H NMR (400 MHz, DMSO-d_6): δ = 8.20 (s, 3H), 2.98–2.87 (m, 1H), 1.96–1.03 (m, 10H) ppm. ^{13}C NMR (100 MHz, DMSO-d_6): δ = 49.87, 30.62, 24.94, 24.18 ppm.
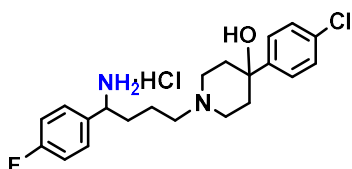
4-(4-(4-chlorophenyl)-4-hydroxypiperidin-1-yl)-1-(4-fluorophenyl)butan-1-amine

hydrochloride

^{1}H NMR (400 MHz, DMSO-d_6): δ = 8.66 (s, 3H), 7.63–7.54 (m, 2H), 7.44 (d, J = 8.40 Hz, 2H), 7.38 (d, J = 8.42 Hz, 2H), 7.28–7.19 (m, 2H), 5.56 (s, 1H), 4.29–4.25 (m, 1H), 3.18–3.01 (m, 6H), 2.41–2.28 (m, 2H), 2.06–1.47 (m, 6H) ppm. ^{13}C NMR (100 MHz, DMSO-d_6): δ = 161.04, 147.03, 133.87 (d, J = 3.02 Hz), 131.64, 129.95 (d, J = 5.04 Hz), 128.18, 126.77, 115.85, 115.65, 68.05, 54.89, 53.14, 48.20, 34.87, 31.48, 19.85 ppm.
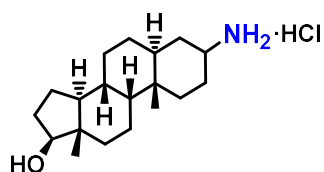
(5S,8R,9R,10S,13S,14S,17S)-17-hydroxy-10,13-dimethylhexadecahydro-1H-cyclopenta[a]phenanthren-3-amine hydrochloride

^{1}H NMR (400 MHz, DMSO-d_6): δ = 8.08 (s, 3H), 4.23–4.00 (m, 1H), 3.47–3.39 (m, 1H), 3.34 (s, 1H), 1.87–1.77 (m, 2H), 1.77–1.66 (m, 2H), 1.66–1.58 (m, 2H), 1.54–1.53 (m, 1H), 1.53–1.42 (m, 4H), 1.38–1.26 (m, 2H), 1.26–1.06 (m, 5H), 0.97–0.80 (m, 4H), 0.77–0.71 (m, 3H), 0.62 (s, 3H) ppm. ^{13}C NMR (100 MHz, DMSO-d_6): δ = 80.07, 53.29, 50.81, 46.27, 42.60, 38.04, 36.69, 35.59, 35.07, 31.20, 30.85, 30.58, 29.90, 27.81, 23.88, 23.08, 19.97, 11.37, 11.15 ppm.

3. Results and discussion

3.1. Characterization of Co_2P NRs

The representative transmission electron microscopy (TEM) images confirm that the prepared cobalt phosphide nanoparticles own the uniform rod morphology with a diameter of ~10 nm and length over 50 nm (**Figures 4-2** (a, b)). The high-resolution TEM (HR-TEM) image and the selected area electron diffraction (SAED) patterns are shown in **Figures 4-2** (c). The measured lattice fringe *d*-spacing values of cobalt phosphide are 0.176 nm corresponds to the (020) surfaces of Co_2P (**Figures 4-2** (c) inset). The observed diffraction pattern can be indexed these from Co_2P orthorhombic structure, indicating the high crystalline nature of the obtained Co_2P NRs [23]. Scanning transmission electron microscopy (STEM) image with elemental mapping proves the presence of the Co and P, which are homogeneously distributed within each nanorods (**Figures 4-2** (d-g)). Moreover, the stoichiometric ratio of Co to P investigated by the corresponding energy dispersive X-ray (EDX) spectrum is close to 2:1 (**Figure 4-2** (h)). To investigate the electrochemistry nature of the cobalt species in Co_2P NR, the *in situ* electron paramagnetic resonance (EPR) measurement has been used. Interesting, bulk-Co_2P gave rise to a very broad ESR signal due to its magnetic property, while Co_2P NR does not show any signals in the ESR spectrum which emphasis the significant effect of nanosizing. In summary, a well ordered Co_2P nanorods is successful synthesized.
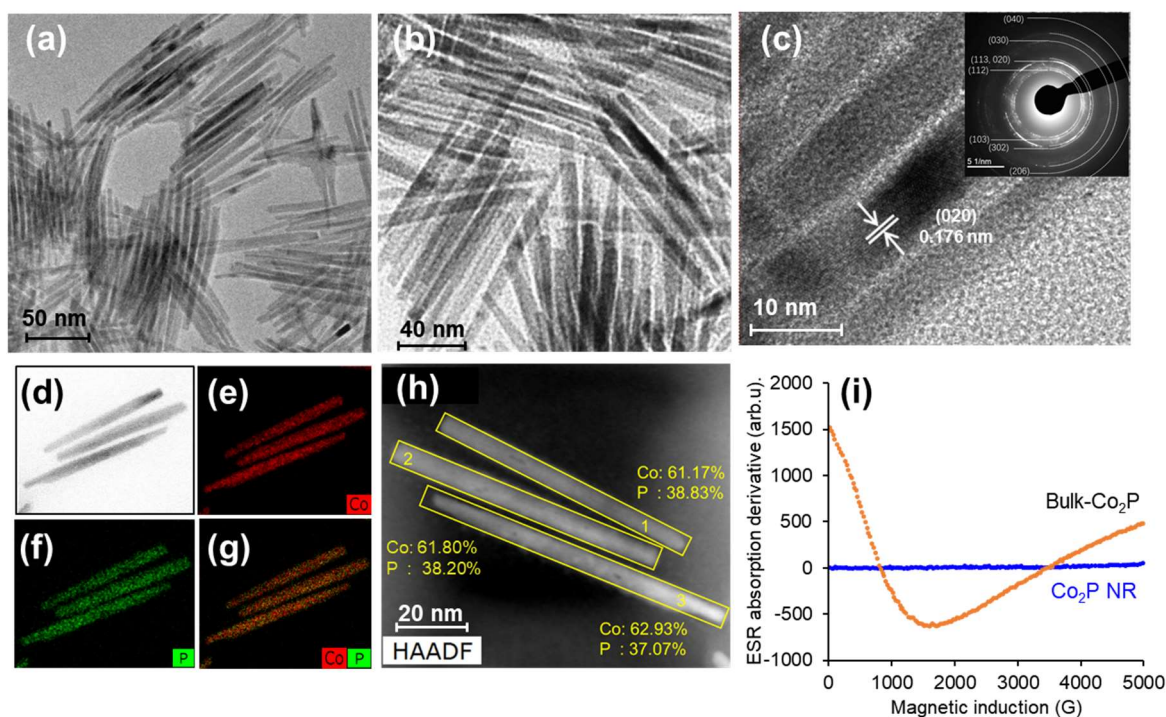
Figure 4-2. (a) and (b) TEM images of the Co_2P NRs showing a rod-like morphology. (c) HR-TEM image of the Co_2P NRs with the inset illustrating the corresponding SAED pattern. (d) STEM image of the Co_2P NRs. Elemental mapping images of (e) Co and (f) P. (g) Composite overlay image of (e) and (f). (h) EDX analysis of Co_2P NRs in the yellow squares. (i) ESR spectrum of bulk-Co_2P (black line) and Co_2P NR (blue line).

The Co *K*-edge XAFS analysis was carried out to determine the electronic properties and local structures of Co species in Co_2P NRs in air atmosphere. The edge position of the X-ray absorption near-edge structure (XANES) spectra of the Co_2P NRs and CoP nanoparticles (NPs) as well as the reference samples, bulk Co_2P, Co foil, and CoO, are shown in **Figure 4-3** (a). The spectra of the Co_2P NRs and CoP NPs are similar to that of Co foil and much different from that of CoO, demonstrating the metallic state of Co species in cobalt phosphide nanoparticles. From the results of fourier-transform extended X-ray absorption fine structure (FT-EXAFS) spectra as shown in **Figure 4-3** (b), bulk Co_2P, the Co_2P NRs, and CoP NPs exhibit the two peaks at 1.6–2.0 Å and 2.0–2.5 Å, contributing the Co–P and Co–Co bonds, respectively. The absence of Co–O bonds also confirms the air-stable state of Co_2P NRs without oxidization.
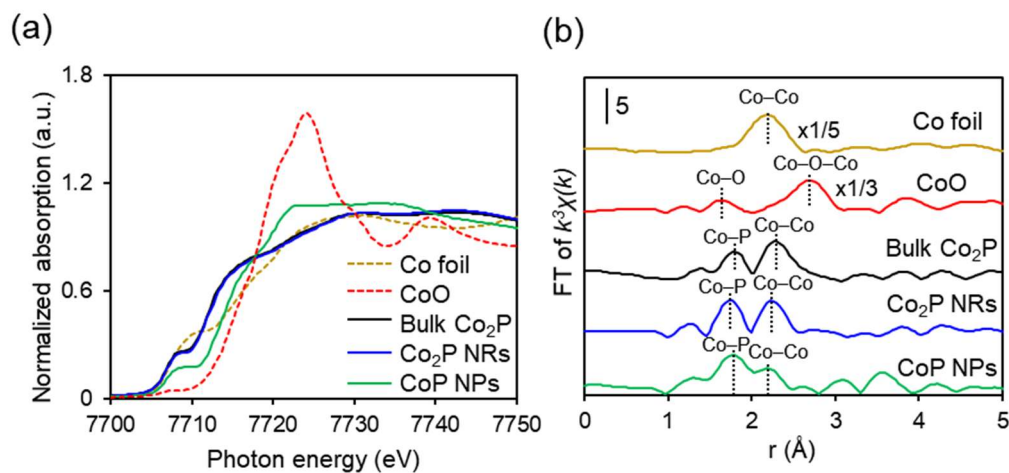
Figure 4-3. Co K-edge (a) XANES and (b) FT-EXAFS spectra of Co foil, CoO, bulk Co_2P, Co_2P NRs, and CoP NPs.

The local structure of the Co_2P NRs was determined via curve fitting analysis as summarized in **Figure 4-4** and **Table 4-1**. Clearly, Co–Co bonds of Co_2P NRs and bulk Co_2P are much longer than that of Co foil (2.56–2.60 Å vs. 2.49 Å) in **Table 4-1** due to orthorhombic Co_2P structure with tetrahedral CoP_4 network with vertex and edge sharing. More importantly, the coordination number (CN) ratios of Co–Co bond to Co–P bond (CN_{Co-Co}/CN_{Co-P}) of Co_2P NRs and bulk Co_2P are quite different: Co_2P NRs has smaller CN_{Co-Co}/CN_{Co-P} ratio (1.6) than that of bulk Co_2P (2.0) and the ideal value (1.8) calculated from the crystal structure of orthorhombic Co_2P, indicating there is a higher number of coordinatively unsaturated Co–Co sites on the its surfaces.
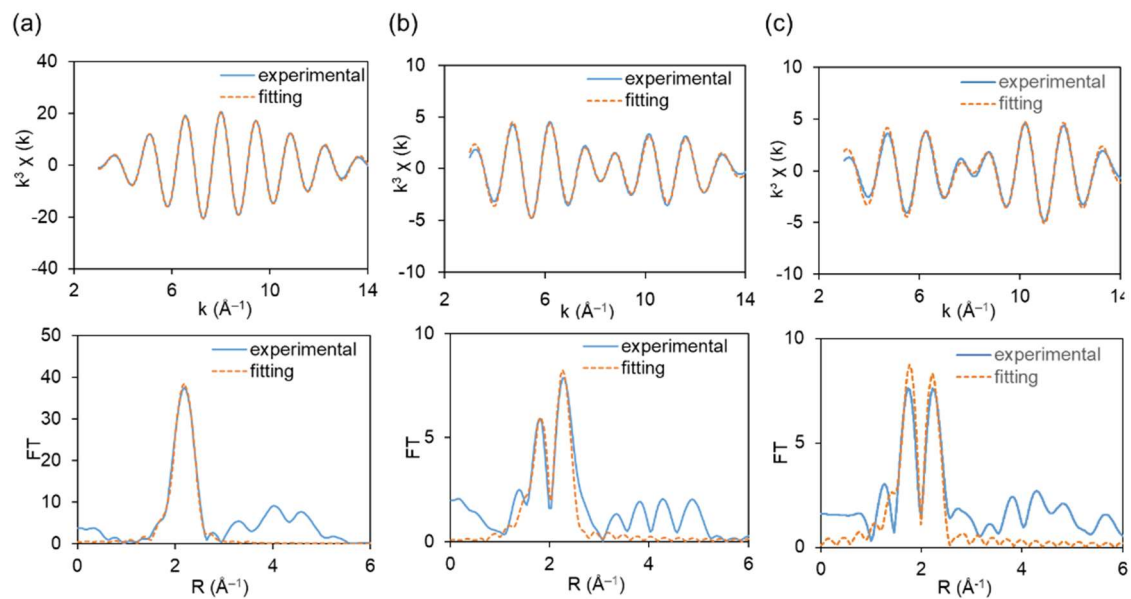
Figure 4-4. EXAFS fitting curves in k-space (left panel) and R-space (right panel) of Co foil, bulk Co₂P, nano-Co₂P, and nano-Co₂P/Al₂O₃.

Table 4-1. Curve-fitting results of Co *K*-edge EXAFS for Co foil, bulk Co₂P, and Co₂P NRs.

Sample	Shell	CN[a]	r (Å)[b]	D.W. [c]	R factor (%)
Co foil	Co–Co	10.6 ± 0.2	2.49 ± 0.01	0.007 ± 0.002	2.6
Bulk Co₂P	Co–P	2.0 ± 0.1	2.24 ± 0.03	0.005 ± 0.002	9.4
	Co–Co	4.0 ± 0.2	2.56 ± 0.02	0.010 ± 0.003	
Co₂P NRs	Co–P	1.8 ± 0.2	2.22 ± 0.04	0.007 ± 0.004	7.4
	Co–Co	2.8 ± 0.2	2.60 ± 0.03	0.009 ± 0.004	
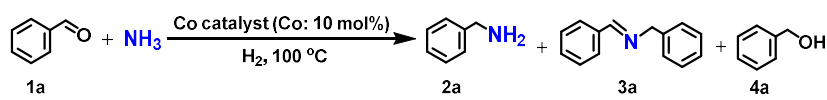
[a]Coordination number. [b]Bond distance. [c]Debye–Waller factor.

3.2. Catalytic performance of Co$_2$P NRs for reductive amination

The investigation of the catalytic activity of Co$_2$P NRs was firstly conducted in the reductive amination of benzaldehyde (**1a**) as the model substrate using three different types of amination sources (an aqueous ammonia solution (aq. NH$_3$), gaseous ammonia (NH$_3$ gas), and ammonium acetate (NH$_4$OAc)) at 10 bar H$_2$ and 100 °C in water (**Table 4-2**). Impressively, the Co$_2$P NRs with aq. NH$_3$ and NH$_3$ gas as ammonia source would give the corresponding primary amine, benzylamine (**2a**), in 93%, 88% yields, respectively (entries 1 and 2). On the other hand, a low yield of **2a** co-existed with the direct hydrogenation product, benzyl alcohol (**4a**), was obtained in the case of NH$_4$OAc (entry 3). After screening the aq. NH$_3$ as the most appropriate ammonia source, notably, Co$_2$P NRs also showed high activity under a low H$_2$ pressure (5 bar H$_2$), giving the **2a** in 94% yields (entry 4). Furthermore, the Co$_2$P NRs-catalyzed reductive amination was still workable even decreasing the H$_2$ pressure to 1 bar to selectively produce **2a** in 87% yield, which represents the first example of cobalt based catalyst for reductive amination under ambient-pressure H$_2$ conditions (entry 5). In sharp contrast, bulk-size Co$_2$P (bulk Co$_2$P), cobalt phosphide nanoparticles with Co: P =1 ratio (CoP NPs), sponge Co, conventional cobalt NPs catalyst prepared by impregnation method (Co/SiO$_2$), and the further reduced one (Co/SiO$_2$_Red) were inactive under such mild reaction conditions, demonstrating the unique catalysis of Co$_2$P NRs (entries 7-11). Moreover, the superior activity of the Co$_2$P NRs also enabled this transformation at a room temperature conditions under a 2 mol% cobalt loading conditions, which is firstly achieved by a non-pricious metal-based reductive amination under ambient temperature (entry 6).

In addition, a scale-up experiment using 2.4 g of **1a** was carried out under 40 bar H$_2$ and 130 °C conditions. The Co$_2$P NRs promoted the reaction well and the hydrochloride salt product could be recovered with a turnover number (TON) as high as 1000 (**Scheme 4-2**), which is the highest value among the up to date homogeneous and heterogeneous non-noble-metal- based catalysts.

Table 4-2. Reductive amination of benzaldehyde (**1a**) with Co_2P NRs and other cobalt catalysts[a]

Entry	Catalyst	H_2	NH_3 source	Time (h)	Yield (%)[b]		
					2a	**3a**	**4a**
1	Co_2P NRs	10	Aq. NH_3	10	93	0	0
2[c]	Co_2P NRs	10	NH_3 gas	10	88	0	0
3[d]	Co_2P NRs	10	NH_4OAc	10	15	0	73
4	Co_2P NRs	5	Aq. NH_3	10	94	0	0
5	Co_2P NRs	1	Aq. NH_3	12	90	0	1
6[e]	Co_2P NRs	40	Aq. NH_3	48	87	0	0
7	Bulk Co_2P	1	Aq. NH_3	12	0	0	0
8	CoP NPs	1	Aq. NH_3	12	0	12	0
9	Sponge Co	1	Aq. NH_3	12	0	11	3
10	Co/SiO_2	1	Aq. NH_3	12	0	0	0
11	Co/SiO_2-Red	1	Aq. NH_3	12	0	0	0

[a]Reaction conditions: Co catalyst (Co: 0.05 mmol), benzaldehyde (0.5 mmol), aq. NH_3 25% (3 mL), 100 °C. [b]Determined by gas chromatography-mass spectrometry (GS-MS) using an internal standard. [c]NH_3 gas (2.5 bar), water (3 mL). [d]NH_4OAc (0.2 g), water (3 mL). [e]Co_2P NRs (Co: 0.02 mmol), benzaldehyde (1.0 mmol), aq. NH_3 25% (3 mL), room temperature, 48 h.
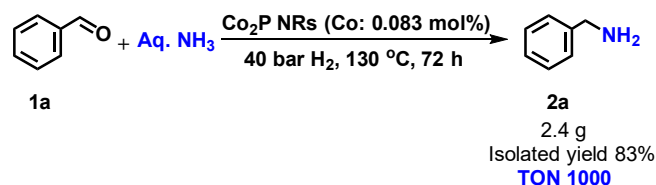
Scheme 4-2. Gram-scale experiment of the reductive amination of **1a** using the Co_2P NRs. Reaction conditions: Co_2P NRs (1.1 mg, Co: 0.018 mmol), **1a** (2.4 g), aq. NH_3 25% (40 mL), ethanol (20 mL), 40 bar H_2, 130 °C.

As a result, Co$_2$P NRs exhibit unpresented excellent performance for reductive amination reaction among the reported non-noble-metal catalysts developed to date, which still suffer from high H$_2$ pressures, high temperatures or low activities (**Table 4-3**).

Table 4-3. Comparison of activity between Co$_2$P NRs and reported non-noble-metal-based catalysts for reductive amination.

| Catalyst	Metal	Reaction Conditions	NH$_3$ Source	Carbonyl Compound	TON	Ref.
Co$_2$P NRs	Co	1–10 bar H$_2$, aq. NH$_3$ or ethanol, 100–120 °C (Scale-up condition: 40 bar H$_2$, 130 °C)	aq. NH$_3$ or NH$_4$OAc	aldehyde, ketone	10 (1000)	This work
Co-DABCO-TPA@C-800	Co	40 bar H$_2$, 5–7 bar NH$_3$, t-BuOH or THF, 120 °C	NH$_3$ gas	aldehyde, ketone	29	Jagadeesh, R. V. et al. *Science* **2017**, *358*, 326–332
Co@NC-800	Co	10 bar H$_2$, aq. NH$_3$, ethanol, 130 °C	aq. NH$_3$	aldehyde	147	Yuan, Z. et al. *J. Catal.* **2019**, *370*, 347–356
Raney Co	Co	10 bar H$_2$, 1 bar NH$_3$, CH$_3$OH, 120 °C	NH$_3$ gas	furfural	6	Wei, J. et al. *ChemCatChem* 2019, *11*, 5562–5569
Co(BF$_4$)$_2$·6 H$_2$O+Triphos	Co	40 bar H$_2$, 1 bar NH$_3$, TFE, 100 °C	NH$_3$ gas	aldehyde, ketone	33	Jagadeesh, R. V. et al. *Nat. Commun.* **2019**, *10*, 5443
Co-DABCO-TPA@C-800	Co	40 bar H$_2$, 5–7 bar NH$_3$, t-BuOH or THF, 120 °C	NH$_3$ gas	aldehyde, ketone	26	Beller, M. et al. *Nat. Protoc.* **2020**, *15*, 1313–1337
Ni-TA@SiO$_2$-800	Ni	20 bar H$_2$, 5-7 bar NH$_3$, t-BuOH, 120 °C	NH$_3$ gas	aldehyde, ketone	16	Jagadeesh, R. V. et al. *Angew. Chem. Int. Ed.* **2019**, *131*, 5118–5122
Ni/Al$_2$O$_3$	Ni	10 bar H$_2$, aq. NH$_3$, 80 °C	aq. NH$_3$	aldehyde, ketone	29	Kempe, R. et al. *Nat. Catal.* **2019**, *2*, 71–77
Fe/(N)SiC	Fe	65 bar H$_2$, aq. NH$_3$, 140 °C	aq. NH$_3$	aldehyde, ketone	10	Kempe, R. et al. *ChemSusChem* **2020**, *13*, 3110–3114
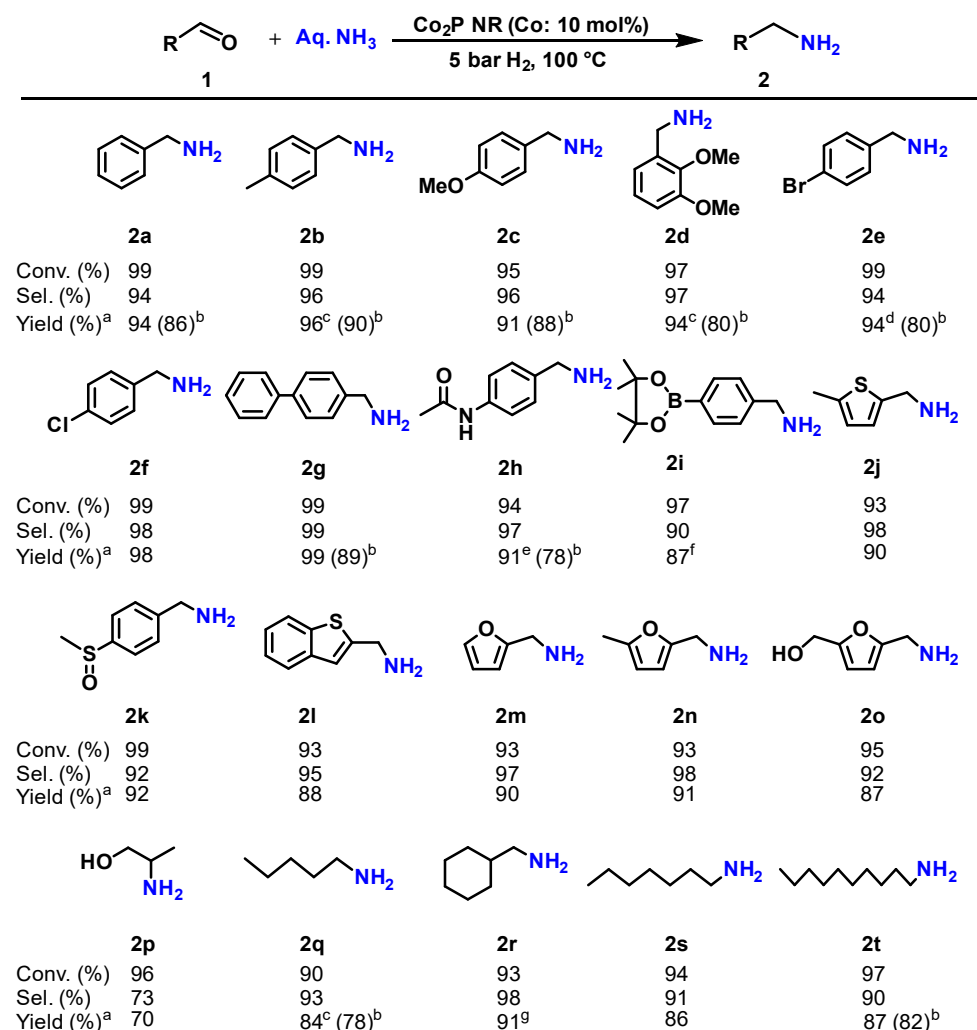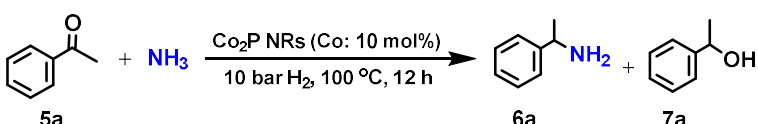
Scheme 4-3. Substrate scope for the Co₂P NR-catalyzed reductive amination of aldehydes with aq. NH₃. Reaction conditions: Co₂P NRs (4.0 mg), aldehyde (0.5 mmol), aq. NH₃ 25% (3 mL), 5 bar H₂, 100 °C, 10 h. [a]Yields were determined by GC-MS using an internal standard. [b]Isolated yield as a hydrochloride salt. [c]120 °C, 6 h. [d]70 °C. [e]80 °C, 10 bar H₂. [f]80 °C. [g]Aq. NH₃ 25% (5 mL), 120 °C.

Next, the wide applicability of the Co₂P NRs was demonstrated through the reductive amination of aldehydes with various function groups as shown in **Scheme 4-3**. Aromatic aldehydes with different moieties like methyl (**1b**), methoxy (**1c, 1d**), halogen (**1e, 1f**), phenyl (**1g**), amide (**1h**), and boronic ester (**1i**) were tolerant and smoothly converted into the corresponding primary amines in

high yields. While sulfur compounds are prone to cause deactivation problems of catalysts due to the strong coordination of sulfur moiety to the metal active sites, aldehydes with sulfur (**1j-l**) in their structures were also good substrates in this Co_2P NRs-catalyzed reaction, providing the primary amine products in excellent yields. Moreover, Co_2P NRs efficiently promoted the reductive amination of biomass-derived substrates (**1m-o**), producing the corresponding primary amines with > 87% yields. Furthermore, this catalyst also could be employed for aliphatic substrates to give the aliphatic primary amines in high yields (**1p-t**).

Table 4-4. Reductive amination of acetophenone under various reaction conditions using the Co_2P NRs catalyst[a].

| Entry | NH₃ Source | Solvent | Yield (%)[b] | |
			6a	7a
1	3 mL aq. NH₃	-	49	47
2	2.5 bar NH₃ gas	ethanol	0	0
3	0.2 g NH₄OAc	ethanol	83	0
4	0.1 g NH₄OAc	ethanol	81	0
5	0.05 g NH₄OAc	ethanol	74	0

[a]Reaction conditions: Co_2P NRs (4.0 mg), acetophenone (0.5 mmol), solvent (3 mL), 10 bar H_2, 12 h. [b]Determined by GS-MS using an internal standard method.

To further investigate the application of Co_2P NRs, the reductive amination of ketones as substrates was carried out. The optimal experiment results were shown in **Table 4-4**. Among the tested amination reagents in the reductive amination of acetophenone (**5a**), the combination of NH_4OAc and ethanol provided the highest yield of corresponding amine (83%), while others resulted in low amine yields or the formation of alcohols.

$$R_1\text{-CO-}R_2 \;(5) + NH_4OAc \xrightarrow[\text{10 bar } H_2,\ 100\ ^\circ C]{\text{Co}_2\text{P NRs (Co: 10 mol\%)}} R_1\text{-CH(}R_2\text{)-}NH_2 \;(6)$$

	6a	**6b**	**6c**	**6d**
Conv. (%)[a]	90	97	>99	96
Sel. (%)	92	91	96	93
Yield (%)[a]	83 (80)[b]	86[c] (82)[b]	96	89[d]

	6e	**6f**	**6g**	**6h**
Conv. (%)[a]	96	84	92	82
Sel. (%)	92	88	93	89
Yield (%)[a]	88[e] (85)[b]	74[f]	86[g] (85)[b]	73[f]

	6i	**6j**	**6k**	**6l**	**6m**
Conv. (%)[a]	87	99	83	92	96
Sel. (%)	87	96	86	91	99
Yield (%)[a]	76[c]	96[g] (88)[b]	71	84 (82)[b]	95

	6n	**6o**
Yield (%)	81[b]	77[b]
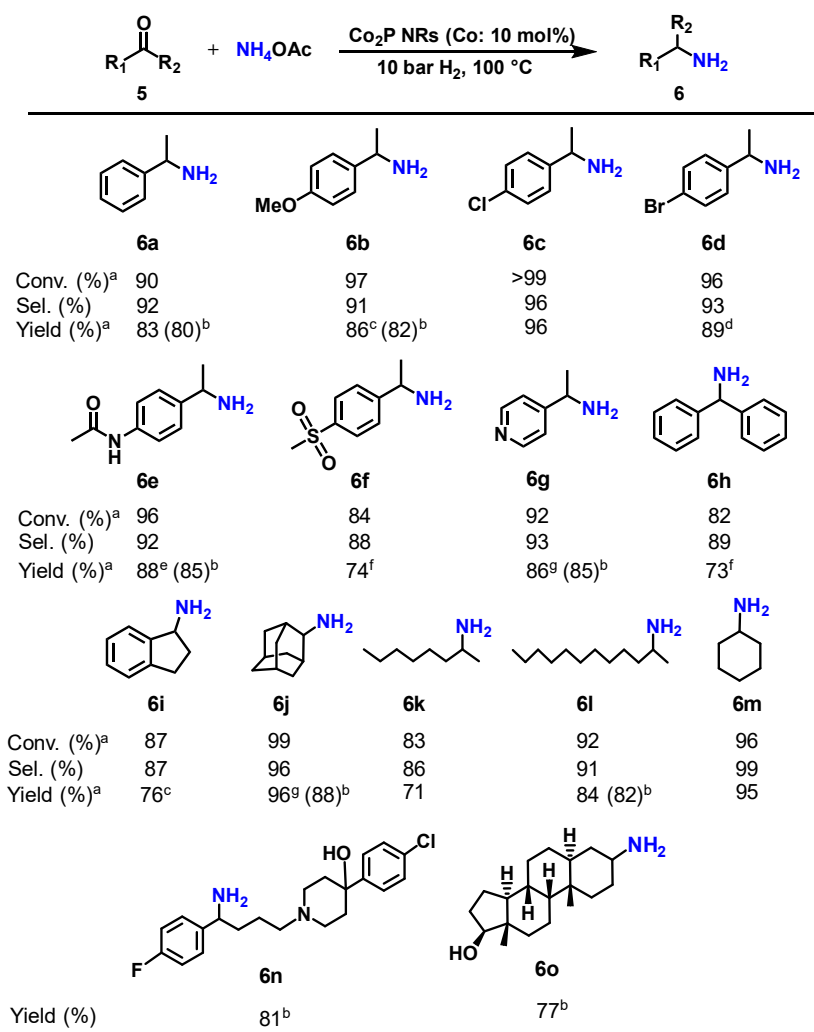
Scheme 4-4. Substrate scope for the Co$_2$P NR-catalyzed reductive amination of ketones with ammonium acetate. Reaction conditions: Co$_2$P NRs (4.0 mg), ketone (0.5 mmol), NH$_4$OAc (0.2 g), ethanol (3 mL), 10 bar H$_2$, 100 °C, 12 h. [a]Yields were determined by GC-MS using an internal standard. [b]Isolated yield as a hydrochloride salt. [c]NH$_4$OAc (0.1 g), 20 bar H$_2$, 110 °C. [d]110 °C. [e]NH$_4$OAc (0.1 g), 80 °C. [f]20 bar

After screening the reaction condition, Co$_2$P NRs were evaluated in the reductive amination of ketones substrates (**Scheme 4-4**). Similarly, Co$_2$P NRs are highly active for a wide range of aromatic and heteroaromatic ketones containing functional groups like methoxy, halogen, amide, methyl, and sulfone functionalities, converting to their corresponding branched primary amines in high yields.

Moreover, structurally complex ketones including steroid-based molecules (**5n**, **5o**) were also transformed to the desired products in good yield. These results strongly highlight the wide substrate scopes.

Furthermore, the highly active of Co₂P NRs made it possible to perform this reaction under just 1 bar H₂ pressure. Some selected aldehydes and ketones as shown in **Scheme 4-5** were effectively converted to their corresponding primary amines with 74-95% yields, confirming the versatility and highly efficiency of this Co₂P NRs-catalyzed reductive amination method to synthesis primary amines.
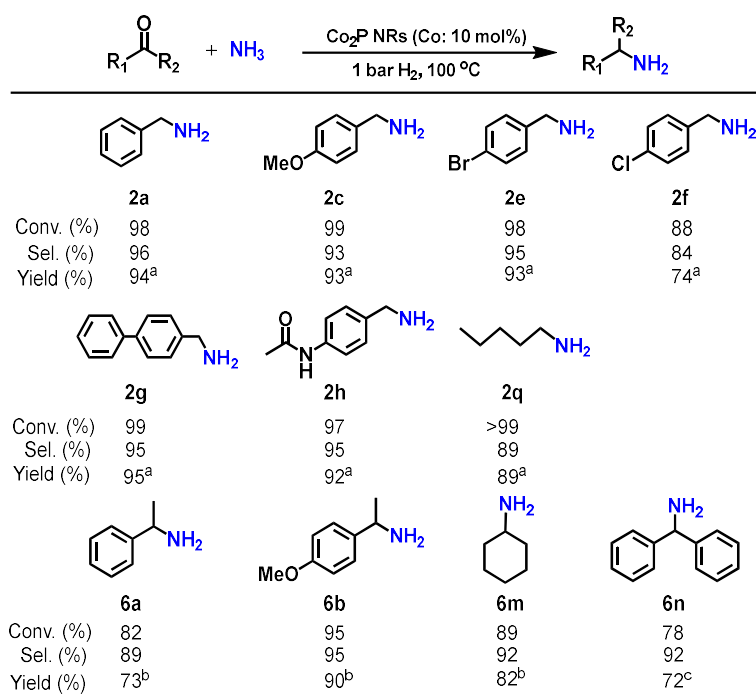
Scheme 4-5. Reductive amination of carbonyl compounds by the Co₂P NRs at 1 bar H₂. Reaction conditions: Co₂P NRs (4.0 mg), substrate (0.5 mmol), 1 bar H₂, 100 °C, 12 h. [a]Aq. NH₃ 25% (3 mL). [b]NH₄OAc (0.1 g), ethanol (3 mL). [c]NH₄OAc (0.15 g), ethanol (3 mL), 110 °C, 20 h. The yields were determined by GS-MS using an internal standard.

3.3. The high reusability and durability of Co₂P NRs

Unlike conventional non-noble-metal-based catalysts requiring strict anaerobic conditions due to the air-sensitivity, Co₂P NRs could operate under air condition and were easily recovered by

105

simple filtration from reaction mixture after reaction. The recovered catalyst was reusable and the high activity could be remained even after 4th cycle, showing the convenient recyclability and high reusability (**Figure 4-5**). The initial reaction rate of each reuse experiment also exhibited almost the same yield of primary amine (white diamonds in **Figure 4-5**) to support the high stability of Co_2P NRs.
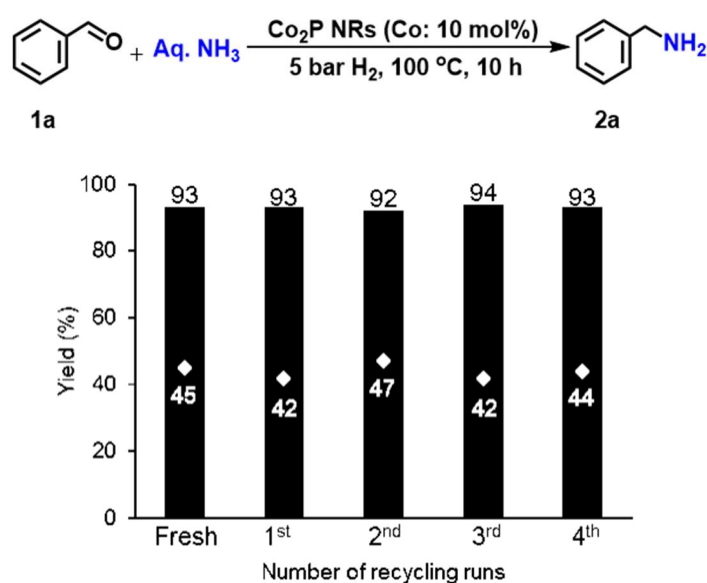
Figure 4-5. Reusability of the Co_2P NR-catalyzed reductive amination of **1a** with aq. NH_3. Reaction conditions: Co_2P NRs (4.0 mg), **1a** (0.5 mmol), aq. NH_3 25% (3 mL), 5 bar H_2, 100 °C, 10 h. The initial reaction rate experiments (diamond) were conducted under the same reaction conditions for 5 h. Yields were determined by GS-MS using an internal standard.

To get insight into the unique air-stable metallic nature and high durability of Co_2P NRs, the XANES spectra of Co_2P NRs was performed with increasing the temperature from room temperature (R. T.) to 700 °C in air. As shown in **Figure 4-6**, the spectra blew 400 °C conditions are almost the same as the R. T. one, which means the structure of Co_2P NRs is unchanged and Co species in Co_2P NRs are still in zero valence state. While raising the temperature to 400 °C and above, the spectra clearly shifted to higher energy side, indicating the presence of oxidized cobalt species. These results

strongly emphasize the high durability of Co$_2$P NRs even under heating on exposure to air conditions, which is significantly different from conventional low valence metal catalysts.
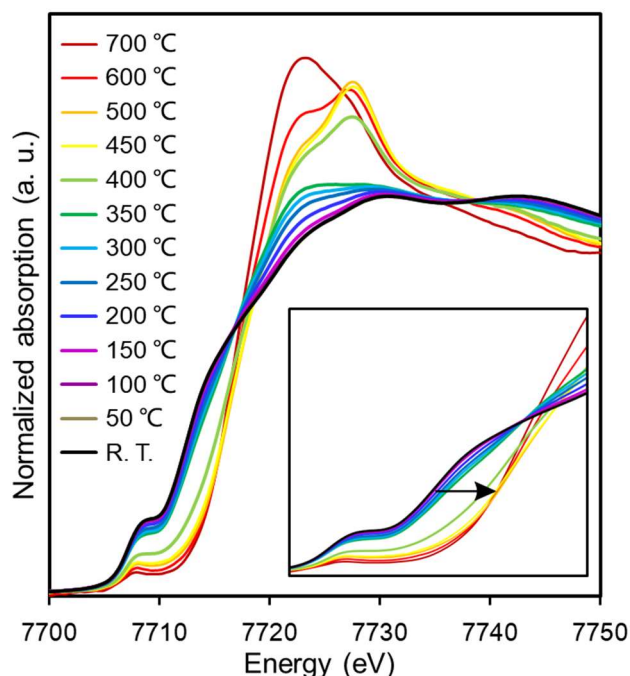
Figure 4-6. Co K-edge XANES spectra of Co$_2$P NRs from room temperature to 700 °C.

3.4. The reaction path investigation

In order to figure out the reaction path, the time profile expriments of Co$_2$P NR-catalyzed reductive amination was investigated (**Figure 4-7**). During the transformation of benzaldehyde amination (**1a**) to benzylamine (**2a**) in presence with aq. NH$_3$ and H$_2$, N-benzylidenebenzylamine (**3a**) firstly appeared and gradually increased at the beginning 2 hours. After that, the amount of **2a** increased apparently and became the main product in the reaction mixture with the decrease of **3a**, indicating **3a** was functioned as intermediate in this reaction. The transformation of **3a** to **2a** is also considered as the rate-determining step due to the additional 8 hours. A possible reaction pathway for the Co$_2$P NRs-catalyzed **1a** to **2a** is proposed based on the time profile results (**Scheme 4-6**). First of all, phenylmethanimine, the product of the condensation reaction of **1a** and NH$_3$, was formed and then

further hydrogenated to produce **2a**. After that, **3a** derived from the condensation reaction of **1a** and

initial generated **2a** was appeared and gradually converted into **2a**, which might through an unstable

geminal amine [24].
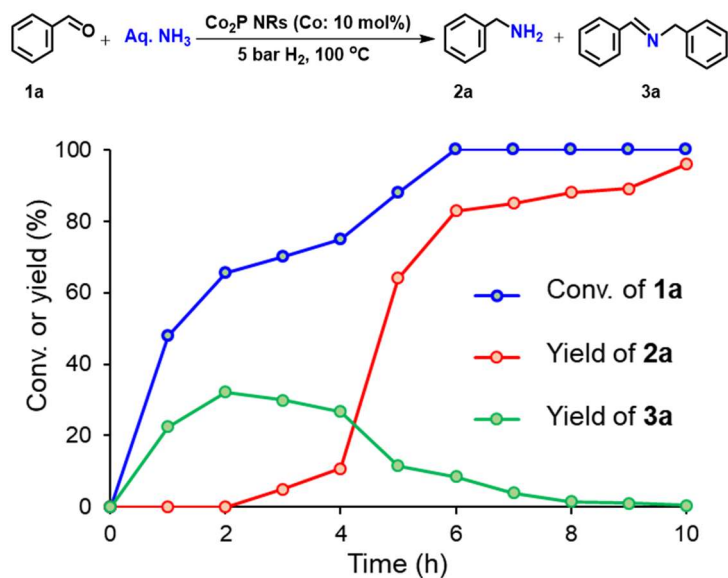
Figure 4-7. Time-course data of the Co_2P NR-catalyzed reductive amination of **1a** with aq. NH_3. Reaction conditions: Co_2P NRs (4.0 mg), **1a** (0.5 mmol), aq. NH_3 25% (3 mL), 5 bar H_2, 100 °C, 10 h. Yields were determined by GS-MS using an internal standard.
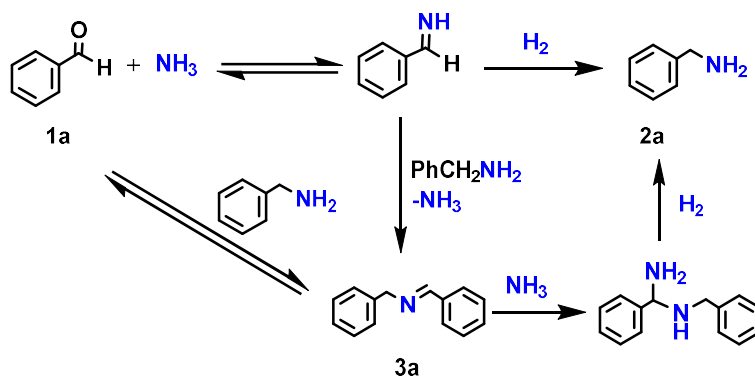
Scheme 4-6. A possible reaction pathway for the Co_2P NR-catalyzed transformation of benzaldehyde (**1a**) to benzylamine (**2a**).

4.   Conclusion

This chapter describes a novel cobalt phosphide nanorods (Co_2P NRs) for the reductive amination of carbonyl compounds, which represents a considerably important reaction for the synthesis of primary amines with high atom efficiency. In sharp contrast to reported non-noble metal catalysts that suffer from air sensitivity (pyrophoricity), low activity, and requirement of high H_2 pressures, the present Co_2P NRs catalyst has both air-stability and high activity under mild reaction conditions, even at 1 bar of H_2 pressure or room temperature, representing the first example of a cobalt catalyst for the reductive amination at ambient conditions. Moreover, the Co_2P NRs is applicable under the scale-up conditions, giving the highest turnover number exceeding 1000 among those of previously reported non-noble-metal catalysts. Therefore, the Co_2P NRs catalyst has high potential to replace conventional air-unstable catalysts and will lead to inexpensive, green, and sustainable reaction processes for producing primary amines from carbonyl compounds.

References

1   Weissermel, K.; Arpe, H. *Industrial Organic Chemistry*, **2008**, Wiley-VCH.

2   Vardanyan, R. S.; Hruby, V. J. *Synthesis of Best-Seller Drugs*, **2016**, Academic Press.

3   Lawrence, S. A. *Amines. Synthesis, Properties and Applications*, **2004**, Cambridge Univ. Press.

4   Ikenaga, T.; Matsushita, K.; Shinozawa, J.; Yada, S.; Takagi, Y. *Tetrahedron* **2005**, *61*, 2105–2109.

5   Raoufmoghaddam, S. *Org. Biomol. Chem.* **2014**, *12*, 7179–7193.

6   Tarasevich, V. A.; Kozlov, N. G. *Russ. Chem. Rev.* **1999**, *68*, 55–72.

7   Hayes, K. S. *Appl. Catal., A* **2001**, *221*, 187–195.

8   Jagadeesh, R. V.; Murugesan, K.; Alshammari, A.; Neumann, H.; Pohl, M.; Radnik, J.; Beller, M. *Science* **2017**, *358*, 326–332.

9   Hahn, G.; Kunnas, P.; de Jonge, N.; Kempe, R. *Nat. Catal*. **2019**, *2*, 71–77.

10 Zhang, Y.; Yang, H.; Chi, Q.; Zhang, Z. *ChemSusChem* **2019**, *12*, 1246–1255.

11 Murugesan, K.; Beller, M.; Jagadeesh, R. V. *Angew. Chem. Int. Ed*. **2019**, *58*, 5064–5068.

12 Bäumler, C.; Bauer, C.; Kempe, R. *ChemSusChem* **2020**, *13*, 3110–3114.

13 Murugesan, K.; Senthamarai, T.; Ghandrashekhar, V.; Natte, K.; Kamer, P.; Beller, M.; Jagadeesh, R. *Chem. Soc. Rev*. **2020**, *49*, 6273–6328.

14 Irrgang, T.; Kempe, R. *Chem. Rev*. **2020**, *120*, 9583–9674.

15 Raney, M. Method of preparing catalytic material, **1925**, U.S. Patent 1563587.

16 Tucker, S. H. Catalytic hydrogenation using Raney nickel. *J. Chem. Educ*. **1950**, *27*, 489–493.

17 Nishimura, S. *Handbook of heterogeneous catalytic hydrogenation for organic synthesis*, **2001**, Wiley-VCH.

18 Jagadeesh, R. V.; Surkus, A.; Junge, H.; Pohl, M.; Radnik, J.; Rabeah, J.; Huan, H.; Schunemann, V.; Bruckner. A.; Beller, M. *Science* **2013**, *342*, 1073–1076.

19 He, L.; Weniger, F.; Neumann, H.; Beller, M. *Angew. Chem. Int. Ed*. **2016**, *55*, 12582–12594.

20 Banerjee, D.; Jagadeesh, R.; Junge, K.; Pohl, M.; Radnik, J.; Brück-ner, A.; Beller, M. *Angew. Chem. Int. Ed*. **2014**, 53, 4359–4363.

21 Jagadeesh, R. V.; Junge, H.; Beller, M. *Nat. Commun*. **2014**, *5*, 4123.

22 Chen, F.; Surkus, A.; He, L.; Pohl, M.; Radnik, J.; Topf, C.; Junge, K.; Beller, M. *J. Am. Chem. Soc*. **2015**, *137*, 11718–11724.

23 Skála, R.; Drábek, M. *Bull. Czech Geol. Surv*. **2001**, *76*, 209–216.

24 Yuan, Z.; Liu, B.; Zhou, P.; Zhang, Z.; Chi, Q. *J. Catal*. **2019**, *370*, 347–356.

Chapter V.

Hydrotalcite-supported Cobalt Phosphide Catalyst for Hydrogenation of Nitriles to Primary Amines under Additive-free Conditions

1. Introduction

Primary amines constitute an important class of chemicals in industry and are significant intermediates for synthesis of various agrochemicals, pharmaceuticals, dyes, and polymers [1-3]. The selective hydrogenation of nitriles with molecule hydrogen offers a green synthesis of valuable primary amines [4-6]. During this hydrogenation reaction, the selectivity of primary amine is one of the main challenges due to the formation of secondary and tertiary amines as by-products: the partially hydrogenated intermediate, imine (**b**), is generated and prone to have a condensation reaction with the initially formed primary amine (**c**) to produce secondary imine (**d**), which will further be hydrogenated to secondary amine (**e**) and go through an additional condensation reaction to provide tertiary amine (**f**) as the final product (**Scheme 5-1**) [7-9].
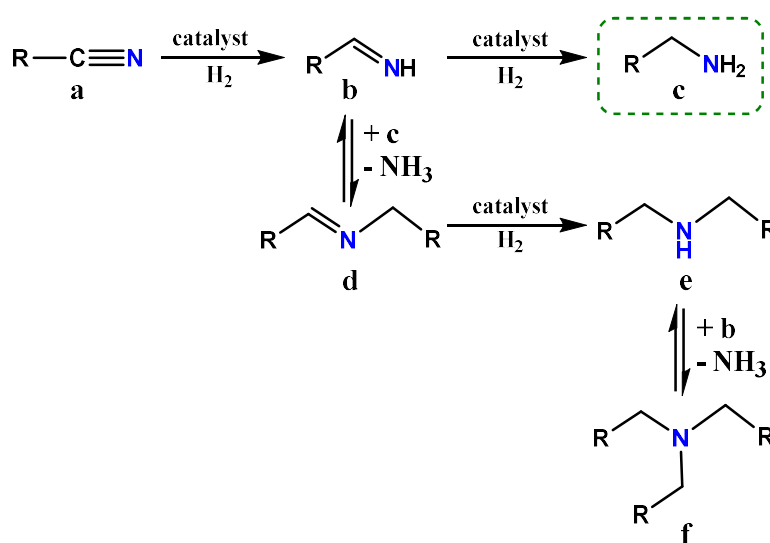
Scheme 5-1. Catalytic hydrogenation of nitriles.

These side reactions are sensitive to the reaction conditions and can be prevented by several methods. For example, strongly acidic solvents (e.g. HCl) can effectively suppress the condensation reaction of the primary amine via the formation of an ammonium salt [10, 11]. Similarly, acylating solvents such as acetic acid or acetic anhydride are also usable to prevent condensation reactions [12].

113

As for industrial nitrile hydrogenation, the most common method to minimize the production of by-products and improve the selectivity of primary amine is to carry out this reaction in the presence of excess ammonia, which can shift the thermodynamic equilibrium into the side in favor of primary amine formation [13-15]. Although the addition of ammonia shows apparent effect for improving selectivity, there also are several problems appeared such as the extra expenses caused by using ammonia (e.g. equipment against the strongly basic condition) and additional post-treatment of remained ammonia [6, 10]. Thus, there is a growing need to develop effective and green catalytic systems for hydrogenation of nitrile under ammonia-free (or additive-free) conditions.

The development of nanostructured heterogeneous catalysts for innovative organic synthesis attracts increasing attention for advancing sustainable processes [16-18]. Their catalytic performance can be tuned by adjusting the size, morphology, and the interaction between active species and support, which are largely affected by catalyst preparation methods and the properties of catalyst itself [19-23].

This chapter represents a well-defined cobalt phosphide with a 100 nm-length rod morphology is successfully synthesized (Co_2P NR) by the modification of preparation method described in chapter **II** and the hydrotalcite-supported Co_2P NR (Co_2P NR/HT) behaviors as an air-stable, active, and reusable catalyst for nitrile hydrogenation reaction, overperforming the state-of-the-art non-precious metal-based catalyst, nano-Co_2P/HT, we reported [24]. Specifically, Co_2P NR/HT catalyst shows a remarkable generality for various nitrile substrates including the sulfur-containing nitrile that normally poisons the active metal species of catalysts. Moreover, Co_2P NR/HT can promote the hydrogenation of nitriles under just 1 bar H_2 pressure, revealing its high activity. Furthermore, its excellent performance also realized the hydrogenation of nitriles to primary amines by non-precious metal-based catalyst under additive-free conditions for the first time.

2. Experimental section

2.1. General

All organic reagents were purchased from Mitsuwa Pure Chemicals, Tokyo Chemical Industry Co., Ltd, Tomita Pharmaceutical Co., Ltd, Tomita Pharmaceutical Co., Ltd, Sigma-Aldrich, and FUJIFILM Wako Pure Chemical.

Co(acac)$_2$ was purchased from Mitsuwa Pure Chemicals. 1-octadecene (technical grade; 90%) was purchased from Sigma-Aldrich. Co. Hexadecylamine and triphenyl phosphite were purchased from Tokyo Chemical Industry Co., Ltd. Hydrotalcite (AD 500NS) was purchased from Tomita Pharmaceutical Co., Ltd.

All substrates were commercially available. valeronitrile (>98%), decanenitrile (>98%), trimethylacetonitrile (98%), benzonitrile (>98%), anisonitrile (>98%), 4-acetylbenzonitrile (>98%), 2-cyanothiophene (>98%), 5-methylthiophene-2-carbonitrile (>98%), adiponitrile (>98%), and isophthalonitrile (>98%) were purchased from Tokyo Chemical Industry Co., Ltd. 4-cyanophenol (>98%), 4-cyanopridine (>98%), and 2-furancarbonitrile (98%) were purchased from FUJIFILM Wako Pure Chemical. 4-(methylthio)benzonitrile (98%) was purchased from Sigma-Aldrich.

Gas chromatography-mass spectrometry (GC-MS) were performed using a Shimadzu GC-2014 instrument equipped with an InertCap for amines (30 m × 0.32 mm i.d.) and a GCMS-QP2010 SE instrument equipped with an InertCap WAX-HT capillary column (30 m × 0.25 mm i.d.). The oven temperature was programmed as follows: 60 °C starting temperature, kept for 3 min, temperature ramp at 10 °C/min to 260 °C, then at -20 °C/min to 120 °C. Other conditions were as follows: 2.44 mL/min column flow rate, 10.0 split ratio; vaporization chamber temperature of 250 °C; detector temperature of 260 °C.

Transmission electron microscopy (TEM) observations were conducted using a JEM-

ARM200F instrument operated at 200 kV. Scanning transmission electron microscopy (STEM) images with elemental maps were collected using a FEI Titan Cubed G2 60-300 instrument, operated at 300 kV, and equipped with a Super-X energy-dispersive X-ray spectroscopy (EDX) detector. Elemental mapping based on quantification analysis of EDX spectra was carried out using Esprit.

X-ray diffraction (XRD) was performed using a Philips X′Pert-MPD diffractometer with Cu-Kα radiation. Co K-edge X-ray absorption spectra were recorded at 25°C using a Si (111) monochromator at the BL01B1 and BL14B2 lines, SPring-8, Japan Synchrotron Radiation Research Institute (JASRI), Harima, Japan. X-ray photoelectron spectroscopy (XPS) analysis was performed on an ESCA1700R system equipped with a dual Mg/Al X-ray source and a hemispherical analyzer operating in fixed-analyzer transmission mode. The spectra were obtained using a pass energy of 58.7 eV and an Al-Kα X-ray source operated at 350 W and 14 kV. Excess charges on the samples were neutralized by argon ion sputtering. The analysis area was 0.8 mm × 2 mm. The working pressure in the analysis chamber was less than 1×10^{-7} Pa. Spectra were acquired in the Co 2p, O 1s, C 1s, and Si 2p regions. The C 1s peak at a binding energy (BE) of 285 eV was used as an internal reference. Inductively coupled plasma-atomic emission spectroscopy (ICP-AES) data were obtained using a Perkin Elmer Optima 8300 instrument. ^{1}H and ^{13}C nuclear magnetic resonance (NMR) spectra were recorded on a JEOL JNM-ESC400 spectrometer.

2.2. Preparation of catalysts

The synthesis of Co$_2$P NR was carried out as follows. Co(acac)$_2$ (1.0 mmol), hexadecylamine (10.0 mmol), and triphenyl phosphite (10.0 mmol) were added to 1-octadecene (10.0 mL) in a Schlenk flask. The mixture was stirred at 120 °C for 1 h under argon flow. Then, the temperature was raised to 300 °C and maintained for another 2 h, yielding a black colloidal solution.

After cooling to 25 °C in air, the black colloid was collected and washed with a mixed solvent consisting of chloroform–acetone (1:1, v/v). The obtained powder was subsequently dried overnight at 25 °C under vacuum to produce Co_2P NR. Typically, Co_2P NR (0.04 g) was re-dispersed in hexane (50 mL). Then, hydrotalcite (1.0 g) was added to the mixture and stirred at 25 °C for 2 h in air. The obtained solid was filtered and dried under vacuum at 25 °C to yield Co_2P NR/HT. Co_2P NR/support catalysts were prepared using Al_2O_3, SiO_2, HAP, and carbon as the support in a similar manner to the preparation of Co_2P NR/HT.

2.3.   Reaction procedure

The reactions with nitrile and H_2 were performed in a 50-mL stainless steel autoclave. Co_2P NR/HT powder (0.025 g), substrate (0.5 mmol), solvent (3.0 mL), and aqueous ammonia (25%, 1.2 mL) were placed into the vessel, and a Teflon®-coated magnetic stir bar was added. After the reactor was sealed, air was purged three times with H_2 and pressurized to 40 bar. Then, the reactor was stirred vigorously at 130 °C for a given time. The reactor was cooled to 25 °C with a water bath after the reaction and the remaining hydrogen gas was released. The reaction solution was analyzed by gas chromatography-mass spectrometry (GC-MS) using biphenyl as an internal standard to determine the conversion and the yield. To obtain the corresponding hydrochloride salts, the catalyst was filtered, and the reaction solution was degassed for ammonia removal. A solution of 1.25 M hydrogen chloride in 1,4-dioxane was added to the reaction solution and the solvent was then removed, yielding the hydrochloride salts for the following NMR analysis.

2.4.   Recycling experiment

After the reaction, the crude reaction mixture was centrifuged to obtain the reaction solution and the yield was determined by GC-MS analysis. Co_2P NR/HT was redispersed in 2-propanol (3.0

mL) and placed in a 50-mL stainless-steel autoclave again with addition of nitrile (0.5 mmol), and aq.

NH$_3$ (25%, 1.2 mL) for reuse experiments.

2.5. Product identification

n-Pentylamine hydrochloride
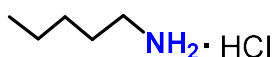
^{1}H NMR (DMSO, 400 MHz): δ = 7.95 (s, 3H), 2.73 (t, J = 7.32 Hz, 2H), 1.56 (m, 2H), 1.33 (m, 4H), 0.88 (t, J = 6.84 Hz, 3H) ppm. ^{13}C NMR (DMSO, 100 MHz): δ = 38.66, 27.86, 26.51, 21.53, 13.63 ppm.

Decylamine hydrochloride
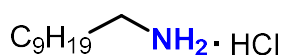
^{1}H NMR (DMSO, 400 MHz): δ = 7.75 (s, 3H), 2.75 (t, J = 8.52 Hz, 2H), 1.51 (m, 2H), 1.25 (m, 14H), 0.86 (t, J = 7.6 Hz, 3H) ppm. ^{13}C NMR (DMSO, 100 MHz): δ = 38.74, 31.20, 28.78, 28.74, 28.58, 28.42, 26.88, 25.70, 21.99, 13.87 ppm.

Neopentylamine hydrochloride
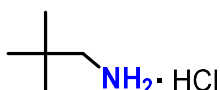
^{1}H NMR (DMSO, 400 MHz): δ = 8.05 (s, 3H), 2.59 (2H), 0.95 (m, 2H) ppm. ^{13}C NMR (DMSO, 100 MHz): δ = 49.68, 30.11, 26.83 ppm.

1-Adamantylmethylamine hydrochloride
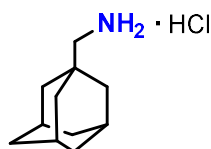
^{1}H NMR (DMSO, 400 MHz): δ = 7.76 (s, 3H), 2.48 (s, 2H), 1.97 (s, 3H), 1.68 (d, J = 12.0, 3H), 1.59 (d, J = 11.6, 3H), 1.50 (s, 6H) ppm. ^{13}C NMR (DMSO, 100 MHz): 49.83, 38.67, 36.02, 30.54, 27.36 ppm.

Benzylamine hydrochloride
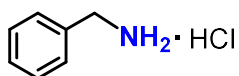
^{1}H NMR (DMSO, 400 MHz): δ = 8.05 (s, 3H), 7.30 (m, 5H), 3.01 (s, 2H) ppm. ^{13}C NMR (DMSO, 100 MHz): δ = 134.04, 128.85, 128.48, 128.31, 42.09 ppm.

(α-naphthylmethyl)ammonium chloride
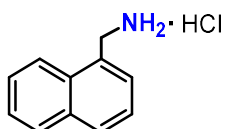
^{1}H NMR (DMSO, 400 MHz): δ = 8.74 (s, 3H), 8.17 (d, J = 7.6, 1H), 7.95 (t, J = 9.6, 2H), 7.69-7.54 (m, 4H), 4.51 (s, 2H). ^{13}C NMR (DMSO, 100 MHz): δ = 133.16, 130.62, 129.92, 128.94, 128.57, 127.24, 126.68, 126.15, 125.29, 123.41, 38.8 ppm.

4-Methoxybenzylamine hydrochloride
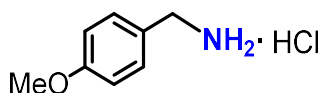
^{1}H NMR (DMSO, 400 MHz): δ = 8.18 (s, 3H), 7.30 (m, 2H), 7.04 (m, 2H), 3.93 (s, 2H), 3.75 (s, 3H) ppm. ^{13}C NMR (DMSO, 100 MHz): δ = 157.85, 129.44, 128.69, 113.52, 54.99, 44.02 ppm.

1-[4-(Aminomethyl)phenyl]ethan-1-one hydrochloride
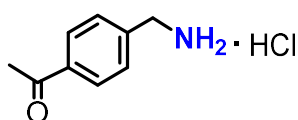
^{1}H NMR (DMSO, 400 MHz): δ = 8.51 (s, 3H), 7.97 (d, J = 8.52 Hz, 2H), 7.66 (d, J = 8.42 Hz, 2H), 4.09 (s, 2H), 2.58 (s, 3H) ppm. ^{13}C NMR (DMSO, 100 MHz): δ = 197.88, 139.15, 136.54, 129.03, 128.22, 41.49, 26.72 ppm.

4-hydroxy-benzylamine hydrochloride
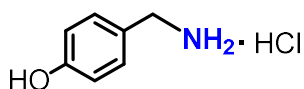
^{1}H NMR (methanol-d_4, 400 MHz): δ = 9.70 (s, 1H), 8.36 (s, 3H), 7.29 (dd, J= 8.00 Hz, 2H), 6.79 (dd, J = 8.00 Hz, 2H), 3.86 (m, 2H) ppm. ^{13}C NMR (methanol-d_4, 100 MHz): δ = 167.18, 139.98, 133.58, 124.74, 51.31 ppm.

4-Picolylamine hydrochloride
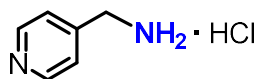
^{1}H NMR (DMSO, 400 MHz): δ = 8.61 (s, 3H), 7.92 (d, J = 4.46 Hz, 2H), 4.23 (s, 2H) ppm. ^{13}C NMR (DMSO, 100 MHz): δ = 149.65, 143.82, 123.23, 41.24 ppm.

Quinolin-3-ylmethanaminium chloride
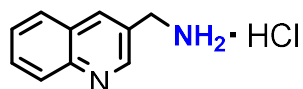
^{1}H NMR (DMSO, 400 MHz): δ = 9.20 (d, J = 2.0 Hz, 1H), 8.77 (s, 1H), 8.72 (brs, 3H), 8.21-8.16 (m, 1H), 8.13-8.11 (m, 1H), 7.97-7.93 (m, 1H), 7.81-7.77 (m, 1H), 4.38 (d, J = 6.0 Hz, 2H) ppm. ^{13}C NMR (DMSO, 100 MHz): δ = 164.76, 147.62, 143.91, 133.59, 129.35, 128.86, 128.18, 127.48, 122.97, 45.59 ppm.

Furan-2-ylmethanamine hydrochloride

^{1}H NMR (DMSO, 400 MHz): δ = 8.46 (s, 3H), 7.73 (m, 1H), 6.55 (m, 1H), 6.50 (m, 1H), 4.06 (m, 2H) ppm. ^{13}C NMR (DMSO, 100 MHz): δ = 147.78, 143.99, 111.04, 110.42, 35.00 ppm.

(4-(Methylthio)phenyl)methanammonium chloride

^{1}H NMR (DMSO, 400 MHz): δ =8.55 (s, 3H), 7.45 (d, J= 8.00 Hz, 2H), 7.29 (d, J= 8.00 Hz, 2H), 3.96 (s, 2H), 2.48 (s, 2H) ppm. ^{13}C NMR (DMSO, 100 MHz): δ = 138.57, 130.42, 129.62, 125.82, 31.66, 14.62 ppm.

Thiophen-2-ylmethanamine hydrochloride
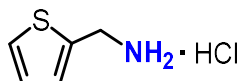
^{1}H NMR (DMSO, 400 MHz): δ =8.67 (s, 3H), 7.57 (d, J= 5.24 Hz, 1H), 7.30 (s, 1H), 7.06 (dd, J= 5.24 Hz, 1H), 4.20 (s, 2H) ppm. ^{13}C NMR (DMSO, 100 MHz): δ = 135.33, 129.05, 127.12, 36.60 ppm.

(5-methylthien-2-yl)methylamine hydrochloride
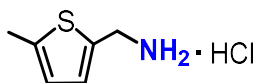
^{1}H NMR (methanol-d_4, 400 MHz): δ = 6.77 (d, J = 3.62 Hz, 1H), 6.49 (dd, J = 4.12, 1.60 Hz, 1H), 3.99 (s, 2H), 2.31 (s, 2H), 2.23 (s, 3H) ppm. ^{13}C NMR (methanol-d_4, 100 MHz): δ = 144.38, 132.85, 128.46, 127.60, 39.69, 16.02 ppm.

1,6-Diaminohexane dihydrochloride

^{1}H NMR (DMSO, 400 MHz): δ = 7.82 (s, 6H), 2.83 (m, 4H), 1.67 (m, 4H), 1.37 (m, 4H) ppm. ^{13}C NMR (DMSO, 100 MHz): δ = 38.42, 26.58, 25.23 ppm.

m-Xylylenediamine dihydrochloride
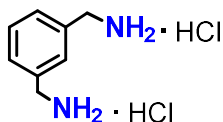
^{1}H NMR (DMSO, 400 MHz): δ = 8.63 (s, 6H), 7.61 (d, J = 2.24 Hz, 1H), 7.53 (d, J = 0.82 Hz, 2H), 7.45 (dd, J = 8.41, 6.93 Hz, 1H), 4.00 (s, 4H) ppm. ^{13}C NMR (DMSO, 100 MHz): δ = 134.25, 129.63, 128.80, 128.64, 41.96 ppm.

3. Results and discussion

3.1. Characterization of Co_2P NRs

The synthesized cobalt nanoalloy was characterized in detail. The X-ray diffraction (XRD) pattern of cobalt nanoalloy exhibits two sharp peaks at 41.1 and 52.3°, which can match well with the crystal structure of the orthorhombic Co_2P phase (**Figure 5-1** (a)) [25]. The Co_2P nanoalloy shows a rod morphology with 10 nm in diameter and 100 nm in length based on the representative transmission electron microscope (TEM) image (**Figure 5-1** (b)). The crystallinity and crystal structure of as-prepared Co_2P NR are also certificated by high-resolution TEM (HR-TEM) analysis. Clear lattice fringes with d spacing of 0.221 and 0.176 nm are observed in the HR-TEM image and indexed to the (112) and (002) plane of Co_2P, respectively (**Figure 5-1** (d)) [26]. In addition, the selected areas electron diffraction (SAED) pattern of Co_2P NR exhibits bright circular rings that are indexed to the orthorhombic structure of Co_2P, confirming its highly crystalline nature as shown in **Figure 5-1** (d) (inset). **Figures 5-1** (e-g) exhibit scanning transmission electron microscopy (STEM) image and the corresponding elemental mapping obtained by energy dispersive X-ray (EDX) technique, demonstrating the presence of the constituent elements, cobalt and phosphorus, are distributed homogeneously within each Co_2P NR. In addition, EDX analysis also shows that the resulting Co_2P NR owns a Co/P ratio of nearly 2 (**Figure 5-1** (h)). All these results clearly indicate the successful synthesis of a single crystal Co_2P NR. The TEM image of Co_2P NR/HT proves that the size and morphology of Co_2P NR are remained after supported on HT (**Figure 5-1** (b)).
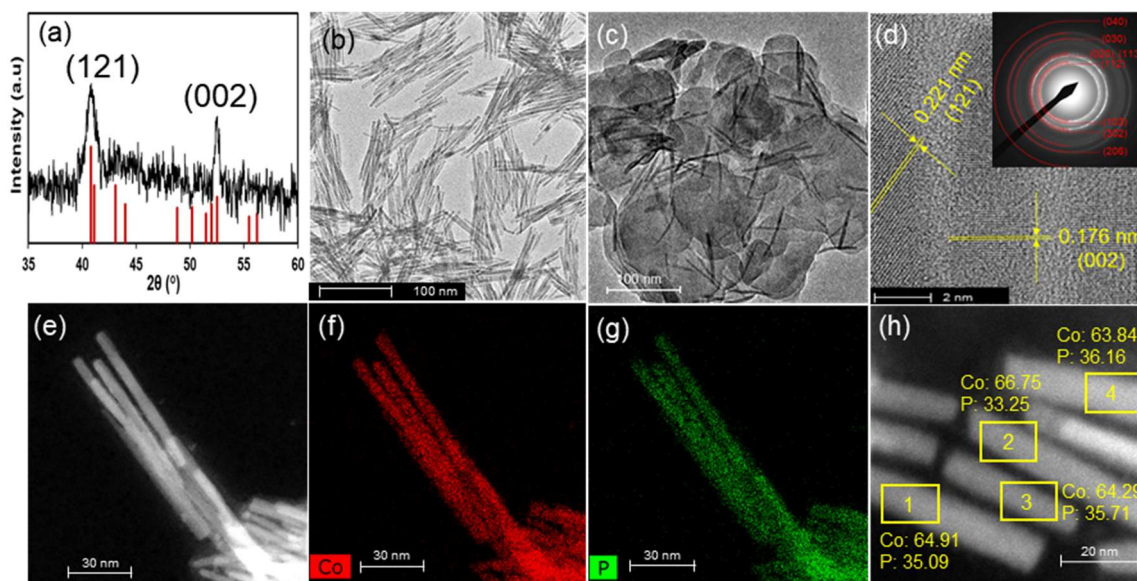
Figure 5-1. (a) XRD pattern of synthesized cobalt nanoalloy. (b) TEM image of the Co_2P NRs showing a rod-like morphology. (c) TEM image of the Co_2P NR/HT. (d) HR-TEM image of the Co_2P NRs with the inset illustrating the corresponding SAED pattern. (e) STEM image of the Co_2P NRs. Elemental mapping images of (f) Co and (g) P. (h) EDX analysis of Co_2P NRs in the yellow squares.

The X-ray photoelectron spectroscopy (XPS) spectra obtained in the Co 2p regions are presented in **Figure 5-2**. The Co 2p spectrum of Co_2P NR shows two main peaks located at 777.8 and 792.8 eV, which are close to the Co $2p_{3/2}$ (777.9 eV) and Co $2p_{1/2}$ (793.5 eV) of cobalt metal (Co^0), demonstrating the air-stable metallic nature of Co_2P NRs [27].
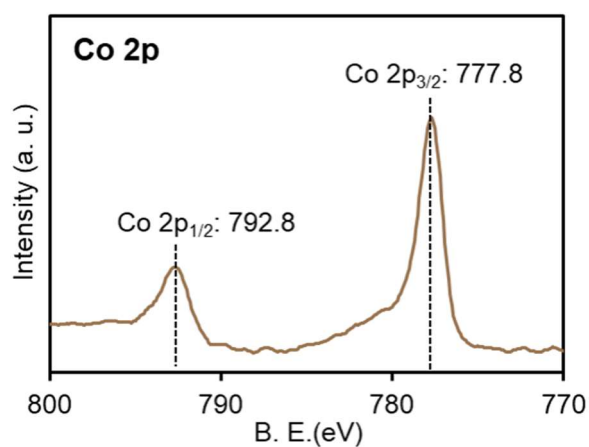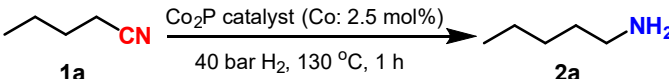
Figure 5-2. Co 2p XPS spectrum of Co_2P NRs.

3.2. Optimization of Co$_2$P NR in hydrogenation of valeronitrile

To investigate the catalytic potential of Co$_2$P NR, various metal oxide-supported Co$_2$P NR were prepared in a similar manner to the that of Co$_2$P NR/HT and then tested in the hydrogenation of valeronitrile (**1a**) at 130 °C, 40 bar of H$_2$ in 2-propanol conditions as model reaction. The results are shown in **Table 5-1**. Co$_2$P NR dispersed on supports all showed improved activity owing to the increase of surface area (entry 1 vs. entries 2-8). Among various metal oxide-supported Co$_2$P NR catalysts tested, Co$_2$P NR/HT showed the best performance, resulting in 93% yield of the primary amine product, 1-pentylamine (**2a**), with excellent selectivity for 1 h (entry 2). Other oxide supports such as Al$_2$O$_3$, MgO, TiO$_2$, CeO$_2$, SiO$_2$, and Nb$_2$O$_5$ were also effective in producing primary amine at moderate to high yields. It is noted that the catalytic activity of Co$_2$P NR/HT is almost 2-fold higher than that of we reported Co$_2$P nanoalloy with hexagonal column, prepared from CoCl$_2$ (entry 9) [24]. To optimize the catalytic performance of Co$_2$P NR/HT, we examined the catalytic activity of Co$_2$P NR prepared with different heating time of P-alloying process (entries 2 and 10-13). Co$_2$P NR could not be obtained after 1 h heating time due to the insufficient phosphidation. While the heating time was prolonged to more than 2 h, the catalytic activity of Co$_2$P NR/HT decreased gradually. Thus, these results revealed that 2 h seems to be the most suitable phosphidation time to form a highly active Co$_2$P NR and the combination with HT yield the best performance.

Table 5-1. Hydrogenation of **1a** using various Co$_2$P catalysts.^{a}

Entry	Catalyst	P-alloying time (h)	Yield of **2a** (%)^b
1	Co$_2$P NR	2	61
2	Co$_2$P NR/HT	2	93
3	Co$_2$P NR/TiO$_2$	2	90
4	Co$_2$P NR/MgO	2	88
5	Co$_2$P NR/Nb$_2$O$_5$	2	85
6	Co$_2$P NR/Al$_2$O$_3$	2	83
7	Co$_2$P NR/CeO$_2$	2	81
8	Co$_2$P NR/SiO$_2$	2	72
9	nano-Co$_2$P/HT	2	49
10	Co$_2$P NR/HT	0.5	0
11	Co$_2$P NR/HT	1	0
12	Co$_2$P NR/HT	5	73
13	Co$_2$P NR/HT	10	48

^{a}Reaction conditions: catalyst (Co: 0.0125 mol), **1a** (0.5 mmol), 2-propanol (3 mL), NH$_3$ aq. (1.2 mL), 40 bar H$_2$, 130 °C, 1 h. ^{b}Determined by gas chromatography-mass spectrometry (GS-MS) using biphenyl as an internal standard.
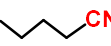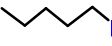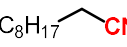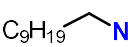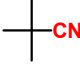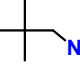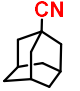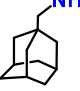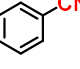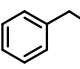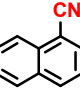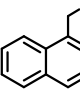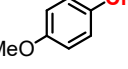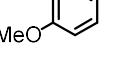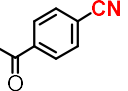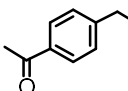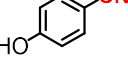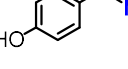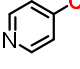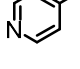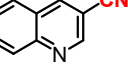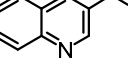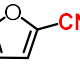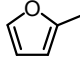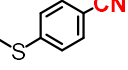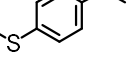
3.3. Applicability of Co$_2$P NR/HT to various nitriles

The applicability of this Co$_2$P NR/HT catalyst was then demonstrated through using a wide range of aliphatic and (hetero)aromatic nitriles as substrate (**Table 5-2**). For example, **1a** as well as long chain ones, dodecanenitrile (**1b**), were smoothly hydrogenated to yield the desired primary aliphatic amines up to 87-92% yield (entries 1-2). Sterically hindered nitriles like t-butylnitrile (**1c**) and 1-adamantanecarbonitrile (**1d**) were also good substrates and transformed into the amine products in high yields (entries 3-4). In regard to aromatic nitriles, benzonitriles with functional groups were hydrogenated and reducible functional groups were well tolerated to give the primary amines in high yields (entries 5-9, **1e-1i**). For example, the ketone group in **1h** was retained under the present conditions, whereas concomitant hydrogenation of ketone occurs in reported catalytic system [28]. In addition, 4-hydroxybenzonitrile (**1g**) was successfully transformed by Co$_2$P NR/HT to give **2g** in 86%, unlike the low (<5%) conversion using previously reported Co-catalyst [29]. Co$_2$P NR/HT also could be employed in the hydrogenation of heteroaromatic nitriles containing nitrogen or oxygen atoms to give the desired products over 85% yields (entries 10-12). Furthermore, Co$_2$P NR/HT was also applicable to sulfur-containing nitriles while sulfur compounds are prone to strongly coordinate to the active site of metals and thus significantly lose the catalytic acitiviies during the reatction. Sulfur-containing nitriles produced the amines in 81-95% yields (entries 13-15). The catalysis of Co$_2$P NR/HT is quite distinguished from that of Co$_2$P NPs (nano-Co$_2$P) described in chapter ***II***, Co$_2$P NR gave 90% yield in the hydogenaition of **2o**, while nano-Co$_2$P/HT only resulted in low yield under the same reaction conditions, highlighting the unique catalysis of Co$_2$P NR (**Scheme 5-2**). Moreover, diamines, like 1,6-hexamethylenediamine (**2p**) and 1,3-benzenedimethylamine (**2q**) are regarded as raw material of valuable industrial polymers also could be obtained by the hydrogenation of dinitriles using Co$_2$P NR/HT catalyst.

Table 5-2. Hydrogenation of nitriles to primary amines by Co_2P NR/HT.[a]

$$R-CN \xrightarrow[\text{40 bar } H_2, 130\,^\circ C]{\text{Co}_2\text{P NR/HT (Co: 2.5 mol\%)}} R \diagdown NH_2$$

Entry	Substrate	Time (h)	Product	Yield (%)[b]	TON	TOF (h^{-1})
1	(1a)	1	(2a)	93	37	37
2	C_8H_{17}—CN (1b)	2	C_9H_{19}—NH$_2$ (2b)	87	35	18
3	(1c)	4	(2c)	76	30	8
4	(1d)	3	(2d)	91	36	12
5	(1e)	4	(2e)	93	37	9
6	(1f)	2	(2f)	88	35	18
7	MeO (1g)	1	MeO (2g)	92	37	37
8	(1h)	1	(2h)	92	37	37
9[c]	HO (1i)	2	HO (2i)	86	34	17
10	(1j)	5	(2j)	93	37	7
11	(1k)	3	(2k)	85	34	11
12	(1l)	4	(2l)	92	37	9
13	(1m)	2	(2m)	95	38	19

14[d]	(1n)	3	(2n)	81	32	11
15[e]	(1o)	6	(2o)	90	36	6
16	(1p)	2	(2p)	76	30	15
17	(1q)	2	(2q)	93	37	19

[a]Reaction conditions: catalyst (Co: 2.5 mol%), substrate (0.5 mmol), aq. NH$_3$ (1.2 mL), 2-propanol (3 mL), 40 bar H$_2$, 130 °C. [b]GC-MS yields using an internal standard. [c]Aq. NH$_3$ (2.0 mL). [d]50 bar H$_2$. [e]150 °C. All the substrates achieved complete conversions.
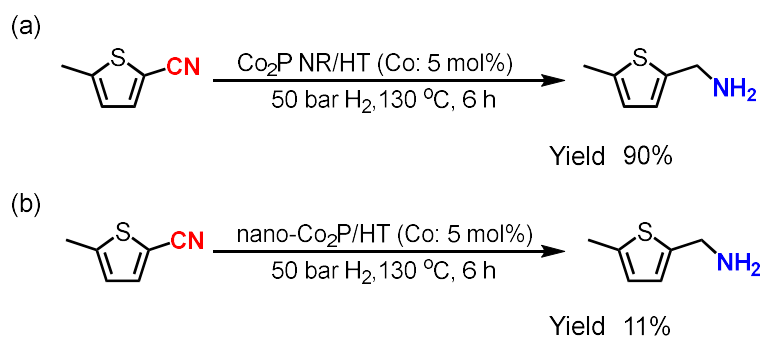

Scheme 5-2. Hydrogenation of 2-cyano-5-methylthiophene by (a) Co$_2$P NR/HT and (b) nano-Co$_2$P/HT. Yields were calculated via GC-MS analysis using an internal standard.

3.4. Nitrile hydrogenation under 1 bar of H_2

Beside the broad substrate-scope of Co_2P NR/HT, the high performance of Co_2P NR/HT was pronounced under milder conditions. Co_2P NR/HT could operate under just 1 bar of H_2 and selected nitriles (**2a**, **2b**, **2e**, **2g**, **2h**, **2p,** and **2q**) were converted into the corresponding primary amines effectively (**Scheme 5-3**).
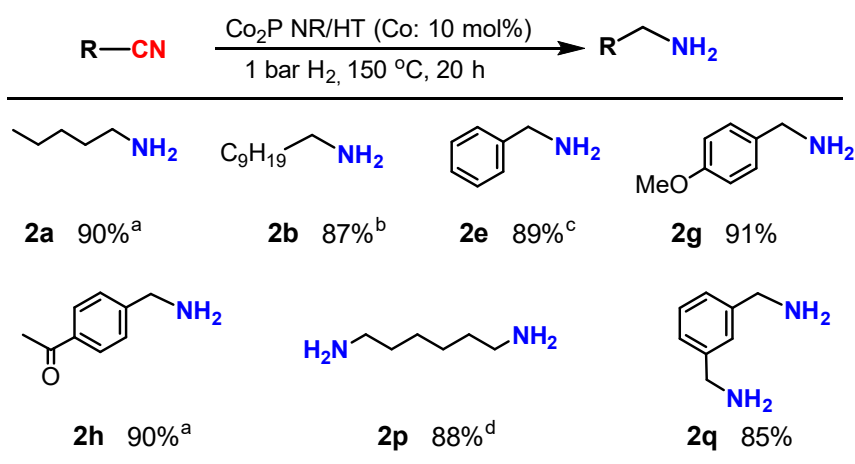
Scheme 5-3. Co_2P NR/HT-catalyzed nitrile hydrogenation to primary amine under 1 bar H_2. Reaction conditions: Co_2P NR/HT (Co: 10 mol%), substrate (0.5 mmol), aq. NH_3 (1.2 mL), 2-propanol (3 mL). Yields were calculated via GC-MS analysis using an internal standard. [a]130 °C, 16 h. [b]16 h. [c]Aq. NH_3 (0.4 mL). [d]Aq. NH_3 (2.0 mL).

3.5. Gram experiment

Furthermore, Co_2P NR/HT-catalyzed gram-scale experiment also proceed smoothly: 2.2 g of **1a** was fully converted and gave the hydrochloride salt of **2a** in 90% isolated yield, indicating its high practicability (**Scheme 5-4**).
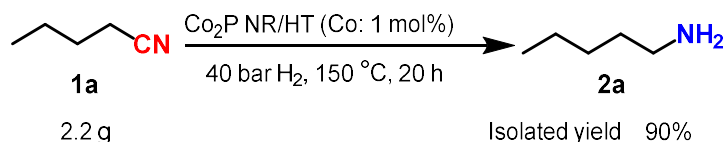
Scheme 5-4. Gram-scale experiment of Co_2P NR/HT in hydrogenation of **1a**. Reaction conditions: Co_2P NR/HT (Co: 1 mol%), **1a** (25 mmol), aq. NH_3 (8 mL), 2-propanol (30 mL), 150 °C, 40 bar H_2, 20 h.

### 3.6. Additive-free hydrogenation of nitrile by Co_2P NR/HT

As mentioned above, ammonia is the most used additive to suppress the formation of secondary amine byproducts in order to improve the selectivity of primary amine during the hydrogenation of nitrile reaction. The application of Co_2P NR/HT for additive-free hydrogenation of nitriles was investigated as shown in **Scheme 5-5**. In the absence of ammonia, 11 kinds of nitriles selectively gave the primary amine products in high yields under 40 bar H_2, 150 °C conditions with 10 mol % of Co_2P NR/HT, which is benefit from the high activity of Co_2P NR/HT that hydrogenates the imine intermediate to primary amine quickly instead of the formation of secondary imine. This successful trial further emphasizes the notable practicality of Co_2P NR/HT and also provides a green catalytic system for producing primary amines.
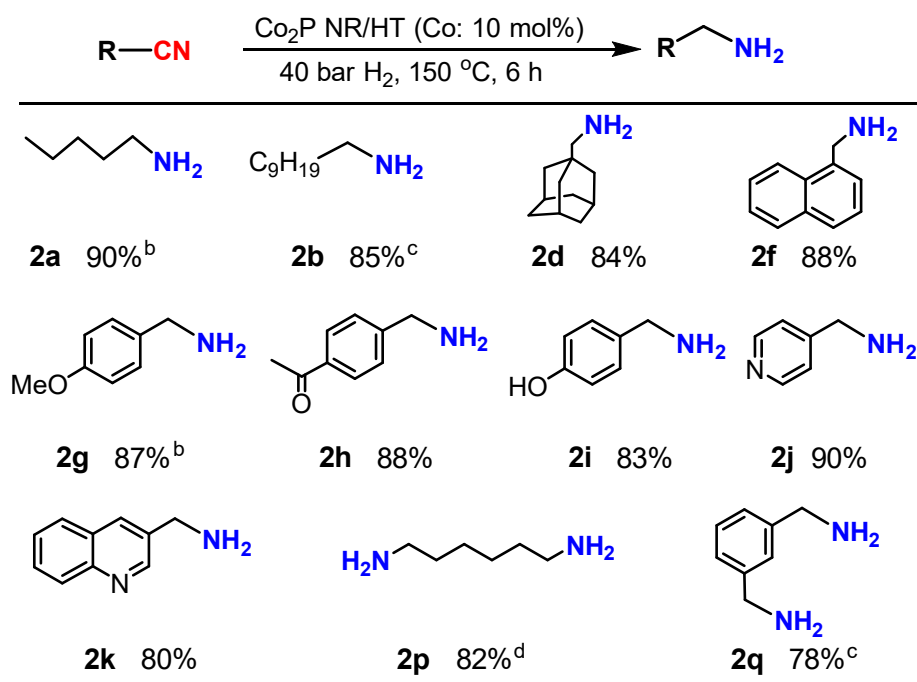
Scheme 5-5. Co_2P NR/HT-catalyzed nitrile hydrogenation to primary amine under ammonia-free conditions. Reaction conditions: Co_2P NR/HT (Co: 10 mol%), substrate (0.5 mmol), 2-propanol (3 mL). Yields were calculated via GC-MS analysis using an internal standard. [a]2 h. [b]10 h. [c]H_2O (1.0 mL), 2-propanol (3 mL), 10 h.

3.7. Durability of Co$_2$P NR/HT

The air-stability of Co$_2$P NR/HT has great advantage in the catalyst-recover and reuse. After the reaction, Co$_2$P NR/HT was easily removed by filtration and operated under air atmosphere safely in sharp consistent with conventional non-noble-metal-based catalysts like Raney catalysts [6]. The recovered Co$_2$P NR/HT catalyst was ready to be used in the next experiment without H$_2$-pre-treatment and any loss of activity even after 5th runs (**Figure 5-3**), demonstrating its high durability and easy-handing. Furthermore, inductively coupled plasma atomic emission spectroscopy (ICP-AES) analysis of the fresh and used catalysts showed the almost same results, which is in well agreement with the high reusability of Co$_2$P NR/HT (**Table 5-3**).
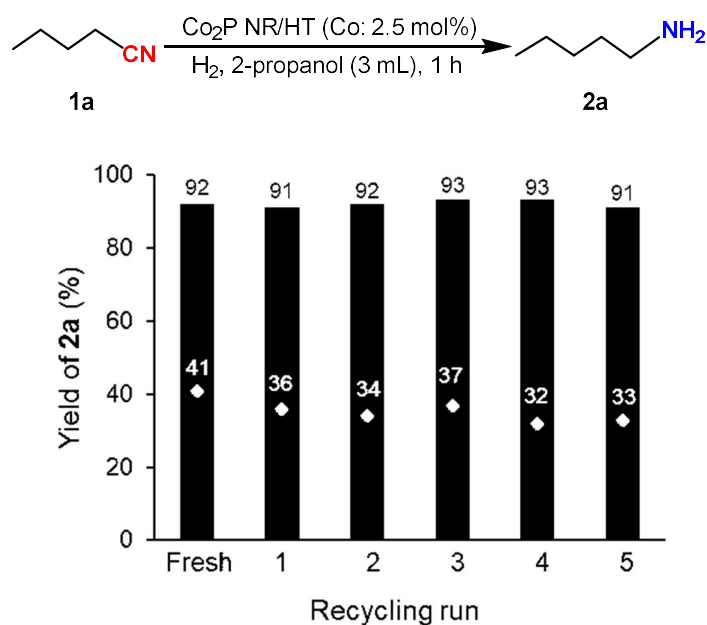

Figure 5-3. Reuse experiment of Co$_2$P NR/HT catalyst. Reaction conditions: Co$_2$P NR/HT (Co: 2.5 mol%), **1a** (0.5 mmol), aq. NH$_3$ (1.2 mL), 2-propanol (3.0 mL), 130 °C, 40 bar H$_2$. Reaction time: 1 h (black bars), 20 min (white diamonds). Yields were calculated via GC-MS analysis using an internal standard.

Table 5-3. ICP-AES analysis of fresh and used Co$_2$P NR/HT.

	wt%			
	Mg	Al	Co	P
Co$_2$P NR/HT_fresh	19.9	7.47	2.70	0.85
Co$_2$P NR/HT_used	20.0	7.51	2.68	0.85

## 3.8. Investigation of activity-structure relationship using XAFS analysis
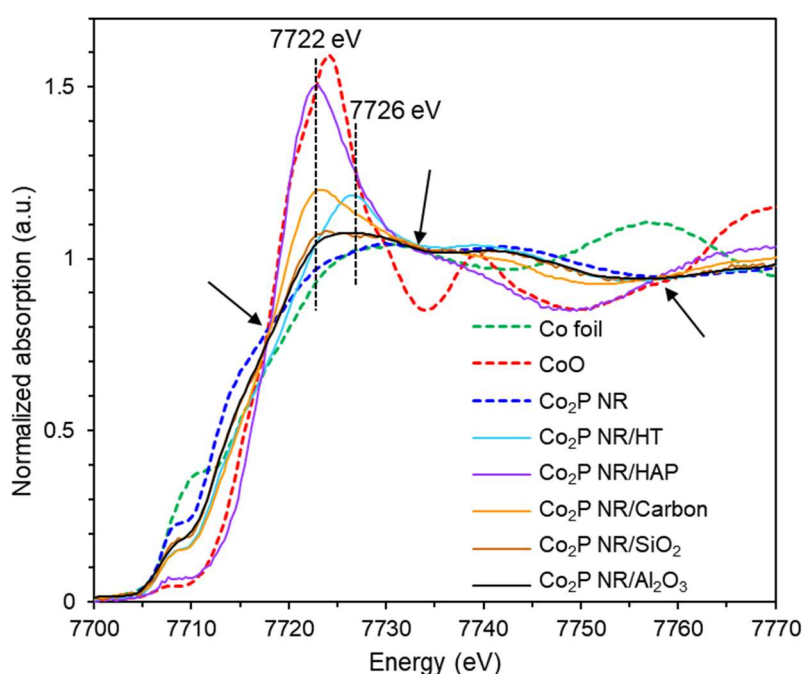
Figure 5-4. Co *K*-edge XANES spectra of Co foil, CoO, Co$_2$P NR, and supported Co$_2$P NRs.

Black arrow: the isosbestic point position in XANES spectra of supported Co$_2$P NRs.

The reason for the high catalytic activity of the present Co$_2$P NR catalyst was investigated by X-ray absorption fine structure (XAFS) analysis. Co *K*-edge X-ray absorption fine structure (XAFS) analysis revealed that the X-ray absorption near edge structure (XANES) spectrum shape of Co$_2$P NR is very similar to that of Co foil, indicating the similar electron states (metallic states) of Co foil (**Figure 5-4**). The spectral feature of Co$_2$P NR/HT verified that of Co$_2$P

NRs, which reveals that the electronic states and/or local structure of Co_2P NR are affected by HT after the immobilization.

Furthermore, the spectral shape of Co_2P NR/HT is significantly different from those of other supported-Co_2P NRs, those have a characteristic Co oxide peak at 7722 eV and three common isosbestic points at 7718, 7733, and 7759 eV, which are not existed in Co_2P NR/HT spectrum. These results showed that Co_2P NR/HT maintains its metallic state after immobilization due to the unique interaction between Co_2P NR and HT, while the combination with other supports are tend to be oxidized that led to the low activity.
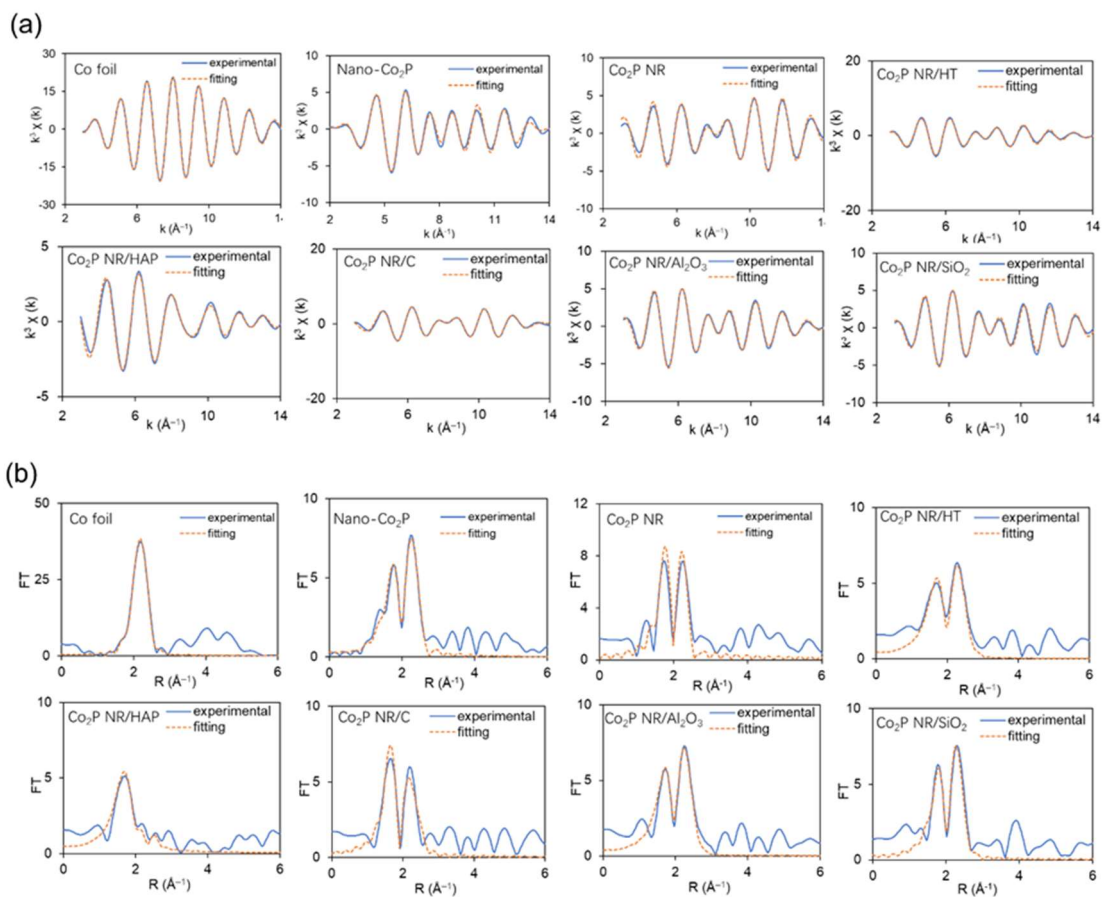
Figure 5-5. EXAFS fitting curves of Co foil, nano-Co_2P, Co_2P NR, and supported Co_2P NRs in (a) k-space and (b) R-space.

The curve fitting analysis was conducted to get insight about the local structure. These results are summarized in **Figure 5-5** and **Table 5-4**. The spectrum of Co_2P NR/HT was well fitted with Co–P and Co–Co shell. On the contrary, Co–O bond as well as Co–P and Co–Co bonds can be observed in other supported-Co_2P NR, which is agree with the partial oxidation results in XANES. Furthermore, Co_2P NR/HT has the smallest coordination number (CN) ratio, CN_{Co-Co}/CN_{Co-P} (1.4) among nano-Co_2P, bulk Co_2P, and other supported-Co_2P NR samples, indicating the presence of high coordinatively-unsaturated Co–Co site in Co_2P NR/HT. Hence, the high activity of Co_2P NR can be also derived from their high coordinatively-unsaturated active site.

Table 5-4. Curve-fitting results of Co K-edge EXAFS.

Sample	Shell	CN[a]	r (Å)[b]	D.W. [c]	R factor (%)
Co foil	Co–Co	10.6 ± 0.2	2.49±0.01	0.007±0.002	2.6
Nano-Co_2P	Co–P	1.8 ± 0.1	2.23±0.02	0.003±0.002	12.5
	Co–Co	3.5± 0.2	2.56±0.02	0.009±0.003	
Co_2P NR	Co–P	1.5 ± 0.1	2.19±0.03	0.007±0.005	13.2
	Co–Co	2.3 ± 0.2	2.58±0.03	0.009±0.005	
Co_2P NR/HT	Co–P	2.0 ± 0.3	2.16±0.05	0.009±0.006	10.8
	Co–Co	2.8 ± 0.3	2.62±0.04	0.010±0.005	
Co_2P NR/HAP	Co–O	3.6 ± 0.3	2,05±0.04	0.010±0.006	13.5
	Co–Co	0.3 ± 0.2	2.63±0.04	0.005±0.004	
Co_2P NR/Carbon	Co–O	2.0 ± 0.2	1.99±0.04	0.003±0.002	10.9
	Co–Co	1.4 ± 0.1	2.58±0.04	0.007±0.005	
Co_2P NR/Al_2O_3	Co–P	1.7 ± 0.2	2.15±0.04	0.007±0.005	10.2

	Co–Co	3.2 ± 0.3	2.59±0.04	0.010±0.005	
Co$_2$P NR/SiO$_2$	Co–P	1.4 ± 0.2	2.20±0.04	0.005±0.004	13.1
	Co–Co	2.4 ± 0.2	2.60±0.04	0.008±0.004	

[a]Coordination number. [b]Bond distance. [c]Debye–Waller factor.

4. Conclusion

This chapter describes a hydrotalcite-supported cobalt phosphide nanorod (Co$_2$P NR/HT) serves as a highly active, air-stable, and reusable non-noble metal heterogeneous catalysts for the selective hydrogenation of nitriles into primary amines. Co$_2$P NR/HT shows high activity for hydrogenation of nitrile under just 1 bar of H$_2$ and also can be employed under additive-free conditions as the first example of non-precious metal-based catalyst. In addition, Co$_2$P NR/HT is uniquely applicable to a broad range of substrates including the sulfur containing nitriles, giving the corresponding primary amines in excellent yields. XAFS analysis exhibited that Co$_2$P NR/HT has air-stable metallic cobalt species with highly coordinatively unsaturated active sites and the presence of a unique interaction between Co$_2$P NR and HT, which can account for its high activity. These findings will significantly contribute to the development of green sustainable technology for producing valuable primary amines from nitriles.

References

1 Roose, P.; Eller, K.; Henkes, E.; Rossbacher, R.; Höke, H. Amines, Aliphatic. *Ullmann's Encyclopedia of Industrial Chemistry*; Wiley-VCH: Weinheim, Germany, **2015**.

2 Bagal, D. B.; Bhanage, B. M. *Adv. Synth. Catal.* **2015**, *357*, 883–900.

3 Herzog, B. D.; Smiley, R. A. Hexamethylenediamine. *Ullmann's Encyclopedia of Industrial Chemistry*; Wiley-VCH: Weinheim, Germany, **2012**.

4 Werkmeister, S.; Junge, K.; Beller, M. *Org. Process Res. Dev.* **2014**, *18*, 289–302.

5 Legnani, L.; Bhawal, B.; Morandi, B. *Synthesis* **2017**, *49*, 776–789.

6 Nishimura, S. *Handbook of Heterogeneous Catalytic Hydrogenation for Organic Synthesis*; Wiley-VCH: Weinheim, Germany, **2001**.

7 Krupka, J.; Pasek, J. *Curr. Org. Chem.* **2012**, *16*, 988– 1004.

8 Chakraborty, S.; Berke, H. *ACS Catal.* **2014***, 4,* 2191–2194.

9 De Bellefon, C.; Fouilloux, P. *Catal. Rev.: Sci. Eng.* **1994**, *36*, 459–506.

10 Rylander, P. N. *Hydrogenation Methods*, Academic Press, London, **1988** (2nd Ed.), 94 –103.

11 Rylander, P. N. *Catalytic Hydrogenation over Platinum Metals*, Academic Press, NY and London, **1967**, 203–226.

12 Takahashi, T.; Ueda, S.; Ichikawa, T.; Kobayashi, Y.; Okami, H.; Hattori, T.; Sawama, Y.; Monguchi, Y.; Sajiki, H. *Adv. Synth. Catal.* **2018,** *360*, 1726–1732.

13 Greenfield, H. *Ind. Eng. Chem. Prod. Rev. Dev*. **1967**, 142.

14 Gomez, S.; Peters, J. A.; Maschmeyer, T. *Adv. Synth. Catal.* **2002**, *344*, 1037–1057

15 Medina Cabello, F.; Tichit, D.; Coq, B.; Vaccari, A.; Dung, N. T. *J. Catal.* **1997**, *167*, 142.

16 Corma, A.; Iborra, S.; Velty, A. *Chem. Rev.* **2007**, *107*, 2411– 2502.

17 Mika, L. T.; Cséfalvay, E.; Németh, Á. *Chem. Rev.* **2018**, *118*, 505–613.

18 Torres Galvis, H. M.; Bitter, J. H.; Khare, C. B.; Ruitenbeek, M.; Dugulan, A. I.; de Jong, K.

P. *Science* **2012**, *335*, 835–838.

19   Anderson, J.A.; García, M. F. *Supported Metals in Catalysis: Catalytic Science Series*, *Imperial College Press*, **2005**.

20   Roldan Cuenya, B. *Thin Solid Films* **2010**, *518*, 3127–3150.

21   Zecevic, J.; Vanbutsele, G.; de Jong, K.; Martens, J. *Nature* **2015**, *528*, 245–248.

22   Arnal, P.; Comotti, M.; Schüth, F. **2006**, *45*, 8224–8227.

23   Pacchioni, G.; Freund, H. *Chem. Soc. Rev.* **2018**, *47*, 8474–8502.

24   Sheng, M.; Yamaguchi, S.; Nakata, A.; Yamazoe, S.; Nakajima, K.; Yamasaki, J.; Mizugaki, T.; Mitsudome, T. *ACS Sustainable Chem. Eng.* **2021**, *9*, 11238–11246.

25   Skála, R.; Drábek, M. *Bull. Czech Geol. Surv.* **2001**, *76*, 209–216.

26   Zhang, H.; Ha, D.; Hovden, R.; Kourkoutis, L.; Robinson, R. *Nano Lett.* **2011**, *11*, 188–197.

27   Wagner, C. D.; Riggs, W. M.; Davis, L. E.; Moulder, J. F.; Muilenberg, G. E. *Handbook of X-Ray Photoelectron Spectroscopy*; Perkin-Elmer: Eden Prairie, **1979**.

28   Chakraborty, S.; Leitus, G.; Milstein, D. *Chem. Commun.* **2016**, *52*, 1812−1815.

29   Tokmic, K.; Jackson, B.; Salazar, A.; Woods, T.; Fout, A. *J. Am. Chem. Soc.* **2017**, 139, 13554−13561.

General Conclusions

This thesis deals with the studies on the development of cobalt phosphide nanoparticle as highly efficient and air-stable catalyst for versatile hydrogenation reactions under liquid-phase conditions such as (I) selective hydrogenation of nitriles to primary amines, (II) selective hydrogenation of furfural derivatives to furfuryl alcohol products, (III) reductive amination of carbonyl compounds to primary amines.

In Chapter I, the author surveys the fundamental background of metal phosphides and focus on the exploration of cobalt phosphide as a potential catalyst for organic synthesis. The characteristics and preparation methods of cobalt phosphides were systematically summarized. In addition, recent reports on the catalysis of cobalt phosphides were reviewed and the limitation of their applicability was also described.

In Chapter II, the author demonstrates a well-defined cobalt phosphide nanoparticle (nano-Co_2P) prepared by phosphorus-alloying strategy for selective hydrogenation of nitriles to the corresponding primary amines. nano-Co_2P catalyst showed significantly high activity in nitrile hydrogenation even under 1 bar H_2 pressure, which is the first example of a non-precious metal catalyst for promoting this transformation under ambient H_2 pressure. In addition, nano-Co_2P catalyst was applicable to the gram-scale reaction, exhibiting a 20- to 500-fold greater activity than reported non-precious metal catalysts.

In Chapter III, the author mentions that an Al_2O_3-supported nano-Co_2P (nano-Co_2P/Al_2O_3) can serve as a highly efficient catalyst for the selective hydrogenation of furfural derivatives to furfuryl

alcohol products. In contrast to conventional air-unstable non-precious metal catalysts, nano-Co$_2$P exhibited unique air-stable metallic nature, which enables easy and safe handling. Furthermore, the spent nano-Co$_2$P catalyst was reusable without significant loss of its activity and selectivity.

The next chapter represents unique catalysis of a newly synthesized single-crystal cobalt phosphide nanorods (Co$_2$P NRs) for reductive amination of carbonyl compounds to primary amines. Whereas conventional Co catalysts were almost inactive, the Co$_2$P NR exhibited high activity and selectivity under an atmospheric pressure of H$_2$ or at room temperature, converting a wide range of carbonyl compounds including aldehydes and ketones into primary amines in high yields.

Finally, the author describes the hydrogenation of nitriles catalyzed by a hydrotalcite (HT, Mg$_6$Al$_2$(OH)$_{16}$CO$_3$·4H$_2$O)-supported cobalt phosphide nanorod catalyst (Co$_2$P NR/HT) in Chapter V. Co$_2$P NR/HT served as a highly effective and reusable catalyst with a broad substrate generality including aromatic, heteroaromatic, aliphatic nitriles, dinitriles as well as sulfur-containing nitriles. Moreover, Co$_2$P NR/HT is the first example of hydrogenation of nitriles to primary amines under ammonia-free conditions using non-precious metal catalyst. Spectroscopic analyses disclose that the cooperative catalysis by Co$_2$P NR and HT are key factors for its high activity and stability.

In terms of the critical role in sustainable chemical processes, the development of highly efficient and stable non-precious metal heterogeneous catalyst by the sophisticated design and synthesis, such as alloying with additional metals or non-metal elements, is of considerable interest. Cobalt phosphide nanoparticles prepared by the phosphorus-alloying with cobalt nanoparticles have both ligand effect and size effect from homogeneous and heterogeneous catalysis and are regarded as a potential catalyst for organic synthesis, which is still underexplored. In this thesis, the author

developed a series of cobalt phosphide nanoparticle catalysts for various hydrogenation reactions, which exhibit excellent activities that far outperform previously reported non-precious metal catalysts. Unlike the dilemma relationship of activity and air stability existed in conventional catalysts, developed cobalt phosphide catalysts uniquely possess air-stable metallic nature that enables the easy and safe handling during the whole reaction, which will significantly ameliorate the complicate processes in nowadays industry caused by the low efficiency and/or air sensitivity of catalyst. Furthermore, cobalt phosphide nanoparticle catalysts were easily separated from the reaction mixture after the reaction and the spent catalyst showed high reusability. The comprehensive analyses revealed that the presence of electron-rich cobalt species derived from phosphorus-alloying and a number of coordinatively unsaturated Co–Co active sites are the key factors for the excellent catalytic performance of developed cobalt phosphide nanoparticles. Furthermore, their activity can be further improved by various nanoengineering and modifications easily due to its easy-handling in air.

The author strongly believes that this study will be a milestone attempt for the development of air-stable and highly efficient non-precious metal catalysts for organic synthesis via a promising method called "phosphorus-alloying strategy". The developed cobalt phosphide nanoparticle catalysts and their catalytic performances in hydrogenation reactions discussed herein will provide potential candidates and beneficial insights to realize the next-generation efficient, sustainable, and environmentally-benign reaction processes for valuable chemical productions.

List of Publications

[1] Takato Mitsudome, **Min Sheng**, Ayako Nakata, Jun Yamasaki, Tomoo Mizugaki, Koichiro Jitsukawa.

"A cobalt phosphide catalyst for the hydrogenation of nitriles"

Chemical Science, **2020**, *11*, 6682–6689.

[2] Hiroya Ishikawa, **Min Sheng**, Ayako Nakata, Kiyotaka Nakajima, Seiji Yamazoe, Jun Yamasaki, Sho Yamaguchi, Tomoo Mizugaki, Takato Mitsudome.

"Air-stable and reusable cobalt phosphide nanoalloy catalyst for selective hydrogenation of furfural derivatives"

ACS Catalysis, **2021**, *11*, 750–757.

[3] **Min Sheng**, Shu Fujita, Sho Yamaguchi, Jun Yamasaki, Kiyotaka Nakajima, Seiji Yamazoe, Tomoo Mizugaki, Takato Mitsudome.

"Single-crystal cobalt phosphide nanorods as a high-performance catalyst for reductive amination of carbonyl compounds"

JACS Au, **2021**, *1*, 501–507.

[4] **Min Sheng**, Sho Yamaguchi, Ayako Nakata, Seiji Yamazoe, Kiyotaka Nakajima, Jun Yamasaki, Tomoo Mizugaki, Takato Mitsudome.

"Hydrotalcite-supported cobalt phosphide nanorods as a highly active and reusable heterogeneous catalyst for ammonia-free selective hydrogenation of nitriles to primary amines"

ACS Sustainable Chemistry & Engineering, **2021**, *9*, 11238–11246.

Related Work

[1] Takato Mitsudome, Shu Fujita, **Min Sheng**, Jun Yamasaki, Keita Kobayashi, Tomoko Yoshida, Zen Maeno, Tomoo Mizugaki, Koichiro Jitsukawa, Kiyotomi Kaneda.

"Air-stable and reusable cobalt ion-doped titanium oxide catalyst for alkene hydrosilylation"

Green Chemistry, **2019**, *21*, 4566–4570.